

2014

NEW MICROFLUIDIC SYSTEM TO INCREASE ROBUSTNESS OF ELECTRODE PERFORMANCE AND DEVELOP POINT-OF-CARE HEMATOCRIT DEVICE

Hwi Yong Lee
Michigan Technological University

Follow this and additional works at: <https://digitalcommons.mtu.edu/etds>

 Part of the [Chemical Engineering Commons](#)


Copyright 2014 Hwi Yong Lee

Recommended Citation

Lee, Hwi Yong, "NEW MICROFLUIDIC SYSTEM TO INCREASE ROBUSTNESS OF ELECTRODE PERFORMANCE AND DEVELOP POINT-OF-CARE HEMATOCRIT DEVICE", Dissertation, Michigan Technological University, 2014.

<https://doi.org/10.37099/mtu.dc.etds/859>

Follow this and additional works at: <https://digitalcommons.mtu.edu/etds>

 Part of the [Chemical Engineering Commons](#)

NEW MICROFLUIDIC SYSTEM TO INCREASE ROBUSTNESS OF ELECTRODE
PERFORMANCE AND DEVELOP POINT-OF-CARE HEMATOCRIT DEVICE

By

Hwi Yong Lee

A DISSERTATION

Submitted in partial fulfillment of the requirements for the degree of

DOCTOR OF PHILOSOPHY

In Chemical Engineering

MICHIGAN TECHNOLOGICAL UNIVERSITY

2014

© 2014 Hwi Yong Lee

This dissertation has been approved in partial fulfillment of the requirements for the Degree of DOCTOR OF PHILOSOPHY in Chemical Engineering

Department of Chemical Engineering

Dissertation Advisor: *Adrienne R. Minerick*

Committee Member: *Caryn Heldt*

Committee Member: *Chang Kyoung Choi*

Committee Member: *Ching-An Peng*

Department Chair: *S. Komar Kawatra*

TABLE OF CONTENTS

PREFACE	5
ACKNOWLEDGEMENTS	6
LIST OF ABBREVIATIONS	7
Abstract	9
Chapter 1 Introduction and outline.....	10
1.1 Introduction	10
1.2 Motivation for the Research and Outline of Dissertation	12
Chapter 2 Technological challenges of microfluidic devices in bio-application: electrolysis, fouling interference, and microelectrode performance.....	13
2.1 Introduction	13
2.2 Electrolysis bubbles.....	15
2.3 Adsorption of biomolecules	22
2.4 Microelectrode performance	27
2.5 Conclusions	30
Chapter 3 Improving electrokinetic microdevice stability by controlling electrolysis bubbles	32
3.1 Introduction	32
3.2 Materials and Methods	36
3.3 Results and Discussion.....	40
3.4 Concluding Remarks	51
3.5 Acknowledgements	52
Chapter 4 Platinum electrode modification by carbonizing surface to improve performance and sensitivity	53
4.1 Introduction	53
4.2 Materials and methods	57
4.3 Results and discussion.....	60
4.4 Concluding remarks	75
4.5 Acknowledgements	76
Chapter 5 Electrochemical hematocrit determination in a direct current microfluidic device	77

5.1 Introduction	77
5.2 Materials and Methods	81
5.3 Results and Discussion.....	85
5.4 Concluding remarks	93
5.5 Acknowledgements	94
Chapter 6 Conclusion and ongoing work	96
References	98
APPENDIX PROOFS OF PERMISSION TO REPRODUCE PUBLISHED MATERIAL	109

PREFACE

The aim of this dissertation is to develop new microfluidic system for hematocrit determination. Chapter 3, 4, and 5 have been published or submitted for publication.

Publication list as follows:

1. H.Y. Lee, C. Barber, and A.R. Minerick, “Improving electrokinetic microdevice stability by controlling electrolysis bubbles”, *Electrophoresis*, 2014, 35, 1782-1789
2. H.Y. Lee, C. Barber, and A.R. Minerick, “Platinum electrode modification by carbonizing surface to improve performance and sensitivity”, *Electrophoresis*, 2014, in review.
3. H.Y. Lee, C. Barber, J.A. Rogers, and A.R. Minerick, “Electrochemical hematocrit determination in a direct current microfluidic device”, *Electrophoresis*, 2014, in review

The descriptions of the coauthors’ contributions follow. Obviously I did rest of the works. Dr. Adrienne R. Minerick, Associate Professor, Department of Chemical Engineering, Michigan Technological University, contributed as my research advisor during this work. Cedrick Barber, Undergraduate student, Department of Chemical Engineering, helped to visualize electrolysis bubbles in paper 1 and red blood cells in paper 3, and measured some of current responses in papers 2 and 3. Jessika A. Rogers measured conductivity and zeta potential of red blood cells in paper 3.

ACKNOWLEDGEMENTS

I would like to sincerely thank Dr. Adrienne R. Minerick for the invaluable opportunity to learn about microfluidic technology. Sincere thanks are also extended to Dr. Faith Morrison for teaching and leading me towards success. Cedrick Barber participated in some of these experiments as my undergraduate assistant and deserves recognition. I greatly appreciate his contribution. Thanks to Portage Health for phlebotomy assistance to obtain the blood samples necessary for these experiments. I would like to appreciate all of MD-ERL members, Tayloria Adams, Maryam Khaksari, Zhichao Wang, and Jeana Dillon.

Thank you to Dr. Caryn Heldt, Dr. Ching-An Peng, and Dr. Chang Kyoung Choi for sacrificing their time to serve on my committee and for being invaluable guides for my research.

LIST OF ABBREVIATIONS

AA: ascorbic acid

ASV: anodic stripping voltammetry

CBC: complete blood count

CF: carbon fiber

CMC: critical micelle concentration

CP: carbon paste

CPC: cetyl pyridinium chloride

CTAB: hexadecyltrimethylammonium bromide

CTAC: cetyl trimethyl ammonium chloride

CV: cyclic voltammetry

DA: 3-hydroxytyramine (dopamine)

DOPAC: 3,4-dihydroxyphenylacetic acid

DPC: dodecyl pyridinium chloride

DTAB: dodecyltrimethylammonium bromide

DTAC: dodecyl trimethyl ammonium chloride

EDS: energy dispersive spectrometry

FE-SEM: field emission scanning electron microscopy

GC: glassy carbon, HRP: horseradish peroxidase

HCT: hematocrit

5-HT: 5-hydroxytryptamine (neurotransmitter serotonin)

LSV: linear sweep voltammetry

MCHC: mean corpuscular hemoglobin concentration

MCV: mean corpuscular volume

MWCNT: multi-wall carbon-nanotube

NADH: β -nicotinamide adenine dinucleotide

PEDOT: poly(3,4-ethylene dioxythiophene)

PB: phosphate buffer

PBS: phosphate buffered saline

POC: point-of-care

RBC: red blood cell

RPG: rough pyrolytic graphite

SDS: sodium dodecyl sulfate

SOS: sodium octyl sulfate

SWCNT: single-wall carbon-nanotube

SWV: square wave square voltammetry

TTAB: tetradecyltrimethylammonium bromide

UA: uric acid

Abstract

The present dissertation aimed to develop a new microfluidic system for a point-of-care hematocrit device. Stabilization of microfluidic systems via surfactant additives and integration of semipermeable SnakeSkin[®] membranes was investigated. Both methods stabilized the microfluidic systems by controlling electrolysis bubbles. Surfactant additives, Triton X-100 and SDS stabilized promoted faster bubble detachment at electrode surfaces by lowering surface tension and decreased gas bubble formation by increasing gas solubility. The SnakeSkin[®] membranes blocked bubbles from entering the microchannel and thus less disturbance to the electric field by bubbles occurred in the microchannel. Platinum electrode performance was improved by carbonizing electrode surface using red blood cells. Irreversibly adsorbed RBCs lysed on platinum electrode surfaces and formed porous carbon layers while current response measurements. The formed carbon layers increase the platinum electrode surface area and thus electrode performance was improved by 140 %. The microfluidic system was simplified by employing DC field to use as a platform for a point-of-care hematocrit device. Feasibility of the microfluidic system for hematocrit determination was shown via current response measurements of red blood cell suspensions in phosphate buffered saline and plasma media. The linear trendline of current responses over red blood cell concentration was obtained in both phosphate buffered saline and plasma media. This research suggested that a new and simple microfluidic system could be a promising solution to develop an inexpensive and reliable point-of-care hematocrit device.

Chapter 1 Introduction and outline

1.1 Introduction

Hematocrit (HCT) is a red blood cell volume percentage in blood. Normal HCT levels are 40 – 54 % for men and 36 – 48 % for women [1]. HCT test is a key medical diagnostic tool. High HCT values may signal medical conditions such as polycythemia, cyanosis, dehydration, decompensating cardiovascular disease, and pulmonary fibrosis. Low HCT values may represent the signs of anemia and leukemia. [2] Since HCT is an important medical indicator, many HCT test methods including microhematocrit [3], Coulter counter [4, 5], CuSO_4 specific gravity [6] and conductivity based point-of-care (POC) HCT devices [7, 8] have been developed. However, these methods are either expensive, environmentally inadvisable or complicated.

Microfluidic devices (also called microdevices, Lab-on-a-Chip (LOC), and micro Total Analytical Systems (μTAS)) are microfluidic platforms that can integrate any combination of reactions, separations, mixing, detections, and other laboratory functions into a single polymer or glass chip in order to perform an entire chemical or bioanalytical assay on the chip. Such microfluidic devices have the advantages of high resolution, low-cost, rapid analysis, low sample consumption in a range of nL to μL , versatility in design and portability [9, 10]. Microfluidic device research was accelerated when the U.S. Defense Advanced Research Project Agency (DARPA) started a fund in the 1990s to develop the portable microfluidic-based medical diagnostic systems for the military.

Since then, their applications have extended to biological assays, medical-diagnostic, life science, chemical synthesis, and many other chemical applications [9, 11, 12]. Due to the breadth and versatility of applications, microfluidic devices are considered a promising technology for the future and are under development across the world.

Point-of-care (POC) tests (also called bed-side test) are a medical test at or near the patient and traditionally outside the clinical laboratory. POC tests are used in order to provide prompt and appropriate treatments to patients in any environmental setting. For POC tests, portable, accurate, and reliable technologies are required. Various POC devices, such as those for measuring and detecting blood glucose, pregnancy, hemoglobin, HCT, and cholesterol, are currently on the market.

The advantages of microfluidic devices, which include allowing rapid and accurate analysis with small sample consumption, match well with the demands of POC devices. Thus, microfluidic devices are considered to be a key platform for the development of POC devices [13, 14]. Inexpensive and reliable microfluidics based POC devices could solve global health issues, especially for the developing world or regions lacking health care resources [14].

However, there are still technical challenges to develop a new microfluidic system for POC devices. Platinum is commonly used as electrode materials of many microfluidic devices due to their good electrochemical properties and high resistance to corrosion. But platinum electrodes in contact with aqueous solution generate electrolysis bubbles limiting voltage-operating window for many microfluidic devices [15, 16]. Biomolecule

adsorption onto electrode surfaces occurs to decrease high free energy at the interface between electrode and thus causes irreproducible signal responses [17-19]. Poor performance of miniaturized microelectrodes due to reduced surface area also have been reported often [20, 21].

1.2 Motivation for the Research and Outline of Dissertation

The present research aims to develop a new and robust microfluidic system for a POC HCT device. In chapter 2, the literature review focuses on research trends to solve problems of electrolysis bubbles, fouling electrodes by adsorbed biomolecules and poor microelectrode performance. Chapter 3 suggests the approach improving microfluidic system stability by controlling electrolysis bubbles. The electrolysis bubble effect was attenuated via surfactant additives and integrated semipermeable membranes. Chapter 4 reports that platinum microelectrode surface modification by carbonizing electrode surface using RBCs. The formed carbon layers on electrode surfaces increased effective electrode surface area and thus improved the electrode performance. Chapter 5 introduces that new and robust microfluidic system for HCT determination. The microfluidic system was drastically simplified by employing direct current. In order to prove the feasibility for HCT determination, current responses of RBC suspensions in phosphate buffered saline and plasma medium over the concentrations of human HCT ranges were measured in the microfluidic system. Chapter 6 summarizes the conclusion of the present work and discuss the future direction of the research.

Chapter 2 Technological challenges of microfluidic devices in bio-application: electrolysis, fouling interference, and microelectrode performance

2.1 Introduction

Microfluidic devices have employed various types of detection techniques, such as laser-induced fluorescence, mass spectrometry, absorbance detection, holographic refractive index, Raman detection, and electrochemical detection [22-29]. Among these techniques, the electrochemical detection has recently gained considerable attention because it is simple, fast, sensitive, inexpensive and easy for miniaturization into microfluidic devices [22, 23, 27-29]. The electrochemical detection for microfluidic devices is very promising and its general principles and trends were already reviewed by many authors [22, 23, 27, 29].

However, there are still many technical challenges to be solved in application of the electrochemical detection. The performance of microfluidic devices with electrochemical detection methods strongly depends on the performance and characteristics of the working electrode material. In general, platinum, gold, palladium, copper, and various types of carbon materials such as carbon ink, carbon paste, carbon fiber and graphene are commonly used as electrode materials due to favorable electrochemical properties. [22, 23, 27]

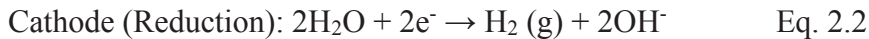
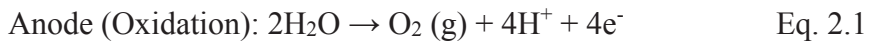
Compared to carbon materials, metals have very high resistance to corrosion and excellent electrocatalytic activity [22]. Among metal materials, platinum is known to be the most inert metal under electrochemical operation. However, recent evidence building upon foundational research has illustrated that platinum is not completely inert under electrochemical operation and it can potentially corrode and deactivate in the microdevice. Experiments have shown that platinum electrodes undergo chemical and morphological changes in biological buffer solutions under electrochemical operation [30]. These changes can potentially alter platinum electrode performance resulting in irreproducible responses within microfluidic system.

In addition, electrolysis gas bubbles [31, 32] and fouling electrodes by adsorbed biomolecules [33] have continuously been considered the factors limiting applications of microfluidic systems with electrochemical detection methods. Poor sensitivity and selectivity problem of miniaturized microelectrodes have been reported often [20, 21]. As microfluidic devices have been used in many applications, various approaches have been suggested to solve these problems.

The purpose of this literature review is to give an overview of research trends in order to solve problems of electrolysis, fouling, and microelectrode performance. The review describes the physical phenomena and effects of electrolysis, fouling, and microelectrode performance in microfluidic systems and summarizes the principle, advantages, and disadvantages of various reported solutions to solve these problems.

2.2 Electrolysis bubbles

Electrolysis bubbles are one of the main reasons electrodes become deactivated in microfluidic devices. In aqueous sample solution, platinum, gold and other metal electrodes electrocatalyze water and generate gas, which forms into bubbles at the electrode surface. For platinum electrodes, oxygen and hydrogen gas bubbles are produced above ~ 3 V [34, 35] and less than ~ 1 kHz AC at $3 V_{pp}$ as follows [36]:



Electrolysis bubbles destabilize and limit the voltage operating window for many microfluidic system in various ways. Gas bubbles covering electrode surfaces deactivate active surface sites and increase electrolyte solution resistance [37, 38]. Growth and detachment motion of bubbles at electrodes increases noise of electric signal responses [32, 38, 39]. Fig 2.1 shows the evolution of gas bubbles on electrode surfaces. Generated electrolysis bubbles remain attached on electrode surfaces due to surface tension. Bubbles coalesce into large bubbles on the surfaces and then detach from the electrode surfaces at a larger bubble diameters because gravity, buoyancy and hydrodynamic drag forces exceed the surface tension. [39, 40]. Detached bubbles enter the microchannel and destabilize the electric field across the microfluidic channel. Moreover, the bubble generation rate is not consistent at the similar operating conditions likely due to electrode surface variations [41].

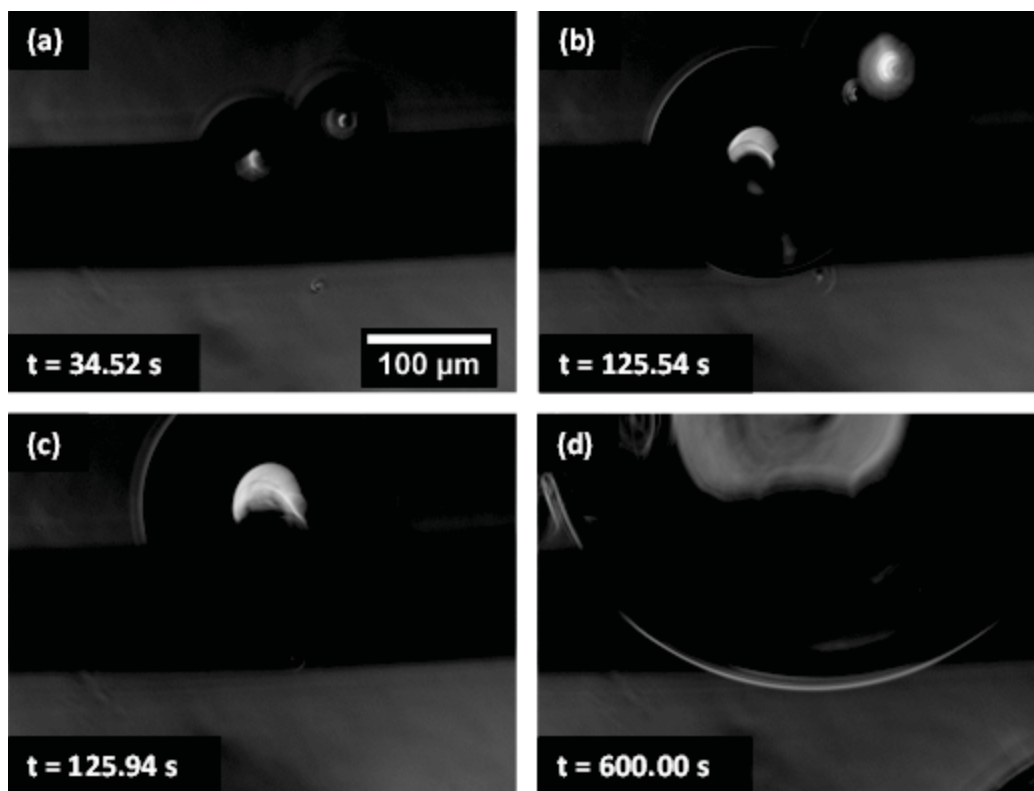


Fig 2.1 *Electrolysis gas bubble evolution at platinum electrode surface in phosphate buffered saline. Two bubbles generated at platinum surface grew in (a) and (b). Those bubbles coalesced into a large bubble in (c) and remain attached on electrode surfaces in (d). These bubbles evolution at electrode surfaces destabilize the electric field and cause irreproducible current responses. Reproduced with permission from [32], copyright 2014 WILEY-VCH Verlag GmbH & Co. KGaA, Weinheim.*

In addition, these gas bubbles and H^+ and OH^- ions can negatively impact and damage biological cells and alter properties such as the zeta potential and the dielectric constant [42-44]. For POC applications, these effects can alter the reliability of reproducibility of diagnostic or analytical tests. Thus, numerous approaches have been introduced to control electrolysis bubbles and stabilize the microfluidic system. Here, we discuss the most promising representative methods: 1) surfactant additives, 2) isolation of electrodes, and 3) bubble free systems.

2.2.1 Surfactant additives to control electrolysis bubbles

Controlling electrolysis bubbles using surfactant additives were suggested since the physics behind bubble stability and detachment is governed by surface tension [31, 32]. Surfactants are chemicals that impact interfacial or surface tension due to their propensity to transport to interfaces and remain there. Surfactant additives in buffer solution attenuate the effect of electrolysis bubble in various ways. First, the surfactant additives increases gas solubility in solution so decrease the volume of generated electrolysis bubbles [32, 45, 46]. In addition, the surfactant decreases the surface tension at electrode/solution interface and thus promote faster bubbles detachment from electrode surfaces at a smaller departure diameter [47, 48] thus creating less disturbance to the electric fields [31]. In bulk solution, surfactant maintain the smaller bubbles size by preventing bubbles from coalescing into larger bubbles [49].

In order to use surfactant additives for biosensing, the surfactant micellar effects on biomolecules should be verified. In order to obtain the significant stabilizing effect via surfactant additives, enough surfactants (above the critical micelle concentration: CMC) needs to be added [31]. However, as the surfactant concentration increases, surfactant molecule might have solubilize the cell membranes by forming mixed micelles with cell membrane lipids and proteins and could eventually have led to cell lysis [50-53]. Ionic surfactants could have contributed to the ionic strength of the buffer medium and would have changed conductivity [46]. These surfactant behaviors can affect and change electrochemical responses of the system.

2.2.2 Isolation of electrodes

The isolation of electrodes is an approach physically blocking bubbles from entering the microchannel and so electrolysis bubbles do not disturb the electric field across the microchannel. The electrode compartments are separated from the microchannel via side channel array [54-57], electrically conductive acrylamide membranes [57-59], or

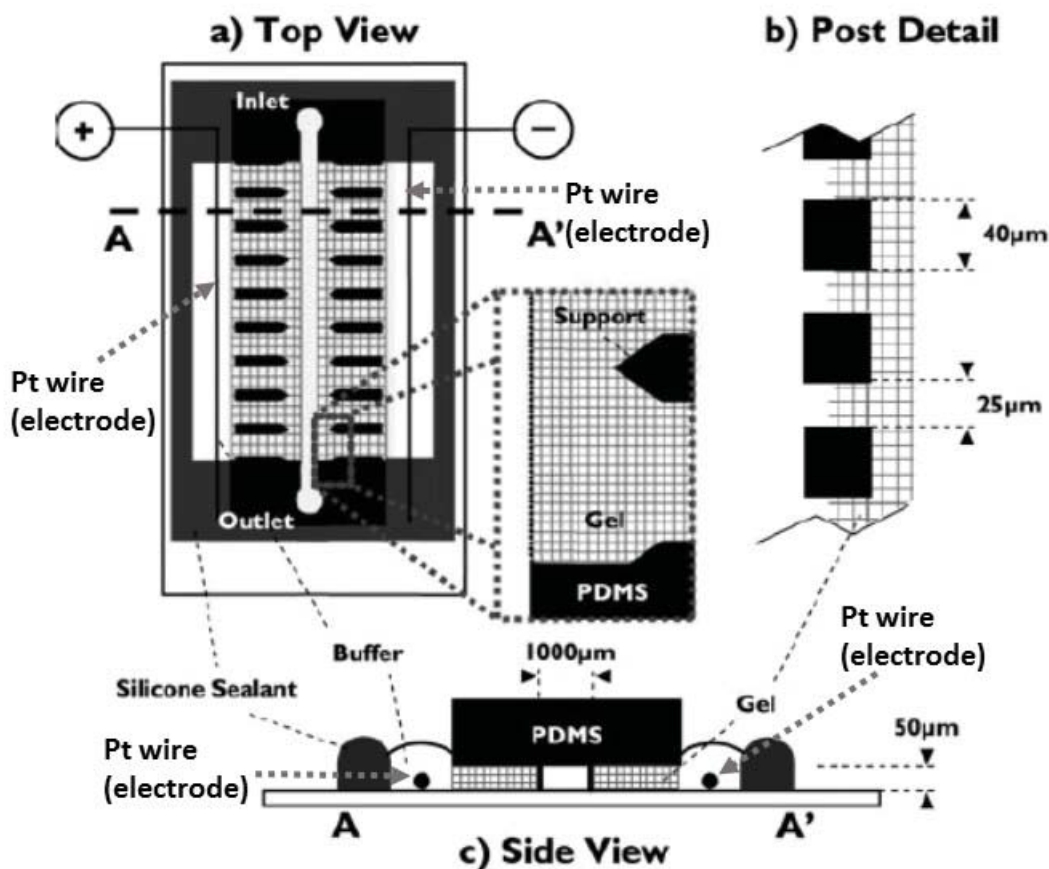


Fig 2.2 Schematic of μ -FFE microfluidic device integrated with acrylamide gel membranes. Acrylamide gel membranes (cross-hatched area) separated electrode reservoirs containing platinum wire electrodes from the sample channel. Ion conductive acrylamide membranes prevented electrolysis bubbles from entering the sample channel while allowed ion conduction. Reformatted and Reproduced with permission from [58], copyright 2014 WILEY-VCH Verlag GmbH & Co. KGaA, Weinheim.

semipermeable porous dialysis membrane [32]. Fig 2.2 shows a microfluidic device with integrated acrylamide membranes for micro free-flow electrophoresis (μ -FFE) to separate analytes depending on their electrophoretic mobilities.

These side channels and membranes, connecting electrode compartments to the microchannel, effectively hinder bubbles from entering the microchannel and permit electrical current to pass through. The side channels should be long and narrow enough to prevent bubbles, which increases the electrical resistance. The disadvantage of microfluidic devices integrated with side channels are poor voltage efficiencies (4 to 60 %) [57, 60]. Mechanical stability issues of acrylamide membranes were also reported [57].

Isolation of electrodes focuses on bubble disturbance in the microchannel. These approaches have widely been used in μ -FFE, separating charged analytes based on electrophoretic mobility differences [57]. In free-flow electrophoresis, disturbance of bubbles in the separation channel significantly changes separation results. These researches focused on preventing bubbles from entering the separation channel in order to obtain a stable flow stream and electric field in the separation channel.

As discussed previously, bubble motions at electrodes (evolution, growth, and detachment) generate significant noise to electrical responses even in open electrode compartments [32, 38]. Many microfluidic devices integrated with side channel arrays or acrylamide membranes have open electrode compartments for easy gas bubble ventilation or additional flow stream to remove bubbles at electrode surfaces [57]. However, the

effect of bubbles at electrodes is still significant even in open electrode compartments [48].

In order to overcome the problems of the poor voltage efficiency and bubbles at electrodes, a unique multiple-depth microfluidic device for μ -FFE was presented [57, 60]. This device was designed to address pressure-driven lubrication flow where, the linear flow velocity in a planar microchannel is proportional to the channel height squared.

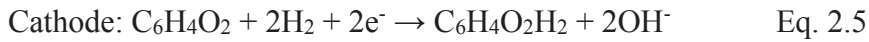
$$v = \Delta P H^2 / 12 \eta L \quad \text{Eq. 2.3}$$

where v is linear flow velocity, ΔP is pressure difference, H is channel height, η is fluid viscosity and L is the channel length. Based on this equation, the multiple-depth microfluidic device for μ -FFE was designed to have electrode channels (electrode compartments) four times deeper than the separation channel (the main microchannel). Thus, the flow rate in the electrode channels is 16 times higher than in the separation channel such that bubbles in the electrode channels were effectively flushed out. This device does not require the side channels or membranes, and has high voltage efficiency (91 %). However, its design and fabrication process is very complicated and the design, containing wide and shallow microchannel, limits the application into other fields. In general, isolating electrode methods have the voltage efficiency problems and limit of design. So its applications are very limited.

2.2.3 Bubble free system

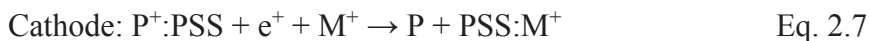
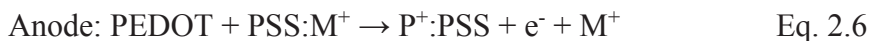
The electrode isolation methods reviewed in section 2.2.2 and surfactant additives reviewed in section 2.2.1 just mitigate the effect of electrolysis bubbles and do not completely remove the interference by electrolysis bubbles. Some approaches target achieving a bubble free system. This section reviews addition of redox couples and bubble free electrode.

In presence of a redox-couple (quinhydrone, a complex of hydroquinone and *p*-benzoquinone) in aqueous buffer, the electrical current was generated via the hydroquinone oxidization and *p*-benzoquinone reduction without gas bubble formation, instead of water oxidation and reduction [61].



However, current generation via the redox-couple has a maximum current limit. The generated maximum current in microfluidic FFE devices was between 30 and 40 μA due to the depletion of the redox-couple at electrode surfaces. In addition, pH gradients formed due to H^+ and OH^- generated by quinhydrone oxidation and reduction.

Bubble-free polymer compound electrodes, (poly(3,4-ethylenedioxythiophene) (PEDOT) blended with poly(styrenesulfonate) (PSS), were also presented. PEDOT:PSS electrodes react with ions from aqueous solution (M^+) without the formation of gas bubble, as given in below reactions [44].



In addition, it is also shown that the pH across the electric field remained more stable than platinum electrodes. However, in order to use the electrodes in biological cell analysis, biocompatibility should be proved.

2.3 Adsorption of biomolecules

Fouling electrode surfaces by adsorbed biomolecules is a very common and serious problem in bio-sensing and bio-microfluidic devices. In thermodynamics, an interface between two different phases has a higher free energy. In order to lower the free energy and stabilize the system, the interface is prone to adsorb any substance from the solvent molecules. Adsorption of biomolecules takes place to lower the free energy at the interface between electrode/sample solvent. [17, 62] The adsorption is often irreversible and causes significant interference in the analysis such as slow electron transfer rate, decreased sensitivity of electrodes, and irreproducible signal responses [63-66].

To overcome the adsorption interferences, many approaches have been suggested including ultrasonication [67], laser ablation [68], and microwave activation [69]. However, these methods are very complicated and require more complex instrumentations and thus not feasible to microfluidic devices. In this section, some approaches, pulsed electrochemical detection (PED) and surfactant additives, feasible to

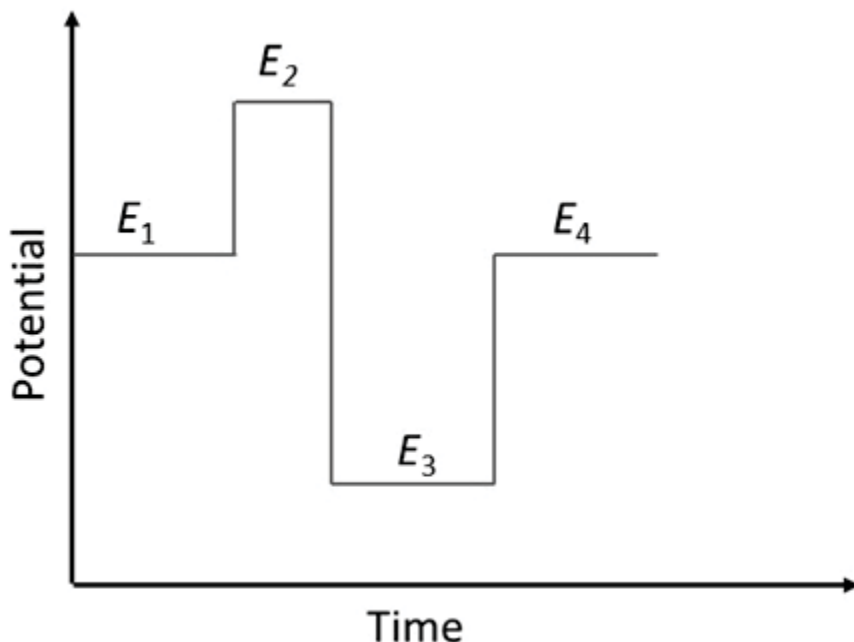


Fig 2.3 Principle of PED. PED involves multistep different potential pulse waveform; E_1 is detection pulse for the desired detection mechanism and fouling electrode surface take places during E_1 . Following E_1 , positive cleaning potential E_2 is applied to desorb adsorbed species causing surface oxide formation. The surface oxide is removed by negative potential E_3 and electrode activity is restored at E_4 .

microfluidic devices and choices of electrode materials to mitigate fouling effects are discussed.

2.3.1 Pulsed electrochemical detection

PED (also called pulsed amperometric detection; PAD) is a technique to remove adsorbed species off the electrode surfaces and to keep electrodes in clean state via application of a large positive cleaning potential [70]. It is widely used for carbohydrate detections with platinum and gold electrodes under amperometric conditions [46, 71, 72].

Table 2.1 *Examples of surfactants mitigating adsorption interferences*

Sample	Surfactant	Working electrode	Detection mode
DA in B-R buffer containing AA and UA [68]	SDS	PEDOT modified Pt electrode	LSV/CV
DA in PB [64]	SDS	RPG	CV
DOPAC in PB [64]	DTAB/TTAB/CTAB	RPG	CV
Horse heart myoglobin in PB [63]	Triton X-100	GC	CV
HRP X-100 in PB [63]	Triton X-100	GC	CV
Isoniazid in B-R buffer [67]	SDS/SOS	CP	CV
5-HT in PB [65]	CTAC/CPC/DTAC/DPC	GC	SWV
Cadmium/lead in acetate buffer/HNO ₃ containing albumin/lysozyme [61]	SDS	GC	ASV
Cadmium/lead/copper in fruit juice/wine/beer/ waste water [66]	SDS	GC	ASV

Fig 2.3 shows the principle of PED. A complete PED measurement involves the application of three different potential; a detection potential (E_1 and E_4), a more positive cleaning potential (E_2), and a cathodic reactivation potential (E_3). Following a detection process, adsorbed carbohydrates are oxidatively desorbed via application of the positive cleaning potential. However, desorption process causes the formation of surface oxides on electrode surfaces [34, 35, 73]. The formed surface oxides are quite inert. The cathodic reactivation potential is applied to remove the oxides and to restore the reactivity of the clean electrode surfaces. [71]

2.3.2 Surfactant additives to mitigate fouling

Surfactants have been proven to be effective in protecting electrodes from fouling in the voltammetric detection of bioorganic analytes, especially in detection of proteins [18, 74-85]. Surfactant additives, simply added to analyte sample solution, adsorb on electrode surfaces via electrostatic/hydrophobic interaction and forms micelle layers. The formed micelle layers modify electrode surface properties and mitigate the fouling effect and thus improve the reproducibility of electrical signals. In addition, surfactants are to alter or enhance reaction pathway and rates at electrodes [86, 87]. Representative examples of surfactant additives reducing fouling were listed in Table 2.1.

Desorption of the adsorbed molecule from electrode surfaces by surfactant additives were reported [79, 80]. In general, surfactant aggregates on electrode surfaces and inhibits the irreversible adsorption of biomolecules and impurities [82, 83]. The surfactant micelle layers intercalate biomolecules and impurities and form mixed micelles and thus the adsorption is prevented. The electron transfer rate can be enhanced if the surfactant micelles align with the intercalated molecules suitably. [81]

These effects of the micelles depend on the structures, dimensions, and polarities of the micelles on electrode surfaces and the positions of electroactive center within the micelles [82, 86, 87]. Thick micelle layers on electrode surfaces increase distance between analytes and electrode surfaces, resulting in decreased electrode sensitivity and responses. In case of ionic surfactant, electrostatic attractions force between micelles

concentrate analytes at electrodes and enhance electron transfer rate, while electrostatic repulsion forces slow down electron transfer rate. [82, 85]

As discussed in surfactant additives to control electrolysis bubbles, the biocompatibility of surfactants and the interaction of ionic surfactant with samples should be considered. These surfactants additive method are commonly used in voltammetric protein analysis. Surfactants can form mixed micelles with organic compounds in bulk solution, causing the changes of the analyte concentration. Denaturation and conformational changes of proteins by ionic surfactants were reported [81].

2.3.3 Alternative electrodes

Electrode surface fouling severely occurs on platinum and gold electrode surface. The fouling problem can be avoided by employing other materials as an electrode. For example, carbohydrate detection can be carried out without the PED process via use of copper [88, 89], cobalt [90, 91], or ruthenium [92] electrodes instead of platinum or gold.

Carbon based electrodes are widely used microfluidic devices. Compared to metal electrodes, carbon based electrodes have minimal fouling [93] as well as lower overpotential and wider electrochemical detection range for organic compound [23, 94]. Various types of carbon materials such as carbon fiber [93, 95, 96], carbon paste [27, 97], carbon ink [98, 99], and glassy carbon [100] have been used as electrodes of many microfluidic devices.

Carbohydrate detection under amperometric or voltammetric conditions involves oxidation of carbohydrates. Carbon electrodes do not allow carbohydrate oxidation at low potentials for practical use so the application of carbon electrodes in carbohydrate detection is limited. [101] However, carbons, especially carbon nanotubes, are widely integrated into chemically modified electrodes due to these properties, as discussed below.

2.4 Microelectrode performance

Microfluidic devices employ miniaturized microelectrodes. In order to obtain precise and accurate analytical result, sensitivity and reproducibility of microelectrodes are critical. However, poor microelectrode performances have been reported often. Miniaturization of electrodes inevitably decrease electrode surface area and lead to poor selectivity, sensitivity, and performance of electrodes [20, 21]. Electrical double layer impedance at electrodes is inversely proportional to electrode surface area. As the electrode surface decrease, the electrical double layer impedance increase and reduces signal current [21]. In addition, microelectrodes are more sensitive to fouling discussed in previous section, due to decreased surface area [102].

In order to solve these problems, many microfluidic devices have employed chemically modified electrodes. In this section, these chemically modified electrodes are discussed. In particular, carbon nanotube (CNT) modified electrodes are widely used due to the

unique properties of CNTs, containing high surface-to-volume ratio with good electrical conductivity. CNT modified electrodes are reviewed separately.

2.4.1 Chemically modified electrodes

Since microfluidic devices have been developed to detect many kind of analytes in various electrochemical detection modes, a variety of chemically modified electrodes have been investigated. These electrodes aims to decrease overpotential and fouling and to increase electrocatalytic activity. Well-tailored chemical modified electrodes have shown excellent electrode performances.

Permselective cation exchange polymer electrolyte Nafion membrane coated glassy carbon electrodes were investigated to reject fouling interferences by albumin in anodic stripping voltammetry of cadmium and lead [103]. Negatively charged Nafion membrane excluded anionic albumin and incorporated cationic cadmium and lead into Nafion membrane on electrode surfaces.

Palladium-coated screen-printed carbon electrodes were developed for detection of various hydrazine compounds [104]. Palladium coating facilitated the oxidation of hydrazine compounds at low operating potentials and minimized the overvoltage effect [105].

Composite electrode act as arrays of microelectrodes and show low background noise of current responses [94, 106]. Graphite-epoxy composite electrodes for detection of

Table 2.2 *Examples of CNT modified electrodes*

Type	Example	Analyte
Deposition	SWCNT deposited GC [87]	Galactose
“	SWCNT/MWCNT deposited GC [88]	NADH
“	MWCNT/Nafion deposited CF [89]	Nitric oxide radical
“	SWCNT/MWCNT deposited Au/Pt/GC [90]	DA/catechol
“	MWCNT/Co deposited tantalum [91]	Glucose
Paste	SWCNT-mineral oil [92]	DA/DOPAC/catechol/ guanine/NADH/H ₂ O ₂
“	MWCNT-mineral oil [93]	Guanine
“	MWCNT-Cu-mineral oil [94]	Carbohydrates/amino acids

dopamine and catechol showed improved performance compared to glassy carbon electrodes [107].

2.4.2 CNT modified electrodes

Distinctive properties of carbon nanotubes (CNTs) such as high surface-to-volume nanoscale structure, ability to accumulate analytes, excellent conductivity, minimization of surface fouling and high chemical stability are very attractive to modify surface properties of microelectrodes in microfluidic devices [102, 108-111].

CNT modified microelectrodes have a large effective surface area with high electrical conductivity. Well aligned porous structures of CNTs hold analytes at electrodes and thus enhance electron reactions. In addition, CNT modified electrodes have minimal fouling, same as other carbon electrodes. [112-114]

Extensive research have been performed to develop CNT microelectrodes for biosensor and already reviewed by many papers [102, 110, 111]. Several methods have been suggested to modify electrode with CNTs such as deposition of CNTs onto conventional electrode surfaces [112, 113, 115-117] and CNT paste forms [114, 118, 119] same as carbon paste electrodes. Some of representative examples are summarized in Table 2.2.

2.5 Conclusions

Electrolysis bubbles, fouling electrodes, and poor microelectrode performance are very common problems in designing a new microfluidic device. As discussed, in order to solve these problems, many approaches have been suggested. However, it is not easy to solve these problems. Platinum electrodes are still widely employed into many microfluidic devices, even if electrolysis bubble disturbance takes place and surface fouling by biomolecules severely occurs. This is because of their high corrosion resistance and good electrocatalytic activity compared to other electrodes. So, many researchers continue to investigate new high performance chemically modified electrodes in order to replace platinum electrodes themselves.

Theoretically, surfactant additives can be used not only to control electrolysis bubbles but also to prevent electrodes from fouling. In order to use surfactant additives, biocompatibility and interactions of surfactants with sample solution, electrodes, and the rest of microfluidic device parts (PDMS and glass slide) should be considered. This is not

easy. In addition, surfactants do not completely remove the interference of electrolysis and fouling but just mitigate their interference.

Integration of chemically modified electrodes seems to be reasonable. Developing electrodes with minimum fouling and high electrocatalytic activity can solve fouling and poor microelectrode performance at once. CNTs are very promising for chemically modified electrodes. However, CNTs are very expensive and thus CNT modified electrodes will significantly raise the cost of microfluidic devices.

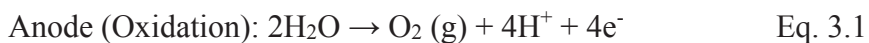
Based on current technologies, there is no right answer to design a new microfluidic device. To design a new microfluidic device is to solve a dilemma. For example, replacing platinum electrodes with carbon electrodes mitigate fouling interference and sacrifice the high corrosion resistance of platinum electrodes. It depends on researchers to decide what needs to be improved and what can be sacrificed.

Chapter 3 Improving electrokinetic microdevice stability by controlling electrolysis bubbles¹

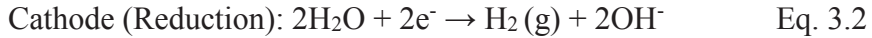
3.1 Introduction

Microdevices, also known as Lab-on-a-Chip (LOC) and μ TAS, are microfluidic platforms that integrate reactions, separations, mixing, detections and other laboratory functions into a single polymer or glass chip. Many utilize electric fields to move and analyze samples. Advantages include high resolution, low-cost, rapid analysis, low sample consumption in a range of nL to μ L, versatility in design and portability [9, 120, 121], and applications in biological assays, medical-diagnostics, and chemical detection.

Platinum has traditionally been regarded as an inert metal suitable for use as electrodes in electrokinetic LOC microdevices for particle and cell separations and interrogations [30]. However, electrolysis gas bubbles limit the voltage-operating window for many devices. Water electrolysis in contact with platinum electrodes generates gas bubbles above ~ 3 V DC [15] and less than ~ 1 kHz AC at 3 Vpp [16, 122]. For platinum electrode catalyzed oxidation and reductions reactions, oxygen and hydrogen bubbles are generated, as follows [123]:



¹ The material contained in this chapter was previously published in: ELECTROPHORESIS, 2014, 35 (12-13): p. 1782-1789.



These electrolysis gas bubbles can interfere with microdevice operation. First, any electrode surface area covered by bubbles is completely inactive [37, 38] and second, electrolyte solution resistance is increased in the presence of gas bubbles [37, 38, 124]. The growth and detachment of bubbles from electrode surfaces create microconvective flows, thus affecting heat and mass transfer rates [37, 39, 125]. After electrode detachment, bubbles can enter microfluidic channels, either completely blocking channel flow or disturbing the shape of electric field lines. In addition, the evolution and detachment of electrolysis bubbles is not consistent in different systems even at similar operating conditions [41]. In aggregate, these effects from electrolysis bubbles result in noise and irreproducible responses in many electrokinetic microfluidic systems.

Attempts to solve the electrolysis bubble problem have included numerous approaches: 1) electrode isolation from microchannels [54, 56, 59, 126-129]; 2) multiple depth channel designs [60, 130]; 3) bubble-free operation via redox couple compounds [44, 61]; and 4) modified buffer solutions [31].

In early microdevices, side channel arrays, connecting electrode compartments to the main microchannel, were employed to isolate electrodes. Side channel arrays physically hinder bubbles from entering the main microchannel, reducing disturbances in the main microchannel electric field [54, 56, 126, 127]. However, the major drawback was that long and narrow side channels were required to effectively block bubble flow, which increased electrical solution resistances resulting in poor voltage efficiencies between 4%

and 60% [60, 127]. Photopolymerized acrylamide gel membranes were used to isolate electrode compartments and behaving like an ion bridge allowing the electrical current to pass through [59, 127-129]. Acrylamide's low electrical resistance improved the voltage efficiency over side channel arrays [127], but low mechanical membrane stability was reported [59, 127, 128].

Multiple depth designs have also controlled electrolysis bubbles [60, 130]. Since linear flow velocity is proportional to planar microchannel heights squared, a microdevice was designed with electrode channels four times deeper than the main channel. The 16 times faster electrode channel flow effectively flushed out electrolytic bubbles without disturbing the electric field and achieving 91% voltage efficiency [60]. Shallow side banks can also isolate electrodes [130]. Multiple depth designs all require greater device footprints and flows, which are not compatible with ultrasmall sample analysis requirements.

Approaches to achieve bubble-free systems [44, 61] have included addition of redox couples, such as hydroquinone and *p*-benzoquinone, to aqueous buffers via oxidation and reduction reactions to generate electrical currents without electrolysis bubble formation [61]. Poly(3,4-ethylenedioxythiophene)(PEDOT) blended with poly(styrenesulfonate) electrodes have also created currents via PEDOT oxidation/reduction without generating electrolysis bubbles [44]. Bubble free system compatibility with biological cells and chemical analytes remains to be tested.

Another unique approach included surfactant additives in buffer solutions to reduce bubble surface tension [31]. Gravity, buoyancy, and hydrodynamic drag forces help detach electrolysis bubbles from electrode surfaces. In opposition, surface tension acts to hold bubbles on electrode surfaces. [37, 39, 40, 124] Surfactants decrease the surface tension in solution to promote faster bubble detachment at smaller departure diameter [48]. In addition, surfactant maintain smaller bubble sizes within microchannels by reducing bubble coalescence into larger bubbles [49]. Our work expands upon this effort by systematically exploring electrolysis bubble behaviors both at platinum electrode surfaces as well as in microchannels to determine if the explanatory surfactant theory in [31] facilitates smaller bubble formation causing fewer electric field disturbances during microdevice operation.

Physical isolation of electrode compartments via side channel arrays or acrylamide membranes showed poor voltage efficiency or mechanical stability problems, respectively. In addition, microdevice fabrication for these approaches is more complex. Instead, we introduced a microdevice with integrated semipermeable porous SnakeSkin[®] dialysis membrane sandwiched between PDMS layers sealed via plasma oxidation. We hypothesized that the SnakeSkin[®] membrane would physically block bubbles yet pores could allow electron transport with less electrical resistance than side channel arrays or acrylamide membranes. This would prevent disturbance to the electric field from electrolysis bubbles in the microchannel leading to stabilization of the microfluidic device system.

Thus, surfactant additives, SDS and Triton X-100, and integrating the semipermeable SnakeSkin[®] membrane were separately investigated to assess impact on electrolysis bubbles and current stability through the microdevice systems shown in Fig-1. Surfactant and SnakeSkin[®] membrane system stabilization efficacies were assessed via current measurements and video microscopy visualizations of electrolysis bubbles at electrode surfaces and in single microchannels.

3.2 Materials and Methods

3.2.1 Materials

Phosphate buffer stock solution (1.36 mM KH_2PO_4 , 8.59mM Na_2HPO_4) was mixed with e-pure water (Resistivity: 18.2 M Ω) then 0.5M HCl was titrated to prepare 1000 $\mu\text{S}/\text{cm}$ (0.405 mM KH_2PO_4 , 2.56 mM Na_2HPO_4 , 0.0114 mM HCl, pH 8) phosphate buffer solution (PBS).

Ionic surfactant sodium dodecyl sulfate (SDS, $\geq 99.0\%$, Sigma-Aldrich, CMC = 8 mM [131]) changes the solution conductivity, so a 1000 $\mu\text{S}/\text{cm}$ PBS and SDS (0.17 mM KH_2PO_4 , 1.07 mM Na_2HPO_4 , 0.05 mM HCl, pH 8) solution was prepared with phosphate buffer stock solution, 9 mM SDS, and e-pure water titrated with HCl to pH 8.

Nonionic surfactant Triton X-100 (T8532, Sigma-Aldrich) has a CMC of 240 μM and does not effect conductivity [31]. For PBS and Triton X-100 solutions, 320 μM Trion X-100 was added to 1000 $\mu\text{S}/\text{cm}$ PBS.

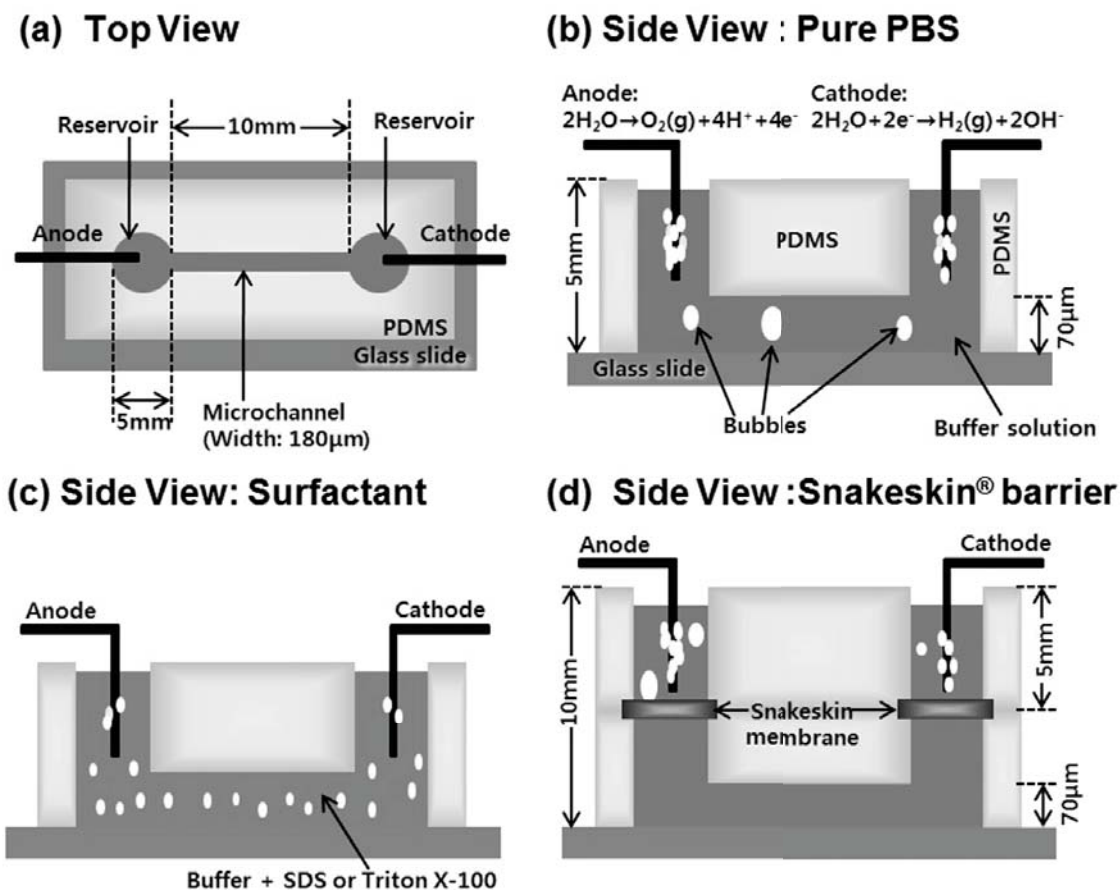


Fig 3.1 Microdevice configurations and postulated electrolysis bubble behaviors. (a) Top view showing 5 mm diameter reservoirs. Platinum electrode diameters were 0.1 mm. (b) Side view with dimensions. In the pure PBS, electrolysis bubbles remain attached to electrode surfaces and coalesce into larger bubbles before detaching. (c) Adsorbed surfactant at electrode surfaces reduces the surface tension at electrode/bubble/buffer solution interfaces, promoting faster bubble detachment with smaller departure diameters. Note (b) and (c) microdevice configurations were identical. (d) Integrated SnakeSkin[®] membranes in 3 mm diameter reservoirs block bubbles from entering

SnakeSkin[®] dialysis membranes (10,000 molecular weight cut off, MWCO, Thermo Scientific) and platinum wire electrodes (0.10 mm diameter, 99.99 %, Sigma-Aldrich) were used without any pretreatment.

3.2.2 Microdevice fabrication

Microdevice configurations are shown in Fig 3.1. Microchannel has dimensions of 180 μm by 70 μm by 10 mm long and was molded via traditional PDMS casting methods from a silicone wafer master [26, 132, 133]. PDMS prepolymer and curing agents at 10:1 ratio were cured at 60 °C for three hours. PDMS microchannel molds were peeled from the wafer, then reservoirs created with a 3 or 5 mm biopsy punch. PDMS and glass microscopy slides were pretreated via plasma oxidation (Harrick Plasma cleaner, Ithaca, NY, U.S.A.) at medium RF for 30 seconds then pressed together and kept in 60 °C oven for three hours to ensure sealing. For the microdevice with integrated SnakeSkin[®] membranes, after sealing the lower PDMS layer on the microscope slide, SnakeSkin[®] membranes were aligned over both reservoirs then the upper PDMS layer was sealed over the lower PDMS layer via plasma oxidation. Note that microdevice configurations were similar as shown in Fig-1(a), (b), (c), and (d), except the integrated SnakeSkin[®] microdevices had 3 mm reservoirs to increase contact area and binding between PDMS layers.

Platinum wire electrodes for anode and cathode were attached on the PDMS surface by general-purpose epoxy (Henkel Corporation, Rocky Hill, CT). Port connectors (LabSmith, Livermore, CA, U.S.A.) were epoxied over anode reservoirs for sample injection.

3.2.3 Current response measurements

Solutions were introduced into the microdevice via a BD Safety-Lok™ 3 ml syringe (BD, Franklin Lakes, NJ, U.S.A.), then 100V DC was applied between anode and cathode positioned across the microchannels for one 10-minute cycle. Current responses were measured with a HVS 448 high voltage sequencer (LabSmith) and saved at 39 points per second. The sequencer was turned off at 10 min and the microchannel flushed with e-pure water. Fresh solution was introduced into the microchannel for the next cycle. For each solution, the experiment was repeated for 23 cycles.

3.2.4 Video Microscopy

Oxygen bubbles at the anode surfaces and in the microchannels were visualized in 100 V for 10 minutes using aDP72 digital camera (OLYMPUS, Center Valley, PA, U.S.A.) attached to an IX-51 inverted microscope (OLYMPUS) equipped with the LUCPlanFLN 20x objective. To image bubbles at the platinum electrode surfaces, the electrodes were bent in L shapes and positioned at reservoir bottoms. This configuration differs from the current response measurement, but it was necessary to visualize bubbles. Electrode surface bubbles in the integrated SnakeSkin® microdevice could not be visualized due to optical interference of the SnakeSkin®. Software cellSens (OLYMPUS) was used for video image recording and analysis.

For each system, electrode surfaces and microchannels were each monitored for five 10-minute cycles. For large bubbles in pure PBS, the whole electrode surface area of $405 \times 314 \mu\text{m}^2$ was monitored and bubble volume was calculated assuming bubbles were

truncated spheres. Small bubble detachment from electrodes was challenging to quantify due to microconvective flows. Thus, small bubbles were observed from smaller electrode surface areas of $153 \times 314 \mu\text{m}^2$.

3.3 Results and Discussion

3.3.1 Current responses

Fig 3.2 (a) and 50-sec inset show current responses of $1000 \mu\text{S/cm}$ PBS at 100V DC applied over 23 10-min cycles. Current responses fluctuated erratically and were not reproducible. From 0 to 9000 seconds, current responses decreased in each 600-second cycle. The inset illustrates current responses were not stable even for 50 seconds. These fluctuations are ascribed to electrolysis bubbles, which block electrode surfaces, increase electrolyte solution resistance, and induce secondary hydrodynamic flow patterns in microchannels and chambers [37, 39, 125]. The large current drops shown in some measurements, such as 3000 - 3600 and 4200 - 4800 seconds, are attributed to larger bubbles covering substantial electrode surface area [134], as discussed later. Fig 3.2 (a) illustrates currents varied wildly within and from cycle to cycle; these overall irreproducible responses can be explained by non-uniform bubble generation and behavior even in the same operating conditions [41].

Attempts to stabilize current responses via SDS and Triton X-100 surfactants at their CMC of 8 mM and $240 \mu\text{M}$ are shown in Fig 3.2 (b) and (c), respectively. Insets illustrate that the relatively small amplitude fluctuations $\sim < 1 \mu\text{A}$ are 6 to 8 times smaller than PBS

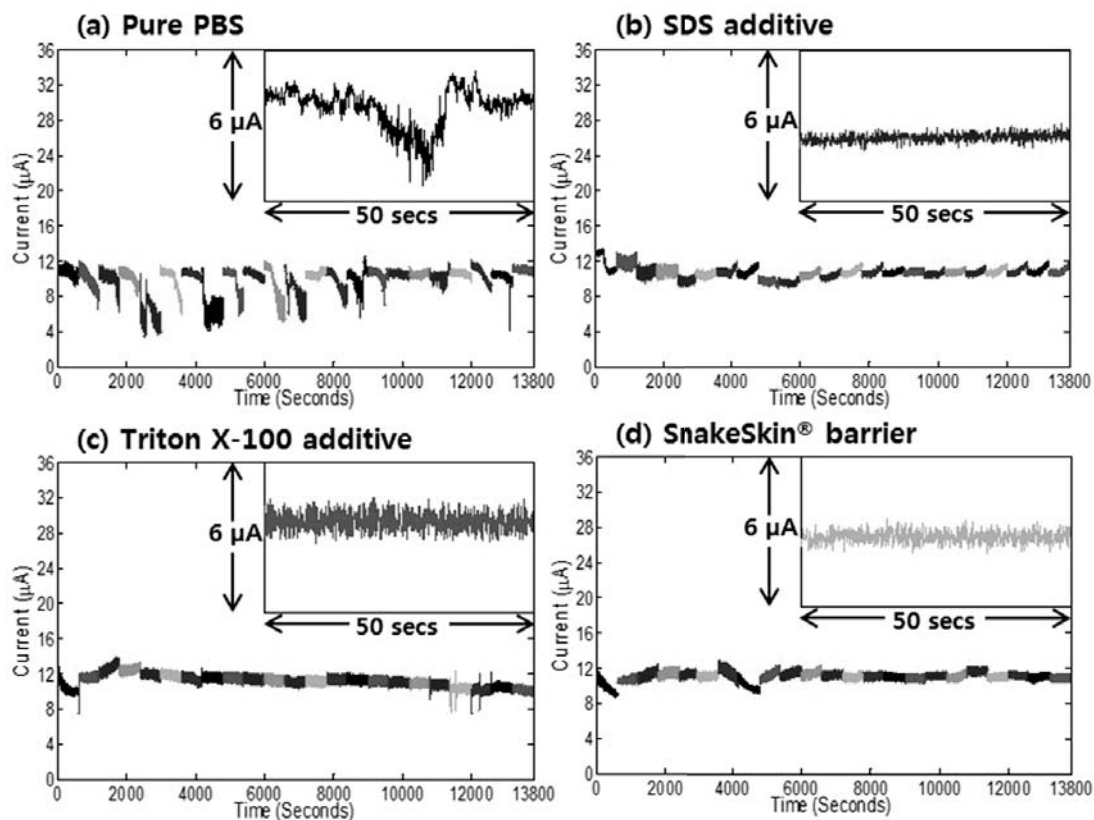


Fig 3.2 Current responses from fixed 100V applied potentials in 1000 $\mu\text{S}/\text{cm}$, pH 8 (a) pure PBS, (b) SDS surfactant, (c) Triton X-100 surfactant, and (d) Snakeskin[®] barrier. Each color represents one 600 sec cycle, begun with new solutions. Insets are representative current response fluctuations for 50 seconds.

current fluctuations in Fig-1 (a). We refer to this as current stabilization. The absence of large huge current drops in SDS and Triton X-100 suggest that larger bubbles were not generated and thus did not disturb the electric field, as cartooned in Fig 3.1 (a), (b), and (c).

However, current responses in SDS slightly increased at the end of each measurement cycle as shown in Fig 3.2 (b). This time dependent behavior may be due to SDS promoting faster bubble detachment. Detached bubbles have been shown to enhance heat transfer and mass transfer of reactants to and products from electrodes by inducing local

turbulent flows at the electrode boundary [125]. It is presumed that faster bubble detachment promoted by SDS enhanced mass transfer in the electrode boundary layer, thus increasing current responses [39].

Current responses in the presence of Triton X-100 are shown in Fig 3.1 (c). Unlike SDS, current responses slightly decreased in each measurement cycle and the cycles trended downward over time. The first 4 cycles deviated from this overall trend, including a steep decrease and small increase from 0 to 180 seconds and increases from 11400 to 13200 seconds. These may be due to mass transport differences of the Triton X-100 to the electrode surface. If Triton X-100 molecules were not uniformly available at the electrode surface, this could account for non-uniform bubble generation and current declines similar to that seen in pure PBS. The first four cycles in SDS also did not follow later equilibrium trends, thus supporting the mass transfer limitation theory. In Triton X-100, representative fluctuations for 50 seconds in the inset remained relatively constant with amplitudes approximately twice those observed in SDS.

In bulk solution, surfactants decrease bubble sizes by reducing surface tension between the gas and the liquid. Thus in our microscale system, the mechanism of SDS and Triton X-100 stabilization of current responses is attributed to lower gas/liquid surface tension that reduces the occurrence of large, field disruptive bubbles. However, the stabilized current response trends are different and can be explained by individual surfactant properties. Since ionic surfactant SDS contributes to the conductivity, the final 1000 $\mu\text{S}/\text{cm}$ solution contained 9 mM SDS and lower phosphate concentrations (0.17 mM

KH₂PO₄, 1.07 mM Na₂HPO₄) than 0.405 mM KH₂PO₄ and 2.56 mM Na₂HPO₄ in the 1000 μ S/cm solution nonionic Triton X-100 solution. In addition, ionic SDS interacts with aqueous buffer solutions by forming micelles and exchanging Na⁺ counter ions with free solution ions [135]. Moreover, the efficiency of lowering surface tension of surfactant depends on the structure and length of the hydrophobic group, the size of the hydrophilic group, and the counter ion of the ionic surfactant [136-138]. These differences could have resulted in different current response trends.

The current responses stabilized by the integrated SnakeSkin[®] membrane are shown in Fig 3.2 (d). Although current decreases were observed, large current drops as illustrated in Fig 3.2 (a) did not occur. This implies that large bubble formation and movement in the microdevice was prevented by the SnakeSkin[®]. The SnakeSkin[®] electrode chamber size was smaller (3 mm instead of 5 mm) due to the increased depth to accommodate the membrane. However, the electrode surface area exposed to the solution remained constant. This greater volume may have decreased solution resistance and current stabilization may be due to the SnakeSkin[®] barrier preventing bubbles from entering the microchannel.

3.3.2 Bubble behaviors at electrode surfaces

To analyze electrolysis bubble behaviors in PBS, SDS, and Triton X-100, oxygen bubbles at the anode surfaces and traveling from the anode to the cathode in the microchannels were visualized under the same conditions as current response

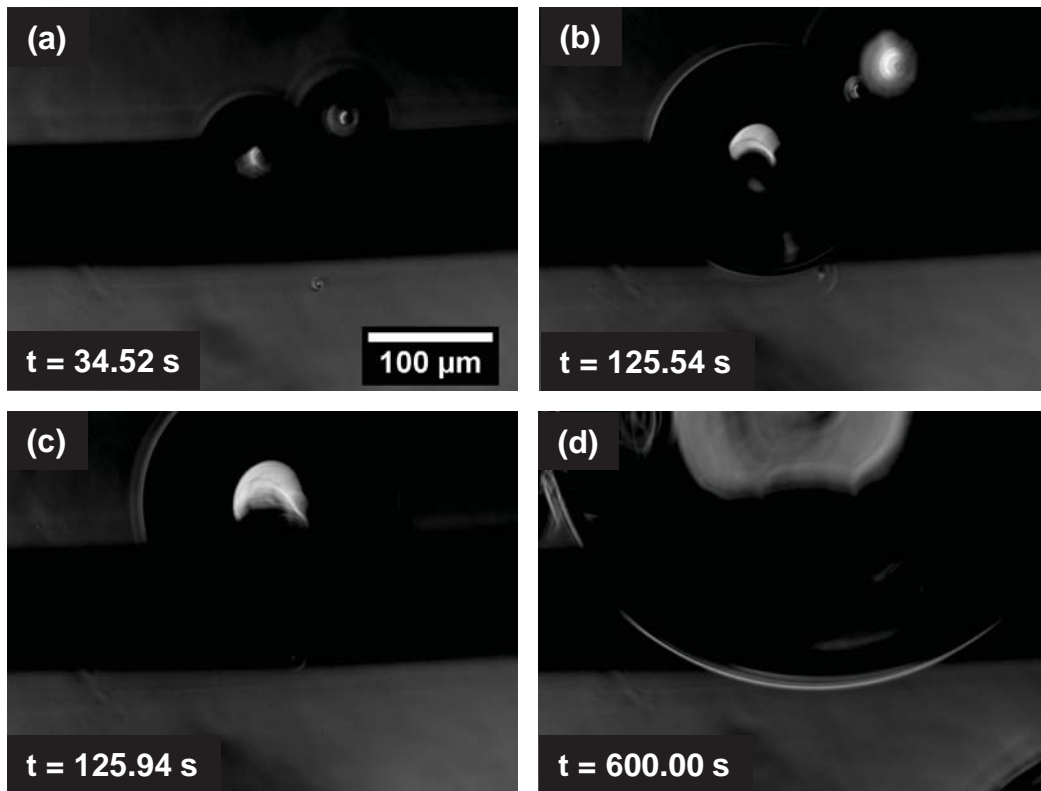


Fig 3.3 Video microscopy images for large bubble evolution from electrode surfaces in the pure PBS system. From 35 seconds (a) to 125 seconds (b), two large electrolysis bubbles grew at the electrode surface. (c) At 126 seconds, the two bubbles coalesced into a larger bubble that vibrated from coalescence momentum. (d) The new bubble continued to grow while remaining attached to the electrode.

measurements. Two distinctively different bubble sizes, large and small, were observed at the electrode surface in pure PBS. The formation and evolution of large and small bubbles at the electrode surface are shown for PBS in Fig 3.3 and PBS, SDS and Triton X-100 in Fig 3.4, respectively.

Once electrolysis bubbles are generated, they remain attached on the electrode and grow. Bubbles coalesce into larger bubbles and vibrate on the electrode surface. Further, bubbles leave electrodes with certain departure diameters when the detaching force, the

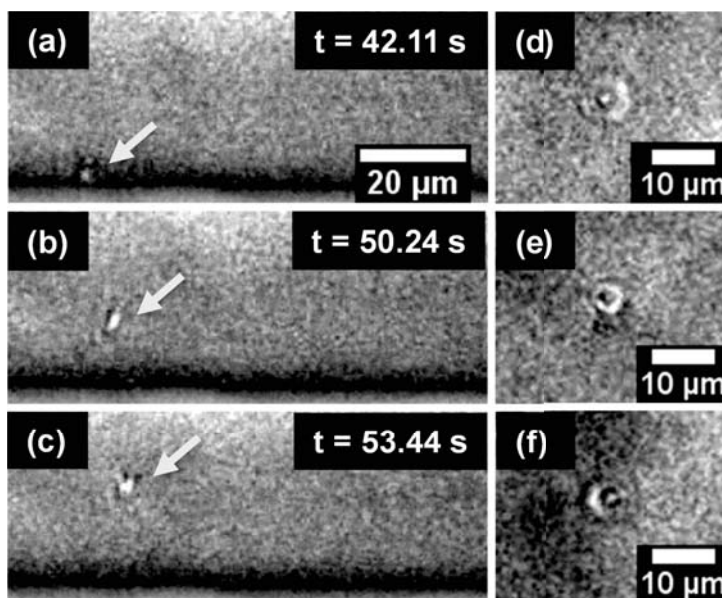


Fig 3.4 Video microscopy images of small bubble detachment from electrode surfaces in pure PBS, SDS, and Triton X-100. (a) Small electrolysis bubbles at the electrode surface marked by arrow. With time, bubbles detach in (b) and migrate away in (c). Relative bubble size comparison in the same focal plane for (d) pure PBS, (e) SDS, and (f) Triton X-100. *Image contrast was adjusted via ImageJ to improve bubble resolvability.

gravity, buoyancy and hydrodynamic drag, are larger than the holding force, the surface tension [40].

As large bubbles grew at the electrode in Fig 3.3 (a) and (b), they shielded more electrode surface area likely correlating to increasing current drops as were illustrated in Fig 3.1 (a). Coalescence of two neighboring bubbles in Fig 3.3 (c) would decrease the electrode surface screened and result in a sudden increase in current [134], but not back to the bubble free value. After coalescence, the bubble kept growing, again decreasing the current. Fig 3.4 shows a subset of the electrode and many more bubbles were observed in the macroscale view, Fig 3.3. All bubbles on the electrode surface would influence

current responses in Fig-1. As microbubbles merge into large bubbles, the resulting vibrations could cause the minor fluctuations in Fig 3.1 current response.

Bubble size and number at the electrode surfaces in pure PBS solutions were tabulated from five 10-min experiments. On average, two or three large bubbles and one or two small bubbles were observed in each experiment. Fig 3.5 (a) shows the total large bubble volume, calculated from truncated spheres, for each of the 5 experiments. Large bubbles remained attached and grew in three experiments, while large bubble detachment was observed twice.

Small bubble detachments were also observed in pure PBS solutions as shown in Fig 3.4 (a), (b), and (c). Detachment of small bubbles can be attributed to enhanced natural convection from temperature gradients induced by Joule heating and bubble movement [37, 139]. Significant electrolyte motion, buoyancy, and increase hydrodynamic drag force lift bubbles off the electrode surface [39].

In SDS and Triton X-100 surfactant solutions, only small bubbles were observed. Bubble counts over 600 seconds in pure PBS, SDS, and Triton X-100 solutions were plotted in Fig 3.5 (b). Average bubble diameter and total bubble volume were tabulated in Fig 3.5 (c) and Fig 3.5 (d) for each solution condition. Small bubble sizes were compared for pure PBS, SDS, and Triton X-100 in Fig 3.4 (d), (e), and (f). Under bright field magnification, bubbles look different depending upon the focal depth due to optical aberrations. Thus, we compared bubbles at the same focal depth as shown in Fig 3.4 (d), (e), and (f) to tabulate outer diameters of the donut-projection of bubbles as reported in

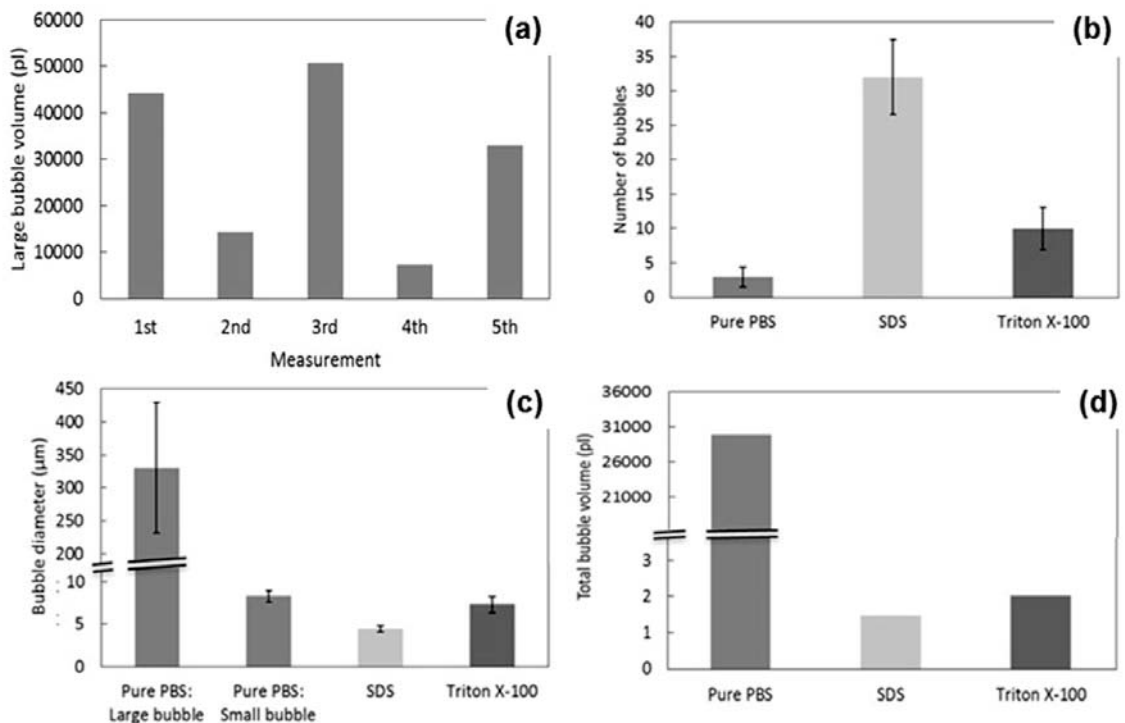


Fig 3.5 Bubble characteristics at electrode surfaces for pure PBS, SDS, and Triton X-100. (a) Total large bubble volumes generated in pure PBS for five 10 minute cycles observed from $405 \times 314 \mu\text{m}^2$ electrode surface area. (b) Total number of bubbles detached from electrode surfaces for five 10 minute cycles from $153 \times 314 \mu\text{m}^2$ electrode surface area, (c) Average bubble diameter. and (d) Total volume of bubbles detached from electrode surfaces were calculated from bubble diameters in (c) for each system. Error bars represent standard deviations ($N > 5$).

Fig 3.5 (c) for $n > 5$ bubbles. SDS produced far more bubbles from the electrode surface than either pure PBS or Triton X-100. However, once bubble size is factored in, total gas volumes within solutions are greatest with PBS and least with SDS. Small bubbles in SDS and Triton X100 were statistically smaller than the small bubbles in pure PBS. This supports the assertion that SDS and Triton X-100 prevented bubble growth at the electrode surface and promoted faster bubble detachment by lowering surface tension. Since no large bubbles were generated in the presence of both SDS and Triton X-100, that suggests both surfactants significantly decreased electrolysis gases suspending in

solution and thus stabilized current measurements. It has been reported that, for elementary and inert gases such as the hydrogen and oxygen in electrolysis bubbles, surface tension decreases and gas solubility increases via the following equation [45].

$$\ln \gamma = \frac{-4\pi r^2 \sigma + E}{kT} \quad \text{Eq. 3.3}$$

Where γ is the Ostwald coefficient of gas solubility, r is gas molecule radius, σ is surface tension, E is interaction energy between gas molecules and the solvent, k is the Boltzmann's constant, and T is temperature. The left term is the natural log of gas solubility, so small decreases in surface tension cause large increases in gas solubility. Thus, in the presence of surfactants, fewer and smaller bubbles form and promote faster bubble detachment, which prevents electrode surface shielding and can account for the stabilized current responses observed in Fig 3.2.

3.3.3 Bubbles in microchannels

Similar bubble analyses were conducted within the 180 μm by 70 μm microchannels for all solution conditions. Large bubbles from the electrode in the pure PBS system did not appear in the microchannel likely due to buoyancy effects. Figure 3.6 (a) illustrates a representative small bubble streak in the electroosmotically flowing channel. Fig 3.6 (b) shows microchannel bubbles counted in the pure PBS, SDS, and Triton X-100 systems over five 10-minute experiments. Total bubble volumes in the microchannel in Fig 3.6 (c)

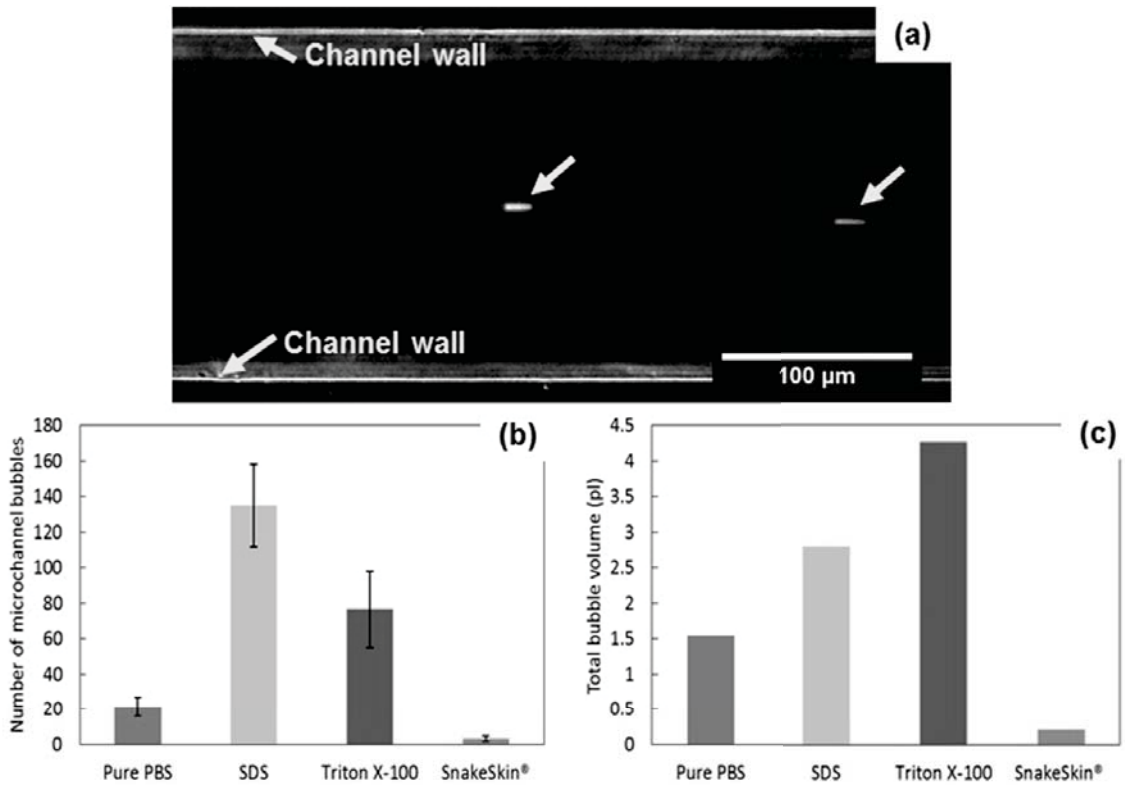


Fig 3.6 Bubbles observed in the microchannels; (a) Representative image showing two bubbles in the microchannel in SDS ($t = 127.54$ seconds). (b) Number of bubbles observed in the microchannels for five 10-minute experiments, and (c) Total volume of bubbles observed, calculated from bubble diameters in Fig-5 (c). Error bars represent standard deviations ($N > 5$). *Image was adjusted via ImageJ to improve contrast.

were calculated assuming Fig 3.5 (c) bubble diameters for each solution system, respectively.

The SDS microchannel contained more bubbles than Triton X-100 and considerably more bubbles than pure PBS or the SnakeSkin[®] microdevice configuration. However, current responses were more stabilize for SDS and Triton X-100, which suggests that microchannel bubbles do not substantially account for electric field disturbances, likely due to the disparate bubble sizes. The large bubbles, such as those demonstrated in Fig 3.3, likely caused the substantial effects on the current responses across the microdevice.

Compared to the microchannel dimensions, small bubbles in the surfactant solutions were two orders of magnitude smaller. Despite greater numbers of small bubbles in the surfactant solutions, large bubble effects at the electrode surface dominate current stability.

As expected, SnakeSkin[®] blocked bubbles from entering the microchannels so fewer bubbles were observed than in the pure PBS system. Data shown in Fig 3.2 (d) illustrated that SnakeSkin[®] successfully stabilized currents, but based on the SDS and Triton X-100 microchannel bubble data, microchannel bubbles do not cause substantial disturbances in the electric field. Disturbances to the electric field by small bubbles are not as significant as the effect of large bubbles, so it is difficult to conclude that the current stabilization is only due to the reduction in microchannel bubbles. The integrated SnakeSkin[®] membrane microdevice reservoir diameter was 3 mm (reservoir volume of 35.33 mm³) which is 36% smaller than the 5 mm (98.13 mm³) microdevices. As previously discussed, enhanced natural convection from Joule heating can facilitate premature bubble detachment; The smaller SnakeSkin[®] reservoir, with steeper temperature gradients could have experienced more vigorously natural convection promoting bubble detachment from electrodes. This is consistent with the current response results in Fig 3.2 (d), which did not show current drops like pure PBS in Fig 3.2 (a). Thus, for the SnakeSkin[®] microdevice, enhancing natural convection in the smaller reservoir could be the more substantial reason for the current stabilization than blocking bubbles from entering the microchannel.

3.4 Concluding Remarks

SDS and Triton X-100 surfactants and the integrated SnakeSkin[®] membrane all stabilized the microdevice system by controlling electrolysis bubbles via different mechanisms. The surfactants promoted more, yet smaller bubbles and faster detachment from electrode surfaces. SnakeSkin[®] excluded bubbles from entering the microchannel, and more importantly increased convective fluid movement enhancing bubble detachment from electrodes.

Decreasing bubble sizes via surfactants has been widely used in macroscale systems; this work shows the physical mechanisms is directly applicable to stabilizing electric fields in microfluidic microdevices. Published research has not previously linked bubble size with electrokinetic microdevice current stability. Surfactants increase gas solubility and thus significantly decrease gas bubble volume, which is directly linked to electric field stabilities within these microfluidic devices.

Research to date has primarily focused on controlling electrolysis bubbles in the main microchannel components of LOC systems, although our data illustrates that behaviors at the electrode surface have substantially greater impacts on current stability. Thus, previously reported research to block bubbles from entering microchannels may be less effective than electrode functionalization approaches. Macroscale systems have reported on gas bubble evolution from electrodes due to bubble motion and natural convection

phenomena. These effects should be more carefully considered in future electrokinetic microdevice development.

Due to the corrosion resistance of platinum, these electrodes will continue to be used in electrokinetic microdevices. Thus, the generation of electrolysis bubbles in DC fields above 3 V and AC fields below ~ 1 kHz are inevitable. The use of surfactants like SDS and Triton X-100 can serve to stabilize electric fields in electrokinetic microdevices.

3.5 Acknowledgements

The authors gratefully acknowledge guidance from Dr. David O. Wipf years ago on solution resistance measurements and from Dr. Aytug Gencoglu for microfabrication.

Chapter 4 Platinum electrode modification by carbonizing surface to improve performance and sensitivity ²

4.1 Introduction

Microfluidic devices are miniaturized systems integrating several conventional laboratory functions - such as sample preparation, separation, and detection - onto a single polymer or glass chip. Because of their numerous advantages including high-resolution, low cost, versatility in design, portability, and rapid analysis with small sample consumption, they are considered to be a key, game-changing platform for many applications such as point-of-care diagnostics, single cell or molecule analysis and manipulation, biosensors, pharmaceutical tests, and many other analysis applications [9, 12, 140, 141].

Many microfluidic devices employ electrochemical detection methods using microelectrodes, with the desire to achieve high sensitivity detection of low concentration analytes. However, miniaturizing electrodes inevitably reduces electrode sensitivity and decreases the signal to noise (S/N) ratio [20]. Electrical double layer impedance is inversely proportion to electrode surface area. As the electrode surface area decreases, the double layer impedance increases and so the signal current and electrode sensitivity decreases [21]. The decreased electrode sensitivity limits applications of microfluidic devices, especially those requiring larger current signals. Thus, there is a demand for

² The material contained in this chapter has been submitted to:
ELECTROPHORESIS.

microelectrode surface modifications to increase surface area, increase sensitivity, and improve performance.

Microfluidic devices developed for biological applications such as biosensors and point-of-care medical diagnostics can experience fouling of electrode surfaces via adsorbed biomolecules. The interface between the electrode surface and biomolecule solution has a higher free energy than the bulk solution. Biomolecules from solution readily adsorb on the electrode surface to lower the free energy at the interface and stabilize the system [33]. Those adsorbed biomolecules foul electrode surface by covering active surface sites to cause significant interferences to electrical responses and decrease the electrode sensitivity and reproducibility [17-19, 142]. Due to relative length scales of electrode surface area to biomolecule size, adsorption interferences are more substantial on microelectrodes.

Electrode materials including metals such as platinum, gold, copper, palladium and carbon based materials such as carbon ink, carbon paste, carbon fiber, and glassy carbon are utilized for a variety of microfluidic device applications [23, 27]. Platinum and gold are chemically inert, biocompatible, and demonstrate favorable electrocatalytic activity and thus are widely used for biological applications. However, platinum and gold are expensive and readily foul with biomolecules from liquid solutions [101]. Comparatively, carbon based electrodes exhibit minimal fouling [93], lower overpotentials, and larger electrochemical potential ranges [23, 27, 94].

Chemically modified electrodes have been investigated to improve electrode performance within microfluidic devices. The electrode surfaces have been tailored to minimize overpotential and fouling, and to increase surface area and electrocatalytic activity. For example, graphite-epoxy composite electrodes for dopamine and catechol detection [107] and palladium-coated screen-printed carbon electrodes for hydrazine separation and detection [104] were investigated. In particular, carbon nanotubes have proven ideal for electrode modification due to their high surface-to-volume nanoscale structure, excellent electrocatalytic activity, high chemical stability, and minimal fouling [102, 117]. Carbon nanotube/copper composite electrodes have been embedded into microfluidic devices for carbohydrate detection [114] and gold deposited carbon nanotube array electrodes were embedded for impedance measurement of prostate cancer cells [143]. Both showed enhanced sensitivity and performance. Carbon nanotube films cast on platinum, gold, and glassy carbon electrodes [117] improved electrode performance and resolution as electrochemical detectors.

Carbon based materials have been investigated as electrode materials in microfluidic devices and other fields due to their high electrocatalytic activity, good corrosion resistance, controllable pore structure, process-ability, and low cost [144-146]. Their applications extend from microfluidic devices to biosensors [116, 118, 119, 147], supercapacitors [144, 145, 148, 149], and batteries [150, 151]. The key goal is to maximize the effective electrode/electrolyte interface area by exploiting carbon structures. It is a consensus in the field that increasing surface area concurrent with well-

optimized three-dimensional (3D) porous structures (size, structure, and distribution of pores) is very critical for the electrode performance [144, 148, 151, 152]. These results are applicable to microfluidic systems to improve the microelectrode performance.

In the present work, we report improvement of platinum electrode performance and sensitivity after what originally presented as red blood cell fouling of the electrode, but progressed into carbonization of the electrode surface. The larger goal of this work was to measure DC electrical resistances of red blood cell (RBC) suspensions in a microchannel for hematocrit determination. As a consequence of this exploration, this paper details irreversible RBC adsorption onto the electrode surfaces, which positively affects the reproducibility of current signals across the microchannel. Initial current responses were irreproducible displaying different current measurements between runs and erratic changes in current within a single run. It was observed that when current responses were repeatedly measured, the platinum electrode performance improved with time.

Systematic experimentation revealed that RBCs adsorb and carbonize the electrode surfaces, thus increasing surface area with a porous 3 dimensional structure that improves performance and stabilizes currents. Platinum electrode surfaces before and after performance improvement were analyzed by field emission scanning electron microscopy (FE-SEM) and energy dispersive spectrometry (EDS).

In addition, platinum electrodes with graphene and active carbon coatings are also presented. Modifying platinum electrode surface using human RBCs was tedious process and coated RBC layers showed mechanical stability problem, as it will be discussed later.

In order to simplify the process and to improve the mechanical stability, platinum electrode surfaces were coated using graphene and active carbons via electrophoretic deposition process (EPD) [148]. These electrode performance for RBC solution current measurements were also tested and surface was characterized by FE-SEM and EDS analysis.

4.2 Materials and methods

4.2.1 Microfluidic device

Fig 4.1 presents a schematic of the microfluidic device used for the current response measurements of RBC solutions. Dimensions of the microchannel were 180 μm by 70 μm by 10 mm long. Brand new platinum wires (0.10 mm diameter, 99.99 %, Sigma-Aldrich) were used as anode and cathode electrodes without any pretreatment. Platinum wires were cut via scalpel and bent by tweezers to immerse 2 mm into each reservoir. General-purpose epoxy (Henkel Corporation, Rocky Hill, CT, U.S.A.) was used to attach platinum wire electrodes on the PDMS surface. Photolithographic fabrication of the PDMS microfluidic layer was the same as previously described [32].

4.2.2 Sample preparation

Blood samples taken from voluntary donors via venipuncture were kept in vacutainers (*Becton, Dickinson and Company*, Franklin Lakes, NJ, U.S.A.) containing 1.8 mg K_2 EDTA (di-potassium ethylenediaminetetraacetic acid) per ml of blood at 4 °C. RBCs

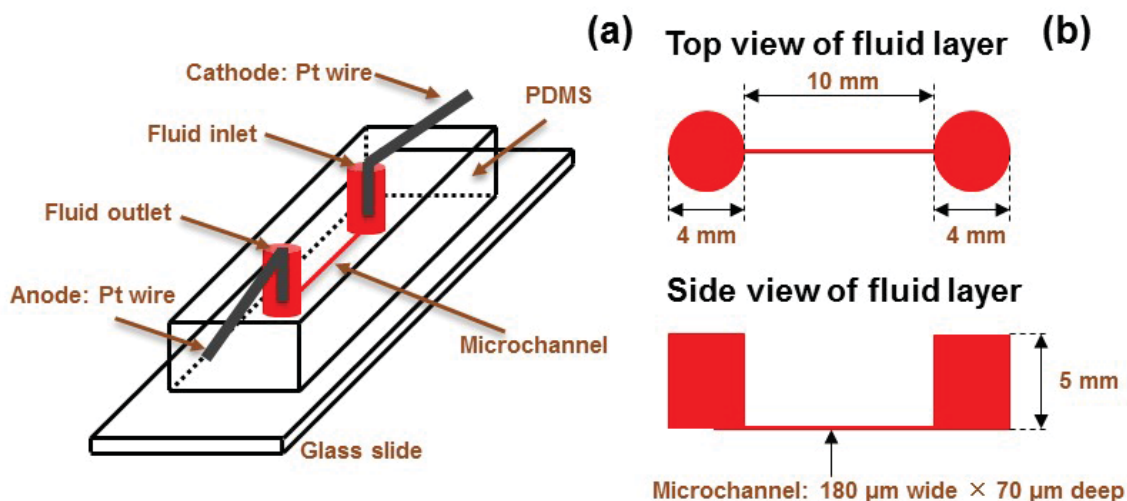


Fig 4.1 Schematic drawing of the single channel microfluidic device. (a) Device configuration illustrating anode and cathode platinum wires (0.1 mm in diameter) submerged in fluidic wells connected by a microchannel 180 μm by 70 μm by 10 mm long as shown in (b). Not drawn to scale.

were isolated from plasma and other blood component by centrifugation at 1400 rpm ($\text{rcf}=110\text{g}$) for 5 minutes via an accuSpin 400 centrifuge (Fisher Scientific, Pittsburgh, PA, U.S.A.). The isolated RBCs were rinsed twice with 0.9 wt% NaCl solution twice by spinning at 1400 rpm for 5 minutes in the accuSpin. Then the RBCs were mixed with 1000 $\mu\text{S}/\text{cm}$ isotonic phosphate buffered saline (PBS, 2.57 mM KH_2PO_4 , 2.57 mM K_2HPO_4 , 2.57 mM NaCl, 274.3 mM dextrose) to make a 60 vol% RBC suspension. Lastly, 320 μM Triton X-100 (T8532, Sigma-Aldrich, Saint Louis, MO, U.S.A.) was added to the 60 vol% RBC suspension and the 1000 $\mu\text{S}/\text{cm}$ PBS solution. Triton X-100 attenuates electrolysis bubble effects by facilitating formation of smaller bubbles, which cause less electrochemical interference than larger bubbles; thus the electrically coupled microfluidic system and current responses are stabilized [32, 153]. It was shown that 320 μM Triton X-100 does not compromise RBC membrane integrity. [36]

Graphene nanoplates (XGnP® Graphene Dispersions – Aqueous, XG science, Inc., Lansing, MI, U.S.A.) and active carbons (KETJENBLACK EC – 600JD, Akzo Nobel Polymer Chemicals LLC, Chicago, IL, U.S.A.) were suspended into e-pure water at 10 vol% and 1 wt%, respectively. The suspension was sonicated for 1 hour before use.

EPD was carried out in a microfluidic device with new platinum electrodes. The suspension was introduced into the microchannel and then 40 V DC applied. Carbon particles (graphene and active carbons) from suspension move toward the opposite charged electrode and coat the electrode surfaces under electric field. The graphene particles with the negative zeta potential [154] coated the anode surface, while the active carbons with positive zeta potential (32.8 ± 1.83 mV, N = 3, measured by a Zetasizer Nano ZS, Malvern Instruments, Malvern, Worcestershire, United Kingdom) were deposited onto the cathode surface. After the EPD process, the graphene coated electrodes and active carbon coated electrodes were dried at 350 °C for 20 minutes and at 80 °C for 8 days in an oven, respectively. Then, the graphene and the carbon deposited electrodes were employed as the anode of a new microfluidic device for RBC current measurement.

4.2.3 Current measurements

Separate current responses of the 1000 μ S/cm isotonic PBS and 60 vol% RBC suspension were measured in an alternate fashion. Both the anode and cathode platinum electrodes were connected to an HVS 448 high voltage sequencer (LabSmith, Livermore, CA,

U.S.A.). The PBS or RBC suspensions were injected via BD Safety-Lok™ 3 mL syringes (*Becton, Dickinson and Company*) through a bonded anode well port connector (LabSmith) and pushed through the microchannel to the cathode well. The 100 V DC was applied for 60 seconds while the current responses were saved to file at a sampling frequency of 39.06 Hz using Sequence software (LabSmith). After each measurement, the entire microfluidic device and microchannel were flushed using e-pure water (Millipore Simplicity 185, Millipore Corporation, Billerica, MA, U.S.A., Resistivity: 18.2 M Ω).

4.2.4 Sample characterization

Platinum electrodes before and after current measurements were imaged using a Hitachi S-4700 FE-SEM operated with a 5.0 keV electron beam. Platinum wire electrodes were cut off the microfluidic device using a scalpel and placed on the stubs using tweezers. The composition of electrode surfaces was determined by EDS with a 15.0 keV electron beam. Platinum electrodes were not coated for the analysis.

4.3 Results and discussion

4.3.1 Current responses

Fig 4.2 (a) shows the current responses sampled at 39.06 Hz of 1000 μ S/cm PBS (blue traces) and 60 vol% RBC suspensions in PBS (red traces) at 100 V. Each bar represents one measurement for one minute. Note that time-axis of the plot is discontinuous to

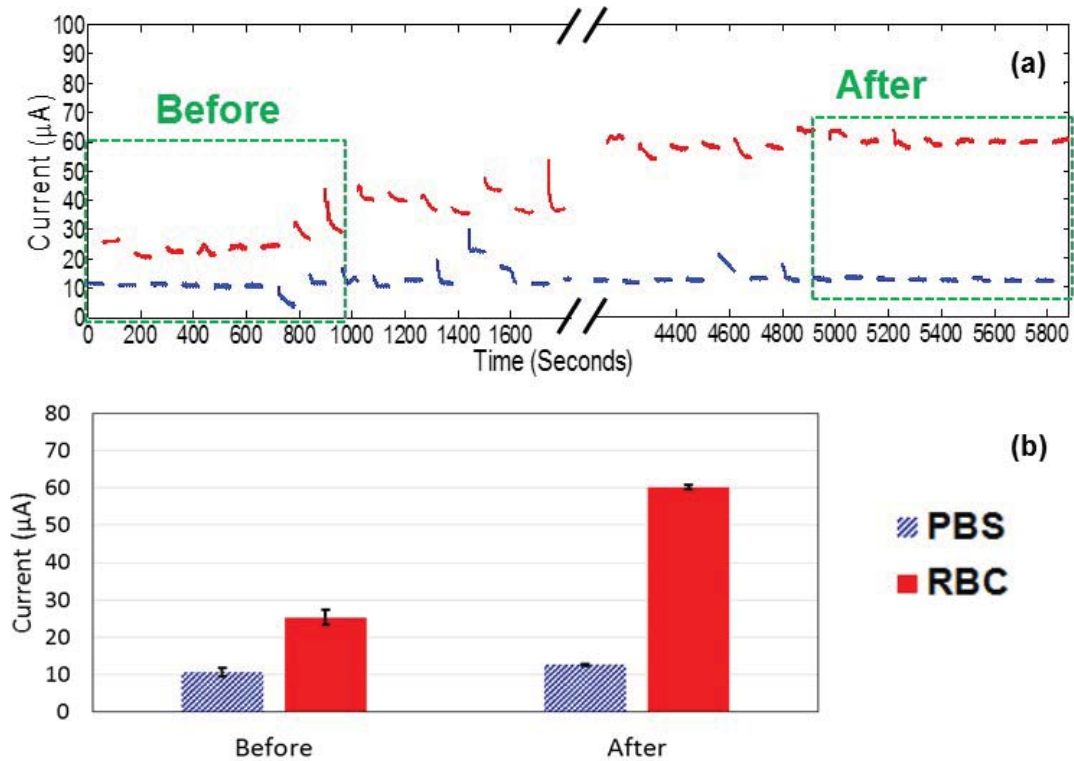


Fig 4.2 (a) Current responses of $1000 \mu\text{S}/\text{cm}$ PBS (blue traces) and 60 vol% RBC suspension (red traces) at 100 V DC versus time. Each bar represents one 60 seconds measurement, begun with new solution. Note that the time axis was broken to enlarge initial and final current responses. (b) Average current responses in the boxes labeled as before and after in (a). Error bars represent 95 % confidence intervals.

emphasize the initial and final responses. The average current responses of the first and last 8 measurements of each solution, highlighted by green boxes in Fig 4.2 (a), are compared in Fig 4.2 (b).

The current responses of the RBC solution gradually increased with each cycle while the baseline PBS remained fairly constant. Some PBS fluctuations such as from 1440 to 1500 seconds and from 1560 to 1620 seconds were likely the result of residual blood cells due to variations in manual flushing of the device with e-pure water. In addition, fewer large fluctuations occurred as the trials progressed indicating that the platinum electrodes

Table 4.1 *S/Ns of current responses before and after in Fig 4.2 (a).*

	Before	After
PBS	55.5	65.5
60 vol% RBC	51.8	170

incrementally became stabilized. These observations were repeated with >10 electrode pairs, although averages reported are for a representative experiment cycle.

The fluctuations of current responses of both the PBS and RBC solutions were attributed to isolated and thus unstable RBC adsorption. It was previously documented that unwanted molecule adsorption fouls biosensor electrode surfaces and results in irreproducible electrochemical responses [17-19, 142]. During the current measurements, it was observed that black layers formed on the platinum surface. We thus hypothesized that during the measurements, RBC adsorption on platinum electrode surfaces was irregular, yet incrementally accumulated. After 10 cycles of RBC current measurements and 10 cycles of PBS, the platinum wire electrodes lost their luster; after 20 cycles of RBC current measurements and 20 cycles of PBS, the anode appeared black in color. RBC current responses, such as from 900 to 960 seconds and from 1740 to 1800 seconds, drastically decreased during the measurement. This phenomenon was attributed to either aggregated clusters of carbonized RBC fragmenting off the electrode, which was experimentally observed, or to collapse and consolidation of the carbonized RBCs onto the electrodes.

In Fig 4.2 (b), the current responses of the 60% RBC suspension before and after were $25.3 \pm 2.13 \mu\text{A}$ and $60.2 \pm 0.67 \mu\text{A}$, respectively. This indicated that, as current signal responses were measured, the platinum electrode electrocatalytic activity (term used here to reflect the relative amount of active surface sites participating in the electron transfer reaction) for the RBC current measurements was increased by 140%. In addition, the current responses were more reproducible as indicated by the reduced confidence interval ranges reflected in the error bars in Fig 4.2 (b). The PBS current responses also illustrated more stable responses. Their values before and after in Fig 4.2 (b) were $10.5 \pm 1.13 \mu\text{A}$ and $12.6 \pm 0.20 \mu\text{A}$. It is presumed that the carbon layers formed on electrode surface might have modified the platinum electrode surface properties and thus improved the performance similar to how other carbon based materials coated electrodes to improve performance [116, 117].

S/Ns before and after were compared in Table 4.1. S/N ratios of both PBS and RBC suspension current responses increased with measurement cycles. The PBS current response signals are nearly the same before and after repeat measurements. Thus, the increased S/N is attributed to reduced noise (stabilized current responses). In RBC suspensions, the increase in S/N was predominantly due to increased current responses and decreased the standard deviation of the current responses. The standard deviation before was 0.922 and after was 0.483.

The entire sequence in Fig 4.2 (a) was reproduced more than ten times ($N > 10$) beginning each time with new platinum electrodes. The result – improved RBC current

responses stabilizing between 60 and 63 μA – was observed each time. The most common sequence length was 30 to 50 cycles of the 60 vol% RBC solution current measurements (plus the repeated PBS current measurements). Once current responses were stabilized at 60 to 63 μA , the entire immersed anode electrode was completely black and fluctuations of current responses were minimal. We hypothesize the black color was due to carbon layers covering the electrode surface. This is consistent with prior literature reporting minimal biomolecule adsorption onto carbon-based electrodes compared to platinum electrodes [114, 155, 156].

The black carbon layers formed on the electrode surfaces were very brittle and could be easily removed from the electrodes mechanically by tweezers or high-pressure air. If the carbon layers were kept intact, the electrodes retained improved performance. However, if the carbon layers were damaged, the current responses decreased below 60 μA . Then, by repeating the same procedure, measuring the PBS and 60 % RBC solution current responses in cycles, the 60% RBC solution currents could be restored to 60 to 63 μA again.

As mentioned previously, our goal was to measure the current responses of RBC suspensions at various volume to volume ratios in DC fields for hematocrit determination. Hematocrit is the volume percentage of RBCs in blood. Theoretically, the current response of blood is inversely proportional to hematocrit due to the nonconductive nature of RBCs [157, 158]. With bare platinum electrodes, different hematocrits could not be discerned because of current instability and the low catalytic

activity of the platinum electrodes as shown in Fig 4.2 (b). Current responses were not reproducible and overlapped at low values regardless of RBC concentrations. After platinum electrodes were coated with carbon layers, the electrodes demonstrated sufficient activity and stability to hematocrit to ~2 vol% resolution [153].

4.3.2 Electrode surface characterization

In order to directly investigate the black layers on the electrode surfaces, unused platinum electrode wire surfaces and the carbonized platinum electrode surfaces showing the improved performance were imaged by FE-SEM. Black layer compositions were analyzed via EDS and the results are shown in Table 4.2. For the EDS analysis, due to the curvature of platinum wire electrodes, the locations along the same ordinate were chosen for quantitative comparison.

Fig 4.3 (a), (b) and (c) illustrate unused platinum wire electrode surfaces at three magnifications. The platinum wire diameter was 0.1 mm and purity reported from Sigma Aldrich was 99.99%. SEM images of the wire were dominated by bright regions with a few, small dark regions. EDS elemental analysis was performed on both regions; representative EDS analysis are marked by A and B, respectively, in Fig 4.3 (c) and correlate to values in Table 4.2. The dark regions are carbon rich, while the bright regions were closer to pure platinum. Overall, the unused platinum surface contained measurable amounts of carbon and oxygen. For all experiments, the platinum wires containing carbon and oxygen impurities were used as electrodes without any pretreatment.

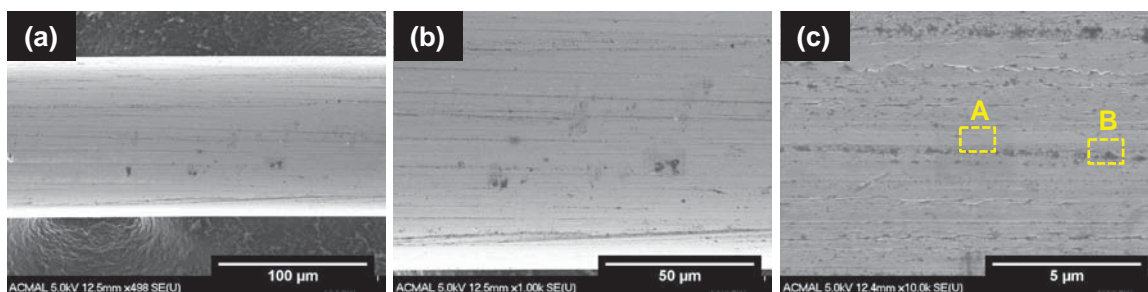


Fig 4.3 FE-SEM images of unused platinum wire electrodes at three magnifications (a) $\times 500$ magnification, (b) $\times 1000$ magnification, and (c) $\times 10000$ magnification. The yellow boxes in (c) indicate the representative regions for EDS analysis shown in Table 4.2.

Fig 4.4 (a), (b), and (c) are the images of platinum electrode surfaces used as a cathode after 31 cycles of the 60 vol% RBC current measurements with 31 intermittent PBS current measurements. This electrode demonstrated stable 60 μ A signals in 60 vol% RBC solutions. Comparison of unused platinum electrode SEM images to the cathode electrode surface, darker regions are more prominent as shown in Fig 4.4 (a). EDS analysis revealed these dark regions are carbon rich as cataloged in Table 4.2. In Fig 4.4 (b), the left most region labeled C has similar composition to the unused platinum electrode surface in Table 4.2. However, the dark region including D contained 31.9 % carbon. Fig 4.4 (c) is a 10000 \times magnification of region D. The images of another cathode electrode after 49 current measurement cycles with PBS and 49 cycles with 60 vol% RBC are shown in Fig 4.4 (d), (e) and (f). Fig 4.4 (d) shows that the platinum electrode was curved and scratched (lettered by E) by a scalpel while cut off the microfluidic device; further F marks carbon tape used to adhere the electrode to the FE-SEM stub. As contrasted with Fig 4.4 (a), (b), and (c), darker carbon regions more extensively cover the electrode surface as illustrated in region G in Fig 4.4 (e). EDS of this region indicated more extensive carbonization, as catalogued in Table 4.2. However, the bright region

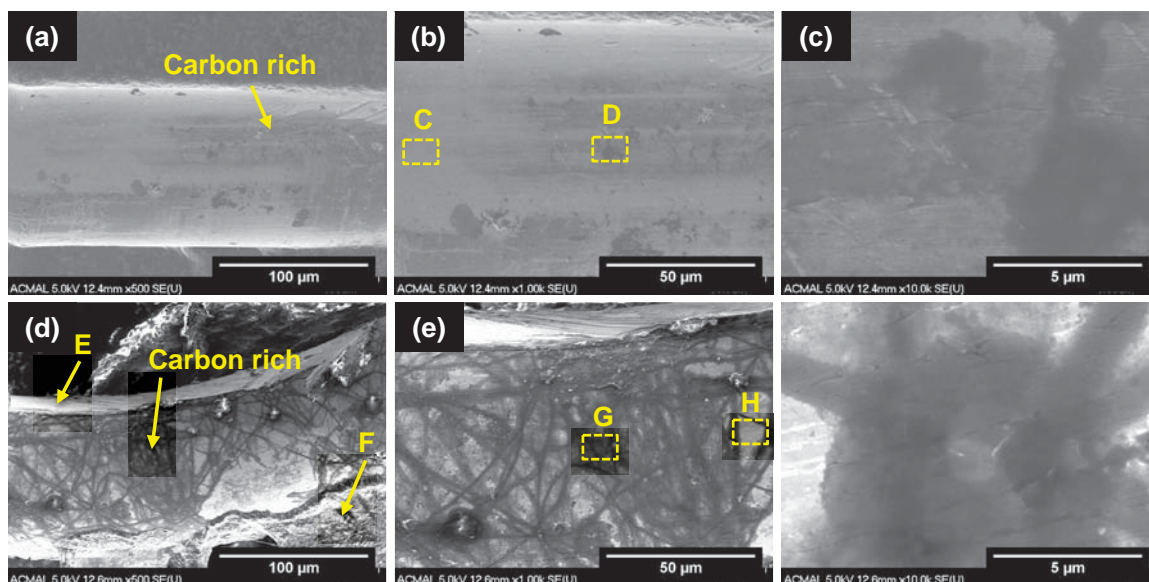


Fig 4.4 FE-SEM images of cathode surfaces. (a), (b), and (c): after 31 cycles of the 60 vol% RBC suspension current measurement (62 cycles if including the PBS current measurements) at $\times 500$, $\times 1000$, and $\times 10000$ magnification, respectively. (d), (e), and (f): after 49 cycles of the 60 vol% RBC current measurement at $\times 500$, $\times 1000$, and $\times 10000$ magnification, respectively. The yellow boxes indicate the representative spots for EDS analysis in Table 4.2.

marked as H in Fig 4.4 (e) still has similar composition to the unused platinum. These results indicate that with increasing measurement cycles, carbon coverage of the cathode electrode surface increased.

The source of the carbonization is attributed primarily to irreversible RBCs adsorption onto the platinum surface because this is the predominant source of carbon within the solution. The solution also contains 320 μM TritonX-100, which is a nonionic surfactant comprised of a hydrophilic polyethylene oxide chain and an aromatic hydrocarbon hydrophobic group $((\text{C}_2\text{H}_4\text{O})_n\text{C}_{14}\text{H}_{22}\text{O}$, $N=9-10$). It was observed that repeated current measurements in only PBS solution containing Triton X-100 did not change electrode surfaces. Other experimental impurities that could serve as sources of carbon include the

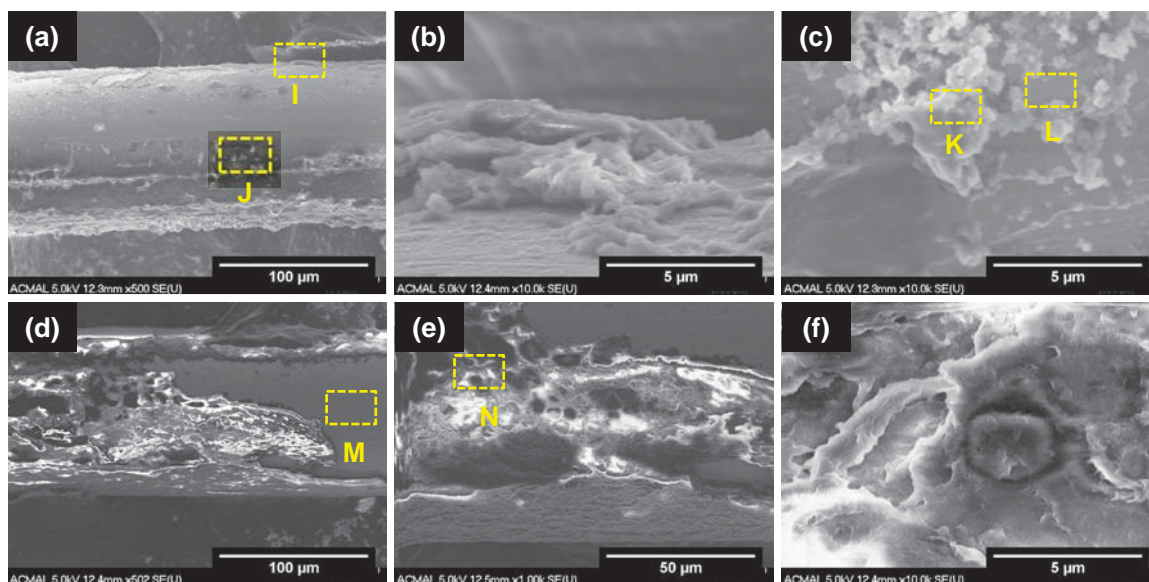


Fig 4.5 FE-SEM images of anode surfaces. (a), (b), and (c): after 31 cycles of the 60 vol% RBC suspension current measurement (62 cycles if including the PBS current measurements) at $\times 500$, $\times 1000$, and $\times 1000$ magnification, respectively. (d), (e), and (f): after 49 cycles of the 60 vol% RBC current measurement at $\times 500$, $\times 1000$, and $\times 10000$ magnification, respectively. The yellow boxes indicate the representative spots for EDS analysis in Table 4.2.

PDMS channel itself and the bonded port connector composed of Ultem[®] (polyetherimide) although these solids have negligible solubility in water [159].

Anode electrode surfaces after the performance improvement were also imaged. Fig 4.5 (a), (b) and (c) show the anode surface after 31 current measurements cycles with PBS and 31 cycles with 60 vol% RBC. This anode was pared with Fig 4.3 (a), (b), and (c) and demonstrated a stable $60 \mu\text{A}$ in 60 vol% RBC solution. Fig 4.5 (b), a magnified view of the I yellow box in Fig 4.5 (a), is a side view of the coated layers. This illustrates that the anode exhibited a rough surface with layers that increased the platinum surface area. A top view of the layers, an enlarged image of the yellow box J, is shown in Fig 4.5 (c). EDS analysis revealed that the K region is a carbon rich layer containing $56.8 \pm 2.59 \text{ wt}\%$

Table 4.2 *Composition of platinum electrode surfaces in Fig 4.3, 4.4, 4.5 and 4.8 analyzed by EDS.*

electrode	label ¹	surface status	element (weight%)			
			C	O	Pt	N
new	A	bright	14.8 ± 1.37	0.82 ± 0.29	84.4 ± 1.62	4
	B	dark	20.0 ± 5.35	1.39 ± 0.67	78.6 ± 6.01	3
cathode	C	bare	14.5 ± 1.05	1.09 ± 0.43	84.4 ± 1.44	3
	D	carbonized	31.9 ± 14.9	2.36 ± 1.24	65.7 ± 16.1	4
	H	bare	13.3 ± 0.26	0.88 ± 0.04	85.8 ± 0.23	3
	G	carbonized	38.6 ± 5.77	3.18 ± 0.55	58.2 ± 6.26	3
anode	L	bare	15.9 ± 1.32	1.37 ± 0.01	84.3 ± 0.17	2
	K	carbonized	56.8 ± 2.59	5.94 ± 0.83	36.1 ± 3.23	2
	M	bare	12.4	1.83	85.8	1
	N	carbonized	55.9 ± 3.34	9.67 ± 0.54	28.9 ± 3.28	3
	p	bare	15.2 ± 0.04	1.24 ± 0.04	83.6 ± 0.08	2
	Q	active carbon	39.5 ± 6.59	2.81 ± 0.26	57.7 ± 6.85	2
	R	carbonized	80.5 ± 8.93	8.70 ± 3.22	10.1 ± 12.1	3

¹ *The capital letters in the label column, corresponding to the labels in Fig 4.3, 4.4, 4.5, and 4.8, indicate representative regions for the analyses.*

carbon as reported in Table 4.2. In K, 1.16 ± 0.19 wt% chlorine was also detected, which is not shown in Table 4.2. Smoother regions, like L, have similar composition as the untreated platinum surfaces, reported in Table 4.2.

Fig 4.5 (a), (b), and (c) indicates that the coated carbon layers developed to three-dimensional (3D) porous structures, which is structurally different from the cathode images. This 3D structure is attributed to the negative zeta potential of RBCs in the PBS driving RBC adsorption to the positively charged anode surface. RBC zeta potential is -31.8 ± 1.1 mV [160] in PBS with 1.7 mM KH_2PO_4 , 5.2 mM Na_2HPO_4 , 150 mM NaCl,

and pH 7.4, which is similar to our PBS medium condition of 2.57 mM KH_2PO_4 , 2.57 mM K_2HPO_4 , 2.57 mM NaCl, 274.3 mM dextrose, and pH 7.2. RBC adsorption is energetically favorable because adsorption reduces the interfacial energy at the electrode-solution interface. In contrast, the negatively charged cathode would repel intact RBCs, so 3D adsorption was not observed on the cathodes as shown in Fig 4.4.

An additional anode electrode was examined after 49 cycles of RBC current measurements and 49 cycles of PBS. The FE-SEM images shown in Fig 4.5 (d), (e), and (f) represent the anode status right after current measurements in Fig 4.2, which displayed $60.2 \pm 0.67 \mu\text{A}$ with the 60 vol% RBC suspension at 100 V DC. The entire solution-exposed anode surface upon obtaining stable current measurements was completely covered by carbon layers. Handling of the anode electrodes was challenging because the black carbon layers were brittle and easily damaged. Note that in Fig 4.5 (d), on right side containing M the 3D carbon layer clearly peeled off and thus, this region had the same composition as the unused platinum electrode. The carbon layer composition representatively marked by N in Fig 4.5 (e) was reported in Table 4.2. In these carbon layers, $4.46 \pm 2.14 \text{ wt}\%$ of chlorine and $1.08 \pm 0.58 \text{ wt}\%$ of potassium were also detected, not shown in Table 4.2. Compared to the anode after 31 cycles of current measurements in Fig 4.5 (a), (b), (c), the carbon layers extended to cover the entire surface.

This microfluidic system has previously been shown to generate electrolysis bubbles [32]; thus, electrolysis reactions occur concurrent with carbon adsorption to the electrodes. During current measurements, electrolysis of water generates oxygen and

hydrogen gas bubbles at the anode and cathode electrode surfaces, respectively [123]. These gas bubbles could affect RBC adsorption at the anode and carbon adsorption at the cathode. Gas bubbles on the electrode surfaces make surface sites inactive. Growth and detachment of bubbles from electrodes can also create microconvective flows at and near electrodes [32, 37, 39], which would interfere with transport to the surface. Thus bubble behavior could impede RBC and carbon adsorption. This phenomenon was reported in electrophoretic deposition, which is a colloidal coating process that is similar to RBC adsorption in the sense that charged particles in suspension are deposited onto polarized electrode surfaces with opposite charges under an externally applied electric field. In electrophoretic deposition, electrolysis bubbles can incorporate into the deposit layers and lead to porous and inhomogeneous deposited structures [155, 156, 161]. In our experiments, the applied 100 V DC is high enough to generate large amount of bubbles and may also lead to a porous structure. The inhomogeneity of the structure is illustrated in Fig 4.5 (a), (b) and (c).

Based on the data presented herein, we have attributed improved electrode performance to the formation of carbon layers on the anode surface and carbon films on the cathode surfaces. During current measurements, adsorbed RBCs lysed on the electrode surfaces and progressively carbonized to form the observed black carbon layers on the electrode surfaces. As the RBC current measurement cycles progressed, RBC adsorption compounded and eventually formed thick black carbon layers, which were especially pronounced on the anode. The anode carbon layers developed into 3D porous structures

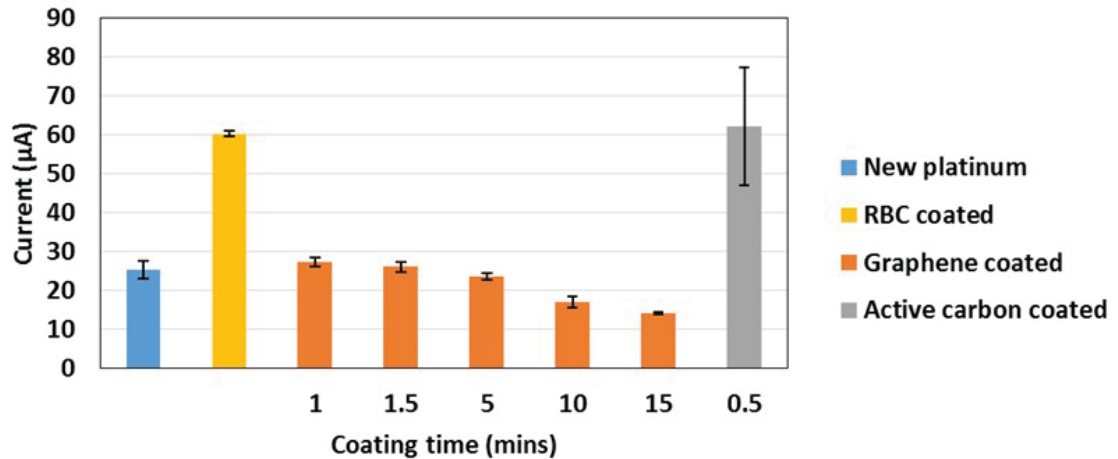


Fig 4.6 Comparison of graphene coated and active carbon coated electrode performance for current measurements of 60 vol% RBC in PBS at 100 V DC. Error bars represent 95 % confidence intervals.

that increased the electrode surface area. Based on improved current responses, it is assumed that these adsorbed carbon layers have favorable electron conduction properties. Consistent with findings in other carbon electrode systems, the critical factor with carbon-based modification of electrode surfaces is to achieve maximum effective surface area with well-optimized porous structures. The stabilization of current and increased electrocatalytic activity of the platinum electrodes in our microfluidic device suggests that carbon layers formed via RBC adsorption developed into optimized porous structures for stable RBC current measurements.

4.3.3 Graphene and active carbon coated electrodes

Electrode performance with graphene and active carbon coated electrodes for current measurements of 60 vol% RBC solution were compared with new platinum electrode performance in Fig 4.6. In EPD process, the thickness and area of deposited layers

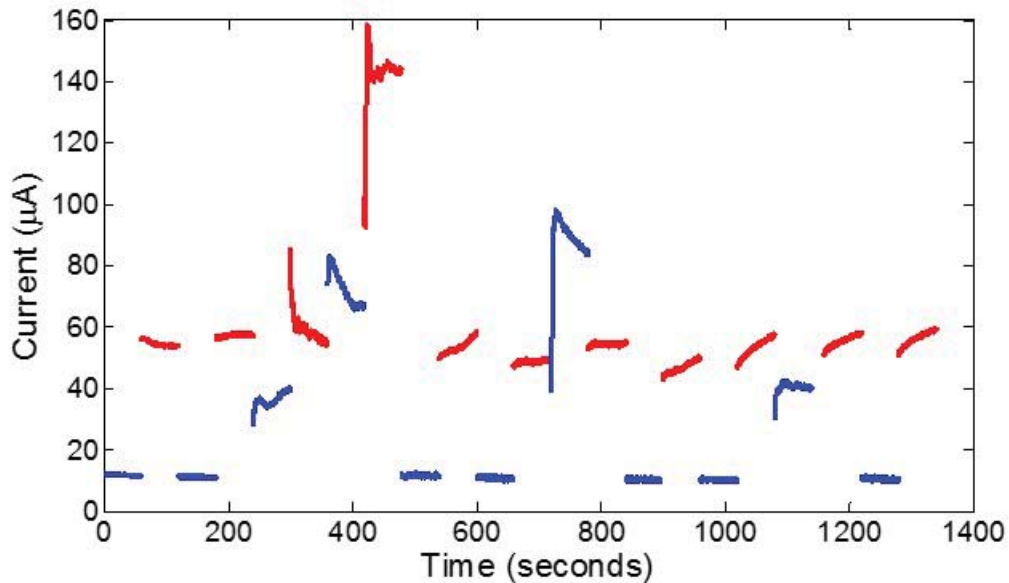


Figure 4.7 Current responses of 1000 $\mu\text{S}/\text{cm}$ PBS (blue traces) and 60 vol% RBC suspension (red traces) with active carbon coated electrode at 100 V DC versus time. Each bar represents one 60 seconds measurement, begun with new solution.

depends on coating time. As coating time increased, electrode surfaces became darker and lost luster. The graphene coated electrodes did not improve electrode performance and as graphene surface coverage increased (longer coating time), electrode performance decreased. Decrease in performance may be due to the thick graphene layers. Thick graphene layers would have increased the resistance to electron transfer and decreased current responses. Average current responses with electrode coated for 10 and 15 minutes were below 20 μA .

Active carbon coated electrode apparently improved performance. Compared to $25.3 \pm 2.38 \mu\text{A}$ of new platinum electrode average current response, active carbon electrode increased current responses to $62.1 \pm 15.2 \mu\text{A}$. Fig 4.7 shows the current responses with this active carbon coated electrode. Some RBC current responses, such as from 300 to

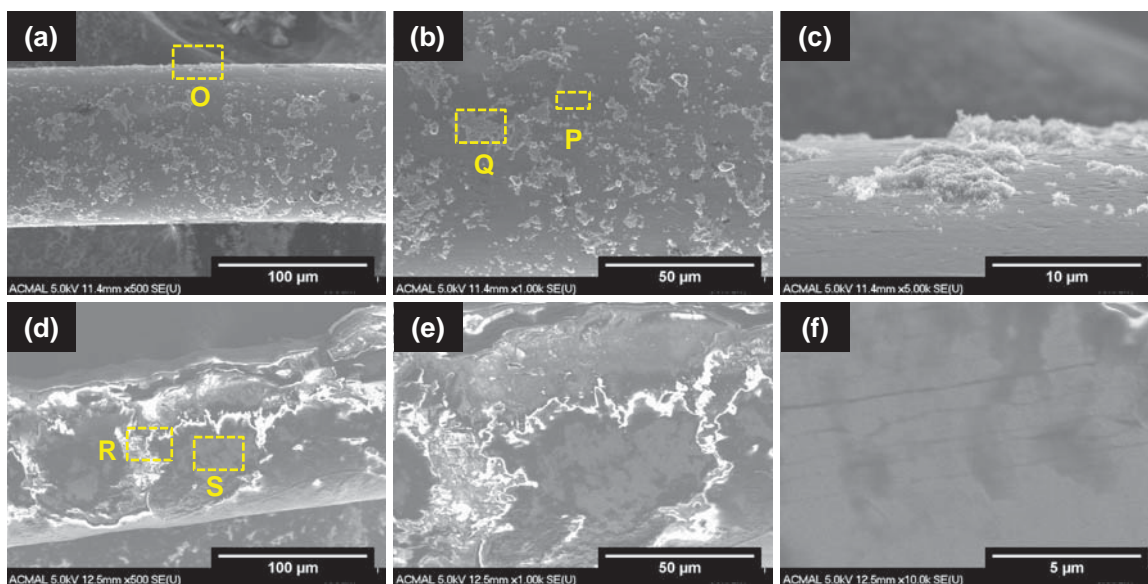


Figure 4.8 FE-SEM images of active carbon coated platinum electrode surfaces. Active carbons from 1 wt% solution were deposited for 30 seconds at 40 V. (a), (b), and (c): Before current measurement at $\times 500$, $\times 1000$, and $\times 5000$ magnification, respectively. (d), (e), and (f): after 11 cycles of the 60 vol% RBC current measurement at $\times 500$, $\times 1000$, and $\times 10000$ magnification, respectively. The yellow boxes indicate the representative spots for EDS analysis in Table 4.2.

360 seconds and from 420 to 480 seconds showed huge fluctuation and deviation compared to other responses. $15.2 \mu\text{A}$ confidence interval is due to these fluctuated responses. Without these two measurement, average current responses of rest measurement was $53.5 \pm 2.12 \mu\text{A}$. This is lower than $60.2 \pm 0.77 \mu\text{A}$ with RBC coated electrode.

Fig 4.8 shows FE-SEM images of active carbon coated electrode surfaces. Electrode surfaces before the measurement was shown in Fig 4.8 (a), (b), and (C). In images, black regions such as P in Fig 4.8 (b) has similar compositions to the unused platinum electrode surface as reported in Table 4.2. White color regions such as Q in Fig 4.8 (b) are active carbon coated layer and contains $39.5 \pm 6.59 \text{ wt}\%$ carbon. Fig 4.8 (c) is a $5000\times$

magnification of the yellow box O in Fig 4.8 (a). It shows that active carbon layers on electrode surfaces increased surface roughness. Fig 4.8 (d), (e), and (f) showed electrode surfaces after RBC current measurements. Most of surface area were carbonized by irreversibly adsorbed RBCs. The carbonized surface area composition, representatively marked by R in Fig 4.8 (a), was reported in Table 4.2. In the carbonized layers, small amount of sodium (0.17 ± 0.11 wt%), potassium (0.05 ± 0.07 wt%), and iron (0.13 ± 0.14 wt%) were also detected. Fig 4.8 (f) a magnification of the yellow box S in Fig 4.8 (d). These results means that RBC adsorption took place and carbonized active carbon coated electrode surfaces. This RBC adsorption must have caused the fluctuations of current responses in Fig 4.7.

4.4 Concluding remarks

Many microfluidic devices employ microelectrodes that have small surface areas that yield weaker electrical signals. Prior biosensor research has revealed that irreversible biomolecule adsorption destabilizes these electrical signals [17-19]. Successful strategies to reduce biomolecule adsorption have included bonding carbon nanotubes or graphene on electrode surfaces.

The present work is an inadvertent extension of this approach with red blood cells as the carbon source. Systematic studies in RBC solutions suspensions revealed that RBCs offer a carbon source for carbon deposition on both the cathode and anode electrodes, although the structure and composition differed greatly between the electrodes. The platinum

electrodes with 3D carbon layers formed from RBC adsorption reached a steady state as indicated by increased current responses with smaller S/N. These carbonization of electrode results using RBCs are consistent with other electrode carbonization literature, which reports that 1) increasing electrode surface area improves the electrode performance, and 2) carbon based or carbon coated electrodes experience less fouling. This suggests that biological sources of carbon may be utilizable to carbon-coat electrodes, and once coated reduce further biomolecule adsorption, and may serve as a lower cost alternative to carbon nanotubes or graphene binding to electrode surfaces.

4.5 Acknowledgements

The authors gratefully acknowledge help from Joe Halt, Zhichao Wang, and Maryam Khaksari for RBC sample preparation and valuable discussion. The authors also gratefully acknowledge prior discussions and efforts years ago on this topic with Soumya Srivastava and David O. Wipf.

Chapter 5 Electrochemical hematocrit determination in a direct current microfluidic device ³

5.1 Introduction

Hematocrit (HCT) is a volume percentage of red blood cells (RBCs) in total volume of whole blood. It is normally 40 – 54 % for men and 36 – 48 % for women [1]. HCT tests are generally performed to screen blood donors and diagnose medical conditions or diseases affecting the quantity of RBCs in blood. Elevated HCT values are signs of polycythemia, cyanosis, dehydration, decompensating cardiovascular disease, and pulmonary fibrosis. Lowered values can be indicators of anemia and leukemia [2].

Point-of-Care (POC) diagnostics is a medical test at or near the site of a patient with a portable, self-contained, handheld testing device. POC devices aim to be inexpensive, simple, small and rugged with rapid and accurate analysis capability to meet medical care market needs. Microfluidic systems are considered a key platform for POC devices due to their unique features of low sample consumption, fast and precise analysis, low cost, and compactness [13, 14]. In addition, inexpensive and reliable microfluidic POC devices are advanced as a key solution for global health issues, especially for the developing world or regions lacking health care resources and diagnostic laboratory infrastructure [14]. The importance of HCT as a screening medical diagnostic has led to the development of many

³ The material contained in this chapter has been submitted to:
ELECTROPHORESIS.

HCT test methods. UltraCrit™ (Separation Technology, Inc., Standford, FL, U.S.A.) for blood donor screen is based upon ultrasound technology [162]. Measuring hemoglobin is an alternative to hematocrit and conversion between the two is done regularly. Mean corpuscular hemoglobin concentration (MCHC) is the average concentration of hemoglobin in RBCs and normally 32 to 36 g/dL [163]. Based on this correlation, HCT can be determined by hemoglobin measurement via the copper sulfate density method [6] and the hemoglobin analyzer HemoCue® (AB Leo Diagnostics, Helsingborg, Sweden) [164], and others [165].

The HCT test is typically conducted in full, wet chemistry laboratory settings by the microhematocrit method, or the Coulter counter method. In the microhematocrit method, the blood is drawn into a glass tube and separated into packed RBC and plasma (fluid around cells) layers by centrifugation; hematocrit is then determined by calculating the ratio of the height of the packed RBCs layer to the total height of whole blood sample [3]. This method does not allow continuous HCT measurements, which may be necessary during surgery and trauma care. Further, centrifuge components are bulky and time-consuming so this is not ideal for adaptation to POC diagnostics.

Another full laboratory alternative, the Coulter counter method, draws diluted blood suspension through a sensing aperture traversing two chambers. Individual nonconductive RBC passing through the aperture changes the electrical impedance in proportion to the RBC volume. The electrical impedance change allows the system to count and size RBCs and thus to determine the total RBC volume passing through the

aperture. HCT is calculated using the total fluid volume passing through the aperture. [4, 5] In addition, mean corpuscular volume (MCV) and other indicators in complete blood count (CBC) tests can be calculated from this information. Although some microfluidic systems employing the Coulter principle were introduced [21, 166], the Coulter counter method is generally considered to be too powerful and unsuitable for a portable microfluidic platform due to its complicated principle.

Another approach to determine HCT is the electrical impedance technique (also called electrical conductivity method) measuring whole blood sample impedance. At low frequencies (below 100 kHz), the AC signals pass through plasma and RBCs due to their insulative membranes act like capacitors. The measured resistance is due to plasma resistance and as such, it increases with the HCT in a reproducible fashion [157, 167-172]. Unfortunately, the impedance technique is a complicated and expensive protocol owing to its working principle – applying sinusoidal electrical signal, measuring responses of the system, and calculating the resistivity over applied frequencies. It requires bulky and intricate equipment to control frequencies and measure impedance. The impedance technique is very accurate and reliable compared to other methods, so many commercialized POC HCT devices are based on the impedance techniques [7, 8] even though miniaturizations require specialized electronic components that increase the device price. In particular, the i-STAT blood analyzer (Abbott Laboratories, Abbott Park, IL, USA) can determine not only HCT, but also sodium, potassium, chloride, pCO₂, blood urea, nitrogen concentration measurements; i-STAT is considered one of the most

successful ‘gold standard’ microfluidic POC diagnostics [8]. However, the i-STAT is too expensive, approximately \$14,000 USD as of 2014, to be used at home or distributed in developing countries for the global health issues.

Employing simpler electronics to test for HCT would significantly reduce costs of a POC device. For this reason, this work explores direct current measures of HCT as a means to avoid the complexity and expense of AC frequency generation and AC impedance detection.

Resistivity measurements of living human tissue, including blood and plasma under DC fields, were conducted in the 1940s through 1960s [173, 174]. The AC impedance technique has been the focus of attention due to greater precision and data dimensions that enable property measurements such as cell interior resistance and membrane capacitance [158, 175, 176]. When DC fields are applied across particle suspension samples like blood, current passes through plasma while the RBCs act like capacitors in a fashion similar to the AC impedance technique. Thus, DC current responses can reflect plasma resistance and RBC fractional volumes thus enabling HCT determination. Blood resistivity is frequency dependent due to the capacitance properties of RBC membranes and decreases as the frequency increases [177]. So the HCT values determined by the AC impedance method depend on the RBC membrane status. Measuring HCT under DC fields (at zero frequency) can exclude the cell membrane dependence.

The purpose of the present work is to design and test a new simple and comparably robust microfluidic system for HCT determination with the goal of reducing complexity

and cost of POC HCT devices. To demonstrate feasibility of the new microfluidic system, RBC solutions suspended in a) phosphate buffered saline (PBS) and b) plasma both to HCT ranges from 10 to 70 vol% were quantified in a simple DC microfluidic device by dynamically measuring current responses.

5.2 Materials and Methods

5.2.1 Microfluidic device

A PDMS microfluidic device was cast using standard soft photolithographic master wafer techniques and O₂ plasma sealing procedures to a standard microscope slide [32]. The microfluidic device incorporated a singular microchannel with the dimensions of 180 μm by 70 μm and 10 mm long was used for current measurements. Both ends of the microchannel were connected to reservoirs of 0.4 mm in diameter. For electrodes, 0.1 mm platinum wires (0.10 mm diameter, 99.99 %, Sigma-Aldrich) were immersed 2 mm into each reservoir.

5.2.2 Sample preparation

From a voluntary A+ donor, 3 mL blood samples were drawn into vacutainers (*Becton, Dickinson and Company*, Franklin Lakes, NJ, U.S.A.) containing 1.8 mg K₂ EDTA (di-potassium ethylenediaminetetraacetic acid) per ml of blood and kept at 4 °C. All samples were tested within 2 days of donation.

3 ml whole blood was centrifuged at 1400 rpm (rcf=110g) for 5 minutes via an accuSpin™ 400 (Fisher Scientific™, Pittsburgh, PA, U.S.A.) to separate RBCs and plasma. Plasma was removed and the RBCs were resuspended with 3 ml 0.9 wt% NaCl solution, then centrifuged at 1400 rpm for 5 minutes. This washing was repeated twice. The rinsed RBCs and plasma were stored at 4 °C and -30 °C, respectively and then used within 2 days and 3 months after donation, respectively.

For the PBS HCT experiments, RBCs were resuspended into 1000 μ S/cm isotonic phosphate buffered saline (PBS, 2.57 mM KH_2PO_4 , 2.57 mM K_2HPO_4 , 2.57 mM NaCl, 274.3 mM dextrose) to desired concentrations (10, 20, 25, 30, 35, 40, 45, 50, 55, 60 and 70 vol%). For the plasma HCT experiments, RBCs were resuspended into the pooled and thawed plasma at the same desired concentrations. Lastly, a previously determined optimal concentration of 320 μ M Triton X-100 was added into each solution to stabilize baseline solution responses by minimizing detrimental electrolysis reaction effects [32].

5.2.3 Current response measurements

RBC solutions were introduced via the microdevice port connector (LabSmith, Livermore, CA, U.S.A.) via BD Safety-Lok™ 3 mL syringes (*Becton, Dickinson and Company*). 100 V DC was applied across the microchannel via the platinum electrodes emmersed in microdevice wells for one minute while concurrently measuring current responses at 39 points per second with the HVS 448 high voltage sequencer (LabSmith). After each one minute cycle, the microchannel was flushed with e-pure water

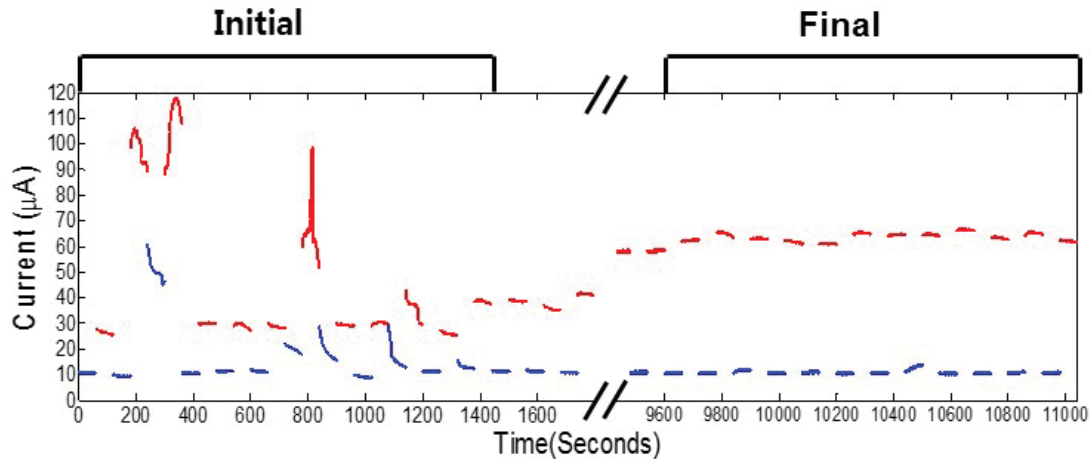


Figure 5.1 The importance of platinum electrode pretreatment. Current responses of 1000 $\mu\text{S}/\text{cm}$ PBS (blue cycle traces) and 60 vol% RBC suspension (higher, red cycle traces) at 100 V DC versus time. Each bar represents one 60 seconds cycle, begun after the microdevice was flushed with new solution.

(Resistivity: 18.2 M Ω). In order to monitor platinum electrode status and ensure microdevice reproducibility and quality control, isotonic PBS solution current responses were also measured with RBC solution in rotating cycles.

5.2.4 Platinum electrode quality control measures

To increase and then maintain platinum electrode performance and stability, platinum electrode pretreatment was necessary as described in separately documented work [129]. All RBC HCT current response experiments were completed with pretreated platinum electrodes. Control experiments were conducted to ensure optimal electrode performance prior to any HCT experiments. 60 vol% RBC suspension in PBS were measured with the PBS in rotating cycles same as the current response measurements for HCT determination. As the electrode current responses of the PBS and the 60 vol% RBC suspension were measured, the electrode surface were carbonized by the adsorbed RBCs

and electrode performance improved as shown in Fig 5.1. These improved performance was attributed to the carbon layers increasing electrode surfaces area with 3 dimensional porous structures and minimizing electrode surface fouling.

5.2.5 Microscopy visualization

To assess cell integrity before and after experiments, RBC images were acquired with a Plan-Neofluar 63x/0,75 Korr Ph2 objective (Zeiss, Thornwood, NY, U.S.A.) on a microscope equipped with an AxioCam MRm camera (Zeiss). Software AxioVision (Version 4.8, Zeiss) was used for digital image processing and 2D RBC diameter measurements.

5.2.6 Cell counts

As an independent verification of manually contrived hematocrit suspensions and to assess the impact of added surfactant on cell integrity, a hemocytometer (Hausser Scientific, Horsham, PA, U.S.A.) was used to count RBCs over time for one hour in presence of 320 μ M Triton X-100. Even 10 vol% RBC solution, which is the most dilute solution used for the current measurement was too dense to count cells on the hemocytometer, so RBC solutions were diluted to 0.1 vol% and cell count calculations adjusted accordingly.

5.2.7 Conductivity and zeta potential measurement

Conductivity of RBCs in PBS was measured using an AB 30 conductivity meter (Fisher Scientific™ accumet™, Pittsburgh, PA, U.S.A.). Zeta potential of RBCs in PBS was determined via a Zetasizer Nano ZS (Malvern Instruments, Malvern, Worcestershire, United Kingdom).

5.3 Results and Discussion

5.3.1 Platinum electrode pretreatment

Current responses of both PBS and RBC suspension were inconsistent with new platinum electrodes. However, pretreatment of the electrodes resulted in highly reproducible results. Fig 5.1 illustrates initial current responses of the 60 vol% RBC suspension (red traces) with new platinum electrodes from 0 to 1440 seconds (labeled ‘Initial’ in Fig-1) were 46.2 ± 16.6 and improved to $63.7 \pm 0.93 \mu\text{A}$ from 9600 to 11040 seconds (labeled ‘Final’). Optimal electrode performance was assessed prior to all subsequent HCT experiments.

5.3.2 Mitigating factors with current response measurements

Representative current responses of RBC solutions (red traces) at 100 V DC are presented in Fig 5.2. In order to monitor the platinum electrode status, the current response of the 1000 $\mu\text{S}/\text{cm}$ PBS (blue traces in the plot) followed by the RBC solution were measured in 60 second cycles. Measured current responses were reproducible once platinum electrode pretreatment was completed [129].

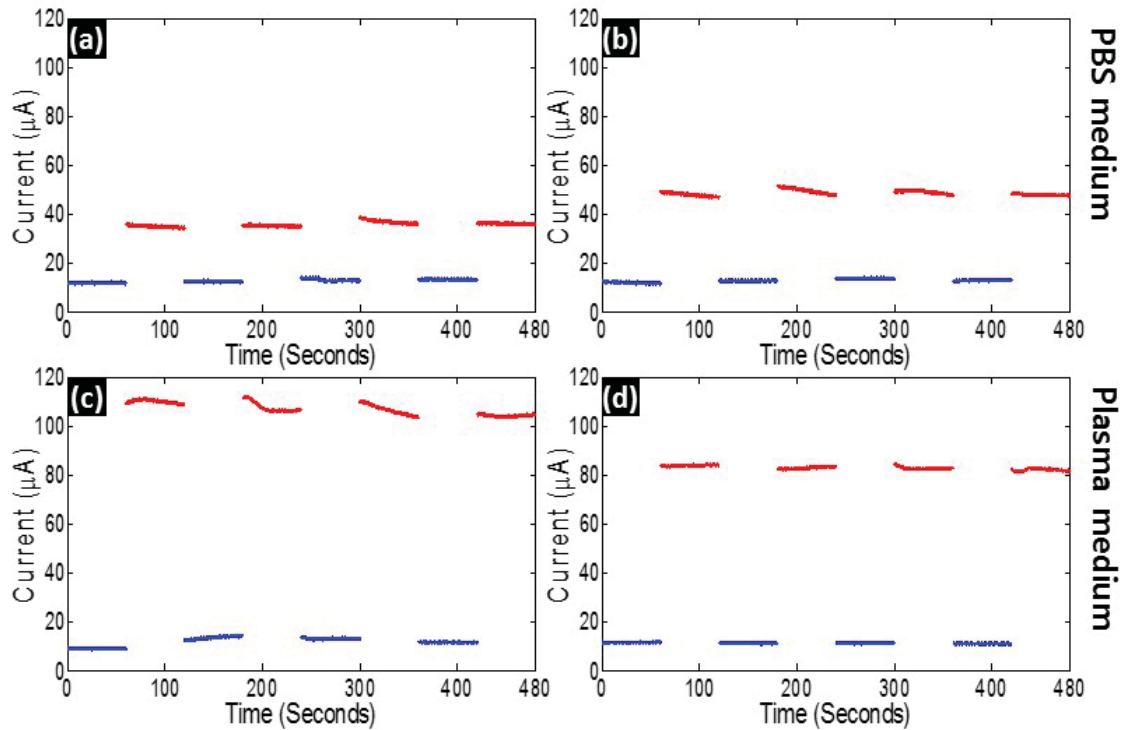


Figure 5.2 Representative current responses of 1000 $\mu\text{S}/\text{cm}$ PBS (blue traces) and RBC solutions (red traces) at 100 V DC versus time. (a) 25 vol% RBC in PBS, (b) 45 vol% RBC in PBS, (c) 25 vol% RBC in plasma, (d) 45 vol% RBC in plasma. Each trace represents one 60 seconds cycle, begun with new solution pumped into the microchannel.

Small fluctuations in the current responses of RBC solutions, PBS, and plasma were observed. In addition to the high frequency noise always experienced by the system, some current responses such as the second 25 vol% RBC in plasma current from 180 to 240 seconds in Fig 5.2 (c) decreased during the 60 second cycle. By examining all RBC traces in Fig 5.2, slight decreases in the current during most measurement cycles were observed. Electrolysis bubbles, RBC adsorption onto electrodes, and RBC sedimentation are factors destabilizing current responses and increasing noise of current signals. In order to obtain reproducible current responses and increase S/N, these factors were considered.

It is well-known that platinum electrodes in aqueous solution generate gas bubbles by electrolysis of water above ~ 3 V DC [15]. The electrolysis bubbles cover active electrode surface sites, increase solution resistance [38], and affect heat and mass transfer rates [39, 125], leading to destabilization of microfluidic system and inconsistent current responses [32]. In order to control the electrolysis bubbles, 320 μ M Triton X-100 was added to each solution. The beneficial mechanisms behind surfactant additives include promoting faster bubble detachments from electrodes, smaller bubble diameters via lower surface tension, and decreasing gas bubbles formation by altering gas solubility. Triton X-100 was previously shown to stabilize our microfluidic system [32].

Secondly, irreversible RBC adsorption is a phenomenon that lowers free energy at the interface between platinum electrodes and the RBC/PBS suspension. Adsorbed RBCs foul the electrode surface and destabilize current responses [17, 33]. In Fig 5.1, large fluctuation of current responses such as from 180 to 240 seconds and from 300 to 360 seconds in the initial time range is attribute to RBC adsorption [129]. However, upon repeat usage of the electrodes, large fluctuations in current responses were not apparent after 9600 seconds. Separate work has revealed that this stabilization is due to carbon layers formed on the electrode [129]. Further, the carbon based electrodes have less tendency to foul than fresh, pure platinum electrodes.

Lastly, RBC sedimentation in static media is noticeable via microscope observations to begin within 30 sec and thus would occur during the measurements [178]. Due to insulative membranes, RBCs are poor conductors. As the cells sediment due to gravity in

both the reservoirs and microchannel, solution resistance would change. In our microdevice configuration, RBC sedimentation in the reservoirs would increase resistance due to poorly conducting RBCs in the current pathway between electrodes [157, 178, 179]. However, electroosmotic flow within the microchannel itself would likely prevent RBC sedimentation. Thus, current responses were measured in one minute cycles to minimize sedimentation influences on the measurements. However, the slight downward drift in most cycles is attributed to sedimentation effects.

5.3.3 Effect of Triton X-100 on RBCs

To control electrolysis bubbles, and thus stabilize the current, 320 μM Triton X-100 surfactant was added to all RBC solutions. Since Triton X-100 is commonly used to lyse RBCs [180-184], the effects of the 320 μM Triton X-100 on RBCs was systematically verified.

Surfactants naturally migrate to interfaces. With cells including RBCs, surfactants insert into the membrane's phospholipid bilayer at sub-solubilizing concentrations. As the bilayer surfactant concentration increases, phospholipid solubilization is reached, normally denoted as D_t^{Sat} , which concurrently signals the beginning of hemolysis. The concentration for complete solubilization, D_t^{Sol} , finishes hemolysis. Between D_t^{Sat} and D_t^{Sol} , inserted surfactant molecules form surfactant/phospholipid mixed vesicles and micelles which result in bilayer curvature changes, formation of pores, and solubilization of the phospholipid and thus cell hemolysis [50, 52, 180, 182, 183].

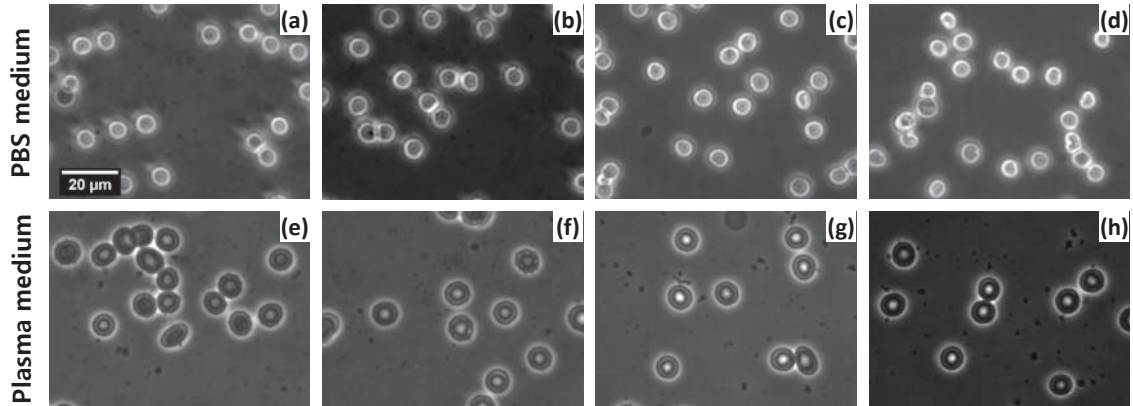


Figure 5.3 Red blood cell microscope images of 10 vol% solutions. Upper row illustrates cells in isotonic 1000 $\mu\text{S}/\text{cm}$ phosphate buffer saline medium. Before (a) and after (b) current measurement under 100 V DC for one minute in the absence of 320 μM Triton X-100. In the presence of 320 μM Triton X-100, RBCs before (c) and after (d) the measurement. Lower row illustrates RBC in plasma in the absence of Triton X-100 before (e) and after (f) the measurement. In the presence of 320 μM Triton X-100, before (g) and after (h) the measurement. Image contrast was adjusted to improve RBC resolvability.

To assess solubilization effects, RBCs were visualized microscopically for cell integrity in the presence and absence of 320 μM Triton X-100, before and after current measurements, and in PBS and plasma mediums as presented in Fig 5.3. For each case, RBC diameters were plotted in Fig 5.4 (a). No significant difference in shape and size of RBCs was observed in each medium. Further, cell counts of 0.1 vol % RBC solutions in presence of 320 μM Triton X-100 for one hour via the hemacytometer were reported in Fig-4 (b), which illustrates that hemolysis was minimal.

Surfactant-induced hemolysis and its rate depend on: i) surfactant molecules and concentrations, ii) lipid concentrations (RBC concentrations) [182-184], iii) medium conditions such as ionic strength, solute sizes, osmolarity, pH, and temperature, and iv) the presence of hemolysis inhibitors such as cholesterol, sucrose, glucose (dextrose),

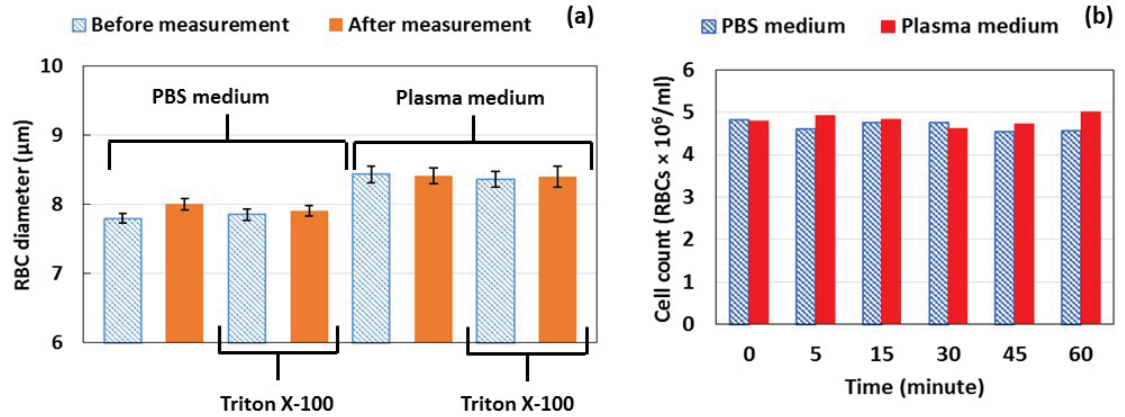


Figure 5.4 Effect of $320 \mu\text{M}$ Triton X-100 on red blood cell sizes and concentration. (a) Comparison of RBC sizes of 10 vol% solution in PBS and plasma, in the presence and absence of Triton X-100. Blue-hashed bars represent before and orange solid bars after current measurements under 100 V DC for one minute. Error bars represent the 95 % confidence intervals ($N = 69 \sim 117$). (b) RBC counts (0.1 vol%) measured via hemocytometer over time in the presence of Triton X-100.

etc.[184-189]. Due to variations in these parameters, it is difficult to make a direct comparison of our results with hemolysis literature, many of which are not consistent. Some Triton X-100 induced hemolysis quantitative results in PBS [180-182, 184] are reported. However, to achieve our desired $1000 \mu\text{S}/\text{cm}$ conductivity, dextrose was a main component of our isotonic PBS buffer (2.57 mM KH_2PO_4 , 2.57 mM K_2HPO_4 , 2.57 mM NaCl, 274.3 mM dextrose). Dextrose has been shown to inhibit hemolysis [184, 187, 188]. Thus, considering these factors, our result that hemolysis was not observed is consistent with parameters in prior literature. Further, these results indicate that $320 \mu\text{M}$ Triton X-100 is below D_t^{Sat} and does not compromise RBCs, while still preventing electrolysis and achieving a stable electrokinetic microdevice system.

5.3.4 HCT determination

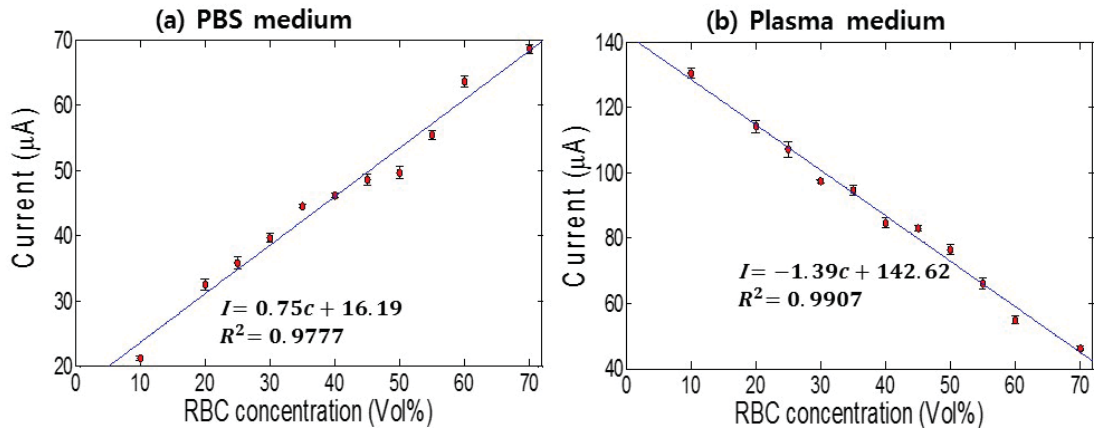


Figure 5.5 Current (I) within the microdevice versus RBC concentration in response to a 100 V DC applied potential. Average currents in (a) PBS medium and (b) plasma. Error bars represent 95 % confidence intervals ($N=4 \sim 12$).

The current response to a 100 V DC potential versus RBC concentration suspended in PBS and plasma were shown in Fig 5.5. The current response increases with RBC concentration in PBS medium while the current response decrease in plasma. It was hypothesized that RBCs would act as insulators due to their lipid membranes such that the solution resistance would increase and current would decrease as RBC concentration increased. The decrease in the current in plasma is consistent with prior AC impedance results [157, 158, 190]. Increases in the current in PBS medium might be ascribed to negatively charged RBC surfaces due to glycoproteins embedded in lipid bilayers [191]. Although RBC membranes are considered nonconductive, these glycoproteins may decrease PBS/solution resistance by adding surface conductivity within the simple salt/dextrose media. The PBS medium and reported plasma conductivities are 1000 and 10,000 $\mu\text{S}/\text{cm}$, respectively [173]. These trends then lead us to postulate that RBC surface conductivity contributions are higher than 1000 $\mu\text{S}/\text{cm}$ and lower than 10000

Table 5.1 Zeta potential of RBCs in PBS.

RBC	Zeta Potential (mV)
0.5 vol%	-34.9 ± 0.34
5 vol%	-17.2 ± 0.75
10 vol%	-19.7 ± 0.68

$\mu\text{S/cm}$. Measured conductivity of 1, 3, 7 vol% RBC solution in PBS were 1329, 1340, and 1596 $\mu\text{S/cm}$, respectively. As RBC concentration increased, conductivity of RBC solution in PBS increased.

The 95% confidence intervals of 45 and 50 vol% in Fig 5.5 (a) and 40 and 45 vol% in Fig 5.5 (b) overlap. In addition, the R^2 value for a linear trendline in plasma is 0.9907, but the fit to a linear trendline in PBS medium is slightly less at 0.9777. This suggests measurements in the PBS medium were less resolvable than those in plasma. With regards to measurement accuracy, minor blood cell aggregation is one potential measurement error. Blood cell associations were observed more often in PBS microchannels during current measurements; this is corroborated by images in Fig 5.3. As expected, plasma is a much better suspension fluid due to its greater buffering capacity and ability to support red blood cell health such that secondary cell effects are minimized. Zeta potential of RBCs in our PBS (2.57 mM KH_2PO_4 , 2.57 mM K_2HPO_4 , 2.57 mM NaCl, 274.3 mM dextrose) were reported in Table 5.1. Zeta potential of 0.5 vol% was -34.9 ± 0.34 mV. This is consistent with reported value -31.8 ± 1.1 mV in similar PBS medium (1.7 mM KH_2PO_4 , 5.2 mM Na_2HPO_4 , 150 mM NaCl) [160]. As

Table 5.2 Comparison of DC microfluidic HCT determination method against other method based on microhematocrit , HemataSTAT II, and ultrasound technology, UltraCrit™.

	HemataSTAT II	UltraCrit™	DC microfluidic
Linearity	16 – 60 % HCT	10.3 – 72.0 % HCT	10 – 70 % HCT
Precision	≤ 4.6 %	≤ 0.8 %	≤ 2.8 %
Accuracy	≤ 0.5 %	≤ 0.4 %	≤ 2.6 %

RBC concentration increased, zeta potential moved toward zero and the absolute values were less than 20. This indicated that RBC solution was not stable and RBC aggregation occurred.

The implications of the data in Fig 5.5 indicate that HCT can be determined by measuring current responses within a simple DC microchannel fluidic system. The tests were completed within one minute and consumed only 125 μ L of blood per measurement. This DC microfluidic system is a simplifying improvement over AC methods and current hematocrit POC devices. Measurement precision and accuracy in plasma medium were $\leq 2.8\%$ and $\leq 2.6\%$, respectively. The performance of our DC microfluidic device for HCT determination was compared with other methods; based on microhematocrit (HemataSTAT II) and ultrasound technology (UltraCrit™), in Table 5.2.

5.4 Concluding remarks

A simple DC current detection method within a microfluidic system for a POC HCT device was presented. Feasibility for HCT determination was shown via measuring

current responses of RBC suspensions in both synthetic PBS and plasma. Key operating parameters including electrolysis bubbles, irreversible red blood cell adsorption, and red blood cell sedimentation were optimized to enable these simple current-based hematocrit measurements. 320 μM Triton X-100 was added to all RBC/PBS or RBC/plasma suspensions to attenuate the production of electrolysis bubbles at electrode surfaces which destabilize the electric field. Control experiments directly confirmed that the added Triton-X100 did not compromise RBC integrity. Carbonized platinum wire electrodes had minimal fouling once they were coated via irreversible RBC adsorption; this improved electrode performance. Further, fluid transport occurred within the device. Current response measurement were performed for one minute before red blood cell sedimentation significantly effected current measurements.

In summary, electrokinetic microfluidic systems have begun to enable POC devices, although very few microfluidic/electrokinetic POC devices have been successfully commercialized. Those POC devices that have been commercialized are fairly complicated, yield sophisticated results, and have correspondingly high cost. This research has illustrated a very simple microfluidic system using battery accessible DC field harness able for an inexpensive, practical POC device.

5.5 Acknowledgements

The authors gratefully acknowledge help from Joe Halt, Zhichao Wang, and Maryam Khaksari for RBC sample preparation and valuable discussion. The authors also

gratefully acknowledge prior discussions and efforts years ago on this topic with Soumya Srivastava and David O. Wipf.

Chapter 6 Conclusion and ongoing work

The present dissertation has illustrated a new microfluidic system for an inexpensive and practical POC HCT device.

In order to improve the microfluidic system stability, surfactant additive (Triton X-100) was added to RBC solutions. Platinum electrode performance was improved by carbonizing electrode surfaces using RBCs. The feasibility of the microfluidic system for HCT determination was shown via current response measurement of RBC suspension in PBS and plasma medium over human HCT concentrations.

We aimed to simplify the microfluidic system to use as a platform for a POC HCT device. Compared to the microfluidic systems based on the conductivity method, the microfluidic system was drastically simplified by employing DC. The microfluidic system determines HCT within one minute and consumed only 125 μL blood sample.

In order to use the present microfluidic system as a POC HCT platform, some of modification are necessary. In the present dissertation, platinum electrode surfaces were coated by RBCs. The RBC layers on electrode surfaces increased effective surface area and minimized fouling and thus platinum electrode performance was significantly improved, as shown in Chapter 4. However, modification electrode surface using RBCs is very tedious and at risk of occupational exposure to bloodborne pathogens. We are investigating alternative materials to modify platinum electrode surfaces as the RBC layers. Some of results are shown in Chapter 4. As of now, only active carbon coated

platinum electrode showed improved performance. Various carbon materials, such as graphene, active carbons, and carbon fibers can be tried to modify platinum electrode surfaces.

Microfluidic technology has been considered a promising solution to develop inexpensive and reliable POC devices. However, it is not easy and simple to integrate the microfluidic technology into POC devices. This research aimed to develop a POC HCT device and faced problems of electrolysis bubble and poor platinum electrode performance. In order to develop POC devices for different purpose such as blood glucose or hemoglobin determination, researchers will encounter different challenges. It is a job and duty of researchers to solve these challenges.

References

1. Hurst, J.W., H.K. Walker, and W.D. Hall, *Clinical methods : the history, physical, and laboratory examinations*. 3rd ed. 1990, Boston: Butterworths. xxxi, 1087 p.
2. Fernandez, A.J. and N.A. Flaxman, *Common laboratory tests, values, and interpretations*. Special Care in Dentistry, 1985. **5**(6): p. 264-269.
3. van Assendelft, O.W. and U.S.N.C.f.C.L. Standards, *Procedure for Determining Packed Cell Volume by the Microhematocrit Method*. 1985: NCCLS.
4. Graham, M.D., *The Coulter Principle: Foundation of an Industry*. Journal of the Association for Laboratory Automation, 2003. **8**(6): p. 72-81.
5. Handin, R.I., S.E. Lux, and T.P. Stossel, *Blood: Principles and Practice of Hematology*. 2003: Lippincott Williams & Wilkins.
6. Van Slyke, D.D., et al., *CALCULATION OF HEMOGLOBIN FROM BLOOD SPECIFIC GRAVITIES*. Journal of Biological Chemistry, 1950. **183**(1): p. 349-360.
7. Myers, G.J. and J. Browne, *Point of care hematocrit and hemoglobin in cardiac surgery: a review*. Perfusion, 2007. **22**(3): p. 179-183.
8. Chin, C.D., V. Linder, and S.K. Sia, *Commercialization of microfluidic point-of-care diagnostic devices*. Lab on a Chip, 2012. **12**(12): p. 2118-2134.
9. Minerick, A.R., *The rapidly growing field of micro and nanotechnology to measure living cells*. AIChE Journal, 2008. **54**(9): p. 2230-2237.
10. Yi, C., et al., *Microfluidics technology for manipulation and analysis of biological cells*. Analytica Chimica Acta, 2006. **560**(1-2): p. 1-23.
11. Ohno, K.-i., K. Tachikawa, and A. Manz, *Microfluidics: Applications for analytical purposes in chemistry and biochemistry*. ELECTROPHORESIS, 2008. **29**(22): p. 4443-4453.
12. Mark, D., et al., *Microfluidic lab-on-a-chip platforms: requirements, characteristics and applications*. Chemical Society Reviews, 2010. **39**(3): p. 1153-1182.
13. Toner, M. and D. Irimia, *BLOOD-ON-A-CHIP*. Annual Review of Biomedical Engineering, 2005. **7**(1): p. 77-103.
14. Yager, P., et al., *Microfluidic diagnostic technologies for global public health*. Nature, 2006. **442**(7101): p. 412-418.
15. Gale, B.K., K.D. Caldwell, and A.B. Frazier, *Geometric scaling effects in electrical field flow fractionation. 2. Experimental results*. Analytical Chemistry, 2002. **74**(5): p. 1024-1030.
16. Waller, P.J., et al., *Evaluation of biological control of sheep parasites using Duddingtonia flagrans under commercial farming conditions on the island of Gotland, Sweden*. Veterinary Parasitology, 2004. **126**(3): p. 299-315.
17. Zourob, M., *Recognition Receptors in Biosensors*. 2010: Springer.
18. Atta, N.F., A. Galal, and R.A. Ahmed, *Poly(3,4-ethylene-dioxythiophene) electrode for the selective determination of dopamine in presence of sodium dodecyl sulfate*. Bioelectrochemistry, 2011. **80**(2): p. 132-141.
19. Marino, A. and A. Brajtertoth, *Ionic Surfactants as Molecular Spacers at Graphite-Electrodes*. Analytical Chemistry, 1993. **65**(4): p. 370-374.

20. Naka, K., et al. *Effect of nano stripe carbonized-polymer electrode on high S/N ratio in electrochemical detection*. in *Micro Electro Mechanical Systems, 2007. MEMS. IEEE 20th International Conference on*. 2007.
21. Zheng, S., M. Liu, and Y.-C. Tai, *Micro coulter counters with platinum black electroplated electrodes for human blood cell sensing*. *Biomedical Microdevices*, 2008. **10**(2): p. 221-231.
22. Wang, J., *Electrochemical detection for microscale analytical systems: a review*. *Talanta*, 2002. **56**(2): p. 223-231.
23. Lacher, N.A., et al., *Microchip capillary electrophoresis/ electrochemistry*. *ELECTROPHORESIS*, 2001. **22**(12): p. 2526-2536.
24. Bruin, G.J.M., *Recent developments in electrokinetically driven analysis on microfabricated devices*. *ELECTROPHORESIS*, 2000. **21**(18): p. 3931-3951.
25. Dolník, V., S. Liu, and S. Jovanovich, *Capillary electrophoresis on microchip*. *ELECTROPHORESIS*, 2000. **21**(1): p. 41-54.
26. McDonald, J.C., et al., *Fabrication of microfluidic systems in poly(dimethylsiloxane)*. *ELECTROPHORESIS*, 2000. **21**(1): p. 27-40.
27. Vandaveer, W.R., et al., *Recent developments in electrochemical detection for microchip capillary electrophoresis*. *ELECTROPHORESIS*, 2004. **25**(21-22): p. 3528-3549.
28. Ouyang, J., et al., *A rapid and sensitive method for hydroxyl radical detection on a microfluidic chip using an N-doped porous carbon nanofiber modified pencil graphite electrode*. *Analyst*, 2014. **139**(13): p. 3416-3422.
29. Nge, P.N., C.I. Rogers, and A.T. Woolley, *Advances in Microfluidic Materials, Functions, Integration, and Applications*. *Chemical Reviews*, 2013. **113**(4): p. 2550-2583.
30. Gencoglu, A. and A. Minerick, *Chemical and morphological changes on platinum microelectrode surfaces in AC and DC fields with biological buffer solutions*. *Lab on a Chip*, 2009. **9**(13): p. 1866-1873.
31. Frost, N.W. and M.T. Bowser, *Using buffer additives to improve analyte stream stability in micro free flow electrophoresis*. *Lab on a Chip*, 2010. **10**(10): p. 1231-1236.
32. Lee, H.Y., C. Barber, and A.R. Minerick, *Improving electrokinetic microdevice stability by controlling electrolysis bubbles*. *ELECTROPHORESIS*, 2014. **35**(12-13): p. 1782-1789.
33. Nakanishi, K., T. Sakiyama, and K. Imamura, *On the adsorption of proteins on solid surfaces, a common but very complicated phenomenon*. *Journal of Bioscience and Bioengineering*, 2001. **91**(3): p. 233-244.
34. *Electrochemical biosensors*. *Chemical Society Reviews*, 2010. **39**(5): p. 1747.
35. *Anodized aluminum oxide-based capacitance sensors for the direct detection of DNA hybridization*. *Biosensors and Bioelectronics*, 2010. **25**(7): p. 1592.
36. Giardi, C., et al., *Nonionic polyoxazoline surfactants based on renewable source: Synthesis, surface and bulk properties*. *Reactive & Functional Polymers*, 2009. **69**(9): p. 643-649.
37. Eigeldinger, J. and H. Vogt, *The bubble coverage of gas-evolving electrodes in a flowing electrolyte*. *Electrochimica Acta*, 2000. **45**(27): p. 4449-4456.
38. Huet, F., M. Musiani, and R.P. Nogueira, *Electrochemical noise analysis of O₂ evolution on PbO₂ and PbO₂-matrix composites containing Co or Ru oxides*. *Electrochimica Acta*, 2003. **48**(27): p. 3981-3989.

39. Zhang, D. and K. Zeng, *Evaluating the Behavior of Electrolytic Gas Bubbles and Their Effect on the Cell Voltage in Alkaline Water Electrolysis*. Industrial & Engineering Chemistry Research, 2012. **51**(42): p. 13825-13832.
40. Lubetkin, S., *The motion of electrolytic gas bubbles near electrodes*. Electrochimica Acta, 2002. **48**(4): p. 357-375.
41. Vogt, H. and R.J. Balzer, *The bubble coverage of gas-evolving electrodes in stagnant electrolytes*. Electrochimica Acta, 2005. **50**(10): p. 2073-2079.
42. Dey, D., et al., *Experimental comparisons with a numerical model of surfactant effects on the burst of a single bubble*. Chemical Engineering Science, 1997. **52**(16): p. 2769-2783.
43. Minerick, A.R., A.E. Ostafin, and H.-C. Chang, *Electrokinetic transport of red blood cells in microcapillaries*. ELECTROPHORESIS, 2002. **23**(14): p. 2165-2173.
44. Erlandsson, P.G. and N.D. Robinson, *Electrolysis-reducing electrodes for electrokinetic devices*. Electrophoresis, 2011. **32**(6-7): p. 784-790.
45. Uhlig, H.H., *The Solubilities of Gases and Surface Tension*. The Journal of Physical Chemistry, 1937. **41**(9): p. 1215-1226.
46. *Advancement in carbon nanotubes: basics, biomedical applications and toxicity : Biomedical applications of carbon nanotubes*. Journal of Pharmacy and Pharmacology, 2010: p. no.
47. Brandon, N.P. and G.H. Kelsall, *Growth kinetics of bubbles electrogenerated at microelectrodes*. Journal of Applied Electrochemistry, 1985. **15**(4): p. 475-484.
48. Kocha, S.S., et al., *Photoelectrochemical decomposition of water utilizing monolithic tandem cells*. Solar Energy Materials and Solar Cells, 1998. **52**(3-4): p. 389-397.
49. Giribabu, K. and P. Ghosh, *Adsorption of nonionic surfactants at fluid-fluid interfaces: Importance in the coalescence of bubbles and drops*. Chemical Engineering Science, 2007. **62**(11): p. 3057-3067.
50. Lichtenberg, D., E. Opatowski, and M.M. Kozlov, *Phase boundaries in mixtures of membrane-forming amphiphiles and micelle-forming amphiphiles*. Biochimica et Biophysica Acta (BBA) - Biomembranes, 2000. **1508**(1-2): p. 1-19.
51. Racker, E., [76] *Reconstitution of membrane processes*, in *Methods in Enzymology*, L.P. Sidney Fleischer, Editor. 1979, Academic Press. p. 699-711.
52. Lichtenberg, D., et al., *Detergent solubilization of lipid bilayers: a balance of driving forces*. Trends in biochemical sciences, 2013. **38**(2): p. 85-93.
53. Linke, D., *Chapter 34 Detergents: An Overview*, in *Methods in Enzymology*, R.B. Richard and P.D. Murray, Editors. 2009, Academic Press. p. 603-617.
54. Fonslow, B.R. and M.T. Bowser, *Free-flow electrophoresis on an anodic bonded glass microchip*. Analytical Chemistry, 2005. **77**(17): p. 5706-5710.
55. Zhang, C.-X. and A. Manz, *High-Speed Free-Flow Electrophoresis on Chip*. Analytical Chemistry, 2003. **75**(21): p. 5759-5766.
56. Raymond, D.E., A. Manz, and H.M. Widmer, *Continuous Sample Pretreatment Using a Free-Flow Electrophoresis Device Integrated onto a Silicon Chip*. Analytical Chemistry, 1994. **66**(18): p. 2858-2865.
57. Kohlheyer, D., et al., *Miniaturizing free-flow electrophoresis – a critical review*. ELECTROPHORESIS, 2008. **29**(5): p. 977-993.

58. Albrecht, J.W. and K.F. Jensen, *Micro free-flow IEF enhanced by active cooling and functionalized gels*. ELECTROPHORESIS, 2006. **27**(24): p. 4960-4969.
59. Kohlheyer, D., et al., *Microfluidic High-Resolution Free-Flow Isoelectric Focusing*. Analytical Chemistry, 2007. **79**(21): p. 8190-8198.
60. Fonslow, B.R., V.H. Barocas, and M.T. Bowser, *Using Channel Depth To Isolate and Control Flow in a Micro Free-Flow Electrophoresis Device*. Analytical Chemistry, 2006. **78**(15): p. 5369-5374.
61. Kohlheyer, D., et al., *Bubble-Free Operation of a Microfluidic Free-Flow Electrophoresis Chip with Integrated Pt Electrodes*. Analytical Chemistry, 2008. **80**(11): p. 4111-4118.
62. Mohammad, A. and S.A. Bhawani, *On Plate Resolution and Identification of Three-Component Mixture of Nonionic Surfactants*. Tenside Surfactants Detergents, 2009. **46**(2): p. 81-84.
63. Gavan, S.A., et al., *Effects Induced by Ethoxylated Nonionic Surfactants on Pyrene-Labeled Hydroxypropyl Cellulose in Aqueous Solution*. Revue Roumaine De Chimie, 2009. **54**(3): p. 227-234.
64. Acosta, E.J. and A.S. Bhakta, *The HLD-NAC Model for Mixtures of Ionic and Nonionic Surfactants*. Journal of Surfactants and Detergents, 2009. **12**(1): p. 7-19.
65. Cong, Z.H., et al., *Effects of different nonionic surfactants on in vitro fermentation characteristics of cereal straws*. Journal of Animal Science, 2009. **87**(3): p. 1085-1096.
66. Armstrong, F.A., H.A.O. Hill, and N.J. Walton, *Direct electrochemistry of redox proteins*. Accounts of Chemical Research, 1988. **21**(11): p. 407-413.
67. Floate, S., et al., *A sonotrode for electroanalysis: the determination of copper in passivating media*. Analyst, 2002. **127**(8): p. 1094-1099.
68. Fulian, Q. and R.G. Compton, *Laser activated voltammetry: application to the determination of phenol in aqueous solution at a glassy carbon electrode*. Analyst, 2000. **125**(3): p. 531-534.
69. Tsai, Y.-C., et al., *Microwave Activation of Electrochemical Processes: Square-Wave Voltammetric Stripping Detection of Cadmium in the Presence of the Surfactant Triton X*. Electroanalysis, 2001. **13**(8-9): p. 639-645.
70. *Biofunctionalization of nanoparticles for cytosensing and cell surface carbohydrate assay*. Journal of Materials Chemistry, 2011. **21**(45): p. 18154.
71. Tsai-Mu, C., et al., *Human haptoglobin phenotypes and concentration determination by nanogold-enhanced electrochemical impedance spectroscopy*. Nanotechnology, 2011. **22**(24): p. 245105.
72. *Nanotubes-/nanowires-based, microfluidic-integrated transistors for detecting biomolecules*. Microfluidics and Nanofluidics, 2010.
73. Ren, X.H., et al., *Nonionic surfactants, are strong inhibitors of cytochrome P450 3A biotransformation activity in vitro and in vivo*. European Journal of Pharmaceutical Sciences, 2009. **36**(4-5): p. 401-411.
74. 2013: p. 193.
75. *Detection of IFN- γ for latent tuberculosis diagnosis using an anodized aluminum oxide-based capacitive sensor*. Biosensors and Bioelectronics, 2013.
76. *Rapid and specific electrochemical detection of prostate cancer cells using an aperture sensor array*. Lab on a Chip, 2013. **13**(5): p. 940.

77. Rusling, J.F. and A.E.F. Nassar, *Enhanced electron transfer for myoglobin in surfactant films on electrodes*. Journal of the American Chemical Society, 1993. **115**(25): p. 11891-11897.
78. 2012: p. 125.
79. Hoyer, B. and N. Jensen, *Suppression of protein interferences in anodic stripping voltammetry by sodium dodecyl sulphate*. Electrochemistry Communications, 2003. **5**(3): p. 257-261.
80. Hoyer, B. and N. Jensen, *Suppression of surfactant interferences in anodic stripping voltammetry by sodium dodecyl sulfate*. Electrochemistry Communications, 2003. **5**(9): p. 759-764.
81. Chattopadhyay, K. and S. Mazumdar, *Direct electrochemistry of heme proteins: effect of electrode surface modification by neutral surfactants*. Bioelectrochemistry, 2001. **53**(1): p. 17-24.
82. Marino, A. and A. Brajter-Toth, *Ionic surfactants as molecular spacers at graphite electrodes*. Analytical Chemistry, 1993. **65**(4): p. 370-374.
83. Hoyer, B. and N. Jensen, *Stabilization of the voltammetric serotonin signal by surfactants*. Electrochemistry Communications, 2006. **8**(2): p. 323-328.
84. Hoyer, B. and N. Jensen, *Use of sodium dodecyl sulfate as an antifouling and homogenizing agent in the direct determination of heavy metals by anodic stripping voltammetry*. Analyst, 2004. **129**(8): p. 751-754.
85. Atta, N.F., et al., *Characterization and electrochemical investigations of micellar/drug interactions*. Electrochimica Acta, 2011. **56**(5): p. 2510-2517.
86. Marcus, R.A., *Chemical and Electrochemical Electron-Transfer Theory*. Annual Review of Physical Chemistry, 1964. **15**(1): p. 155-196.
87. Vittal, R., H. Gomathi, and K.J. Kim, *Beneficial role of surfactants in electrochemistry and in the modification of electrodes*. Advances in Colloid and Interface Science, 2006. **119**(1): p. 55-68.
88. Ye, J. and R.P. Baldwin, *Determination of carbohydrates, sugar acids and alditols by capillary electrophoresis and electrochemical detection at a copper electrode*. Journal of Chromatography A, 1994. **687**(1): p. 141-148.
89. Schwarz, M.A., et al., *A two-electrode configuration for simplified amperometric detection in a microfabricated electrophoretic separation device*. Analyst, 2001. **126**(2): p. 147-151.
90. Cataldi, T.R.I., et al., *Study of a cobalt-based surface modified glassy carbon electrode: Electrocatalytic oxidation of sugars and alditols*. Electroanalysis, 1995. **7**(4): p. 305-311.
91. Cataldi, T.R.I., et al., *Cobalt-based glassy carbon chemically modified electrode for constant-potential amperometric detection of carbohydrates in flow-injection analysis and liquid chromatography*. Analytica Chimica Acta, 1992. **270**(1): p. 161-171.
92. Wang, J. and Z. Taha, *Catalytic oxidation and flow detection of carbohydrates at ruthenium dioxide modified electrodes*. Analytical Chemistry, 1990. **62**(14): p. 1413-1416.
93. Gawron, A.J., R.S. Martin, and S.M. Lunte, *Fabrication and evaluation of a carbon-based dual-electrode detector for poly(dimethylsiloxane) electrophoresis chips*. ELECTROPHORESIS, 2001. **22**(2): p. 242-248.

94. Kissinger, P. and W.R. Heineman, *Laboratory Techniques in Electroanalytical Chemistry, Second Edition, Revised and Expanded*. 1996: Taylor & Francis.
95. Chen, Z., et al., *Vacuum-assisted thermal bonding of plastic capillary electrophoresis microchip imprinted with stainless steel template*. *Journal of Chromatography A*, 2004. **1038**(1–2): p. 239-245.
96. Bao, N., et al., *Electrochemical detector for microchip electrophoresis of poly(dimethylsiloxane) with a three-dimensional adjustor*. *Journal of Chromatography A*, 2004. **1041**(1–2): p. 245-248.
97. Martin, R.S., et al., *Carbon paste-based electrochemical detectors for microchip capillary electrophoresis/electrochemistry*. *Analyst*, 2001. **126**(3): p. 277-280.
98. Wang, J., G. Chen, and M. Pumera, *Microchip Separation and Electrochemical Detection of Amino Acids and Peptides Following Precolumn Derivatization with Naphthalene-2,3-dicarboxyaldehyde*. *Electroanalysis*, 2003. **15**(10): p. 862-865.
99. Muck, A., et al., *Fabrication of Poly(methyl methacrylate) Microfluidic Chips by Atmospheric Molding*. *Analytical Chemistry*, 2004. **76**(8): p. 2290-2297.
100. Lim, T.-K., H. Ohta, and T. Matsunaga, *Microfabricated On-Chip-Type Electrochemical Flow Immunoassay System for the Detection of Histamine Released in Whole Blood Samples*. *Analytical Chemistry*, 2003. **75**(14): p. 3316-3321.
101. Baldwin, R.P., *Electrochemical determination of carbohydrates: Enzyme electrodes and amperometric detection in liquid chromatography and capillary electrophoresis*. *Journal of Pharmaceutical and Biomedical Analysis*, 1999. **19**(1–2): p. 69-81.
102. Choong, C.-L., W. Milne, and K.K. Teo, *Review: carbon nanotube for microfluidic lab-on-a-chip application*. *International Journal of Material Forming*, 2008. **1**(2): p. 117-125.
103. Hoyer, B., N. Jensen, and L.P. Busch, *Effect of the Pretreatment of Recast Nafion Membranes on Their Rejection of the Albumin Interference in Anodic Stripping Voltammetry*. *Electroanalysis*, 2001. **13**(10): p. 843-848.
104. Wang, J., et al., *Capillary Electrophoresis Chips with Thick-Film Amperometric Detectors: Separation and Detection of Hydrazine Compounds*. *Electroanalysis*, 2000. **12**(9): p. 691-694.
105. Liu, J., et al., *Detection of Hydrazine, Methylhydrazine, and Isoniazid by Capillary Electrophoresis with a Palladium-Modified Microdisk Array Electrode*. *Analytical Chemistry*, 1996. **68**(19): p. 3350-3353.
106. Pumera, M., et al., *Direct voltammetric determination of gold nanoparticles using graphite-epoxy composite electrode*. *Electrochimica Acta*, 2005. **50**(18): p. 3702-3707.
107. Pumera, M., A. Merkoçi, and S. Alegret, *Microchip Capillary Electrophoresis-Electrochemistry with Rigid Graphite-Epoxy Composite Detector*. *Electroanalysis*, 2006. **18**(2): p. 207-210.
108. *Electrodeposition of Supported Gadolinium-Doped Ceria Solid Solution Nanowires*. *Journal of The Electrochemical Society*, 2012. **159**(5): p. E108.
109. *Metallic ions as therapeutic agents in tissue engineering scaffolds: an overview of their biological applications and strategies for new developments*. *Journal of The Royal Society Interface*, 2012. **9**(68): p. 401.
110. Wang, J., *Carbon-Nanotube Based Electrochemical Biosensors: A Review*. *Electroanalysis*, 2005. **17**(1): p. 7-14.

111. Merkoçi, A., et al., *New materials for electrochemical sensing VI: Carbon nanotubes*. TrAC Trends in Analytical Chemistry, 2005. **24**(9): p. 826-838.
112. Deo, R.P. and J. Wang, *Electrochemical detection of carbohydrates at carbon-nanotube modified glassy-carbon electrodes*. Electrochemistry Communications, 2004. **6**(3): p. 284-287.
113. Ye, J.-S., et al., *Nonenzymatic glucose detection using multi-walled carbon nanotube electrodes*. Electrochemistry Communications, 2004. **6**(1): p. 66-70.
114. Wang, J., et al., *Carbon-nanotube/copper composite electrodes for capillary electrophoresis microchip detection of carbohydrates*. Analyst, 2004. **129**(6): p. 512-515.
115. Musameh, M., et al., *Low-potential stable NADH detection at carbon-nanotube-modified glassy carbon electrodes*. Electrochemistry Communications, 2002. **4**(10): p. 743-746.
116. Wang, Y., Q. Li, and S. Hu, *A multiwall carbon nanotubes film-modified carbon fiber ultramicroelectrode for the determination of nitric oxide radical in liver mitochondria*. Bioelectrochemistry, 2005. **65**(2): p. 135-142.
117. Pumera, M., A. Merkoçi, and S. Alegret, *Carbon nanotube detectors for microchip CE: Comparative study of single-wall and multiwall carbon nanotube, and graphite powder films on glassy carbon, gold, and platinum electrode surfaces*. ELECTROPHORESIS, 2007. **28**(8): p. 1274-1280.
118. Valentini, F., et al., *Carbon nanotubes as electrode materials for the assembling of new electrochemical biosensors*. Sensors and Actuators B: Chemical, 2004. **100**(1-2): p. 117-125.
119. Pedano, M., et al., *Adsorption and electrooxidation of nucleic acids at carbon nanotubes paste electrodes*. Electrochemistry Communications, 2004. **6**(1): p. 10-16.
120. Yi, C.Q., et al., *Microfluidics technology for manipulation and analysis of biological cells*. Analytica Chimica Acta, 2006. **560**(1-2): p. 1-23.
121. Ohno, K., K. Tachikawa, and A. Manz, *Microfluidics: Applications for analytical purposes in chemistry and biochemistry*. Electrophoresis, 2008. **29**(22): p. 4443-4453.
122. Shipley, J.W., *THE ALTERNATING CURRENT ELECTROLYSIS OF WATER*. Canadian Journal of Research, 1929. **1**(4): p. 305-358.
123. Minerick, A.R., A.E. Ostafin, and H.C. Chang, *Electrokinetic transport of red blood cells in microcapillaries*. Electrophoresis, 2002. **23**(14): p. 2165-2173.
124. Landolt, D., et al., *An Optical Study of Cathodic Hydrogen Evolution in High-Rate Electrolysis*. Journal of The Electrochemical Society, 1970. **117**(6): p. 839-845.
125. Engstrom, R.C., *Comprehensive Treatise of Electrochemistry, Vol 6, Electrode Transport - Yeager, E, Bockris, Jo, Conway, Be, Sarangapani, S*. Journal of the American Chemical Society, 1983. **105**(24): p. 7211-7212.
126. Zhang, C.X. and A. Manz, *High-speed free-flow electrophoresis on chip*. Analytical Chemistry, 2003. **75**(21): p. 5759-5766.
127. Kohlheyer, D., et al., *Miniaturizing free-flow electrophoresis - a critical review*. Electrophoresis, 2008. **29**(5): p. 977-993.
128. Kohlheyer, D., et al., *Free-flow zone electrophoresis and isoelectric focusing using a microfabricated glass device with ion permeable membranes*. Lab on a Chip, 2006. **6**(3): p. 374-380.

129. Albrecht, J.W. and K.F. Jensen, *Micro free-flow IEF enhanced by active cooling and functionalized gels*. Electrophoresis, 2006. **27**(24): p. 4960-4969.
130. Kobayashi, H., et al., *Free-flow electrophoresis in a microfabricated chamber with a micromodule fraction separator - Continuous separation of proteins*. Journal of Chromatography A, 2003. **990**(1-2): p. 169-178.
131. Dominguez, A., et al., *Determination of critical micelle concentration of some surfactants by three techniques*. Journal of Chemical Education, 1997. **74**(10): p. 1227-1231.
132. Xu, B., et al., *Line laser beam based laser-induced fluorescence detection system for microfluidic chip electrophoresis analysis*. Sensors and Actuators A: Physical, 2009. **152**(2): p. 168-175.
133. Effenhauser, C.S., et al., *Integrated Capillary Electrophoresis on Flexible Silicone Microdevices: Analysis of DNA Restriction Fragments and Detection of Single DNA Molecules on Microchips*. Analytical Chemistry, 1997. **69**(17): p. 3451-3457.
134. Bouazaze, H., et al., *Electrochemical noise study of the effect of electrode surface wetting on the evolution of electrolytic hydrogen bubbles*. Journal of Electroanalytical Chemistry, 2006. **597**(1): p. 60-68.
135. Bunton, C.A., et al., *Ion binding and reactivity at charged aqueous interfaces*. Accounts of Chemical Research, 1991. **24**(12): p. 357-364.
136. Rosen, M.J., *Surfactants and interfacial phenomena*. 1978, New York: Wiley. xiv, 304 p.
137. Duerr-Auster, N., et al., *Binary coalescence of gas bubbles in the presence of a non-ionic surfactant*. Journal of Colloid and Interface Science, 2009. **333**(2): p. 579-584.
138. Janczuk, B., et al., *The Adsorption of Triton X-100 at the Air-Aqueous Solution Interface*. Langmuir, 1995. **11**(11): p. 4515-4518.
139. Yeager, E., *Comprehensive Treatise of Electrochemistry: Electrodictics, : transport*. 1983: Plenum.
140. Yeo, L.Y., et al., *Microfluidic Devices for Bioapplications*. Small, 2011. **7**(1): p. 12-48.
141. Whitesides, G.M., *The origins and the future of microfluidics*. Nature, 2006. **442**(7101): p. 368-373.
142. Nassar, A.E.F., W.S. Willis, and J.F. Rusling, *Electron-Transfer from Electrodes to Myoglobin - Facilitated in Surfactant Films and Blocked by Adsorbed Biomacromolecules*. Analytical Chemistry, 1995. **67**(14): p. 2386-2392.
143. YeoHeung, Y., et al., *Electrochemical impedance measurement of prostate cancer cells using carbon nanotube array electrodes in a microfluidic channel*. Nanotechnology, 2007. **18**(46): p. 465505.
144. Zhang, L.L. and X.S. Zhao, *Carbon-based materials as supercapacitor electrodes*. Chemical Society Reviews, 2009. **38**(9): p. 2520-2531.
145. Pandolfo, A.G. and A.F. Hollenkamp, *Carbon properties and their role in supercapacitors*. Journal of Power Sources, 2006. **157**(1): p. 11-27.
146. Kang, X., et al., *Glucose Oxidase-graphene-chitosan modified electrode for direct electrochemistry and glucose sensing*. Biosensors and Bioelectronics, 2009. **25**(4): p. 901-905.
147. Keefer, E.W., et al., *Carbon nanotube coating improves neuronal recordings*. Nat Nano, 2008. **3**(7): p. 434-439.

148. Chen, Y., et al., *Electrophoretic deposition of graphene nanosheets on nickel foams for electrochemical capacitors*. Journal of Power Sources, 2010. **195**(9): p. 3031-3035.
149. Zhang, H., et al., *One-Step Electrophoretic Deposition of Reduced Graphene Oxide and Ni(OH)₂ Composite Films for Controlled Syntheses Supercapacitor Electrodes*. The Journal of Physical Chemistry B, 2012. **117**(6): p. 1616-1627.
150. Choi, H., et al., *Graphene counter electrodes for dye-sensitized solar cells prepared by electrophoretic deposition*. Journal of Materials Chemistry, 2011. **21**(21): p. 7548-7551.
151. Zhang, D.W., et al., *Graphene-based counter electrode for dye-sensitized solar cells*. Carbon, 2011. **49**(15): p. 5382-5388.
152. Long, J.W., et al., *Three-Dimensional Battery Architectures*. Chemical Reviews, 2004. **104**(10): p. 4463-4492.
153. Abdel-Rahem, R. and A.S. Ayesh, *Surface activity of newly nonionic surfactants at air/water interface and their interaction with clay and teflon*. Tenside Surfactants Detergents, 2008. **45**(3): p. 137-143.
154. Lu, J., et al., *Stable Aqueous Suspension and Self-Assembly of Graphite Nanoplatelets Coated with Various Polyelectrolytes*. Journal of Nanomaterials, 2010. **2010**: p. 11.
155. Besra, L., et al., *Experimental verification of pH localization mechanism of particle consolidation at the electrode/solution interface and its application to pulsed DC electrophoretic deposition (EPD)*. Journal of the European Ceramic Society, 2010. **30**(5): p. 1187-1193.
156. Ammam, M., *Electrophoretic deposition under modulated electric fields: a review*. RSC Advances, 2012. **2**(20): p. 7633-7646.
157. HIRSCH, F.G., et al., *THE ELECTRICAL CONDUCTIVITY OF BLOOD: I. RELATIONSHIP TO ERYTHROCYTE CONCENTRATION*. Blood, 1950. **5**(11): p. 1017-1035.
158. Zhao, T.-X., *Electrical impedance and haematocrit of human blood with various anticoagulants*. Physiological Measurement, 1993. **14**(3): p. 299.
159. Varaprath, S., C.L. Frye, and J. Hamelink, *Aqueous solubility of permethylsiloxanes (silicones)*. Environmental Toxicology and Chemistry, 1996. **15**(8): p. 1263-1265.
160. Bondar, O.V., et al., *Monitoring of the Zeta Potential of Human Cells upon Reduction in Their Viability and Interaction with Polymers*. Acta Naturae, 2012. **4**(1): p. 78-81.
161. Chavez-Valdez, A., M.S.P. Shaffer, and A.R. Boccaccini, *Applications of Graphene Electrophoretic Deposition. A Review*. The Journal of Physical Chemistry B, 2012. **117**(6): p. 1502-1515.
162. Nguyen, K.T., *Evaluation of the ultracrit device for measuring blood donor hematocrit*. Transfusion, 2005. **45**(3): p. 167A.
163. Jandl, J.H., *Blood: Textbook of Hematology*. 1987: Little, Brown.
164. Rippmann, *HEMOCUE AN ACCURATE BEDSIDE METHOD OF HEMOGLOBIN MEASUREMENT?* Journal of clinical monitoring, 1997. **13**(6): p. 373-377.
165. Cable, R.G., *Hemoglobin determination in blood donors*. Transfusion Medicine Reviews, 1995. **9**(2): p. 131-144.
166. Hassan, U., et al., *Flow metering characterization within an electrical cell counting microfluidic device*. Lab on a Chip, 2014. **14**(8): p. 1469-1476.
167. Okada, R.H. and H.P. Schwan, *An Electrical Method to Determine Hematocrits*. Medical Electronics, IRE Transactions on, 1960. **ME-7**(3): p. 188-192.

168. Rosenthal, R.L. and C.W. Tobias, *Measurement of the electric resistance of human blood; use in coagulation studies and cell volume determinations*. The Journal of laboratory and clinical medicine, 1948. **33**(9): p. 1110-22.
169. Geddes, L.A. and C. Sadler, *The specific resistance of blood at body temperature*. Medical and biological engineering, 1973. **11**(3): p. 336-339.
170. Hill, D.W. and F.D. Thompson, *The effect of haematocrit on the resistivity of human blood at 37°C and 100 kHz*. Medical and biological engineering, 1975. **13**(2): p. 182-186.
171. Mohapatra, S.N. and D.W. Hill, *The changes in blood resistivity with haematocrit and temperature*. European journal of intensive care medicine, 1975. **1**(4): p. 153-162.
172. Sandberg, K., B.-A. Sjoqvist, and T. Olsson, *Relation Between Blood Resistivity and Hematocrit in Fresh Human Fetal Blood*. Pediatr Res, 1981. **15**(6): p. 964-966.
173. Burger, H.C. and J.B. van Milaan, *Measurements of the specific Resistance of the human Body to direct Current*. Acta Medica Scandinavica, 1943. **114**(6): p. 584-607.
174. Burger, H.C. and D. van, *Specific electric resistance of body tissues*. Phys Med Biol, 1961. **5**: p. 431-47.
175. Cole, K.S., *Membranes, Ions, and Impulses: A Chapter of Classical Biophysics*. 1968: University of California Press.
176. Zhao, T.-X., B. Jacobson, and T. Ribbe, *Triple-frequency method for measuring blood impedance*. Physiological Measurement, 1993. **14**(2): p. 145.
177. SCHWAN, H.P. and C.F. KAY, *Specific Resistance of Body Tissues*. Circulation Research, 1956. **4**(6): p. 664-670.
178. McClendon, J.F., *COLLOIDAL PROPERTIES OF THE SURFACE OF THE LIVING CELL: I. CONDUCTIVITY OF BLOOD TO DIRECT ELECTRIC CURRENTS*. Journal of Biological Chemistry, 1926. **68**(3): p. 653-663.
179. Wilson, T.M., *The Conductivity of Blood in Coagulation*. Biochem. J., 1907. **2**(7-8): p. 377-0.
180. Preté, P.S.C., et al., *Multiple stages of detergent-erythrocyte membrane interaction—A spin label study*. Biochimica et Biophysica Acta (BBA) - Biomembranes, 2011. **1808**(1): p. 164-170.
181. Rodi, P.M., V.M. Trucco, and A.M. Gennaro, *Factors determining detergent resistance of erythrocyte membranes*. Biophysical Chemistry, 2008. **135**(1–3): p. 14-18.
182. Preté, P.S.C., et al., *Quantitative assessment of human erythrocyte membrane solubilization by Triton X-100*. Biophysical Chemistry, 2002. **97**(1): p. 1-5.
183. Rodi, P.M., et al., *Comparative study of the interaction of CHAPS and Triton X-100 with the erythrocyte membrane*. Biochimica et Biophysica Acta (BBA) - Biomembranes, 2014. **1838**(3): p. 859-866.
184. Shalel, S., S. Streichman, and A. Marmur, *The Mechanism of Hemolysis by Surfactants: Effect of Solution Composition*. Journal of Colloid and Interface Science, 2002. **252**(1): p. 66-76.
185. Isomaa, B., A.C. Engblom, and H. Hägerstrand, *On the time-dependence of amphiphile-induced haemolysis*. Toxicology, 1988. **48**(3): p. 285-291.
186. Bielawski, J., *Two types of haemolytic activity of detergents*. Biochimica et Biophysica Acta (BBA) - General Subjects, 1990. **1035**(2): p. 214-217.
187. Ponder, E., *Hemolysis and related phenomena*. 1948: Grune & Stratton.

188. Rideal, E. and F.H. Taylor, *On Haemolysis and Haemolytic Acceleration*. Proceedings of the Royal Society of London. Series B - Biological Sciences, 1958. **148**(933): p. 450-464.
189. Huntley, J.S. and A.C. Hall, *Aspects of the haemolytic reaction induced by Kanagawa haemolysin of Vibrio parahaemolyticus*. Toxicon, 1994. **32**(11): p. 1397-1412.
190. Geddes, L.A. and L.E. Baker, *The specific resistance of biological material—A compendium of data for the biomedical engineer and physiologist*. Medical and biological engineering, 1967. **5**(3): p. 271-293.
191. Fernandes, H.P., C.L. Cesar, and M.d.L. Barjas-Castro, *Electrical properties of the red blood cell membrane and immunohematological investigation*. Revista Brasileira de Hematologia e Hemoterapia, 2011. **33**: p. 297-301.

APPENDIX PROOFS OF PERMISSION TO REPRODUCE PUBLISHED MATERIAL

The proofs for the reproduced material are attached as follows:

1. Permission for reproduced figure 1.1 in Chapter 1
2. Permission for reproduced figure 1.2 in Chapter 1
3. Permission for reproduced article in Chapter 3

----- This is a License Agreement between Hwi Yong Lee ("You") and John Wiley and Sons ("John Wiley and Sons") provided by Copyright Clearance Center ("CCC"). The license consists of your order details, the terms and conditions provided by John Wiley and Sons, and the payment terms and conditions.

All payments must be made in full to CCC. For payment instructions, please see information listed at the bottom of this form. License Number 3495530445002 License date Oct 24, 2014 Licensed content publisher John Wiley and Sons Licensed content publication Electrophoresis Licensed content title Improving electrokinetic microdevice stability by controlling electrolysis bubbles Licensed copyright line © 2014 WILEY-VCH Verlag GmbH & Co. KGaA, Weinheim Licensed content author Hwi Yong Lee, Cedrick Barber, Adrienne R. Minerick Licensed content date Apr 15, 2014 Start page 1782 End page 1789 Type of use Dissertation/Thesis Requestor type Author of this Wiley article Format Electronic Portion Figure/table Number of figures/tables 1 Original Wiley figure/table number(s) Fig-3 Will you be translating? No Title of your thesis / dissertation New microfluidic system to increase robustness and develop point-of-care hematocrit device Expected completion date Nov 2014 Expected size (number of pages) 200 Total 0.00 USD Terms and Conditions *TERMS AND CONDITIONS* This copyrighted material is owned by or exclusively licensed to John Wiley & Sons, Inc. or one of its group companies (each a "Wiley Company") or handled on behalf of a society with which a Wiley Company has exclusive publishing rights in relation to a particular work (collectively "WILEY"). By clicking i

½accepti½ in connection with completing this licensing transaction, you agree that the following terms and conditions apply to this transaction (along with the billing and payment terms and conditions established by the Copyright Clearance Center Inc., ("CCC's Billing and Payment terms and conditions"), at the time that you opened your Rightslink account (these are available at any time at <http://myaccount.copyright.com>). *Terms and Conditions* * The materials you have requested permission to reproduce or reuse (the "Wiley Materials") are protected by copyright. * You are hereby granted a personal, non-exclusive, non-sub licensable (on a stand-alone basis), non-transferable, worldwide, limited license to reproduce the Wiley Materials for the purpose specified in the licensing process. This license is for a one-time use only and limited to any maximum distribution number specified in the license. The first instance of republication or reuse granted by this licence must be completed within two years of the date of the grant of this licence (although copies prepared before the end date may be distributed thereafter). The Wiley Materials shall not be used in any other manner or for any other purpose, beyond what is granted in the license. Permission is granted subject to an appropriate

acknowledgement given to the author, title of the material/book/journal and the publisher. You shall also duplicate the copyright notice that appears in the Wiley publication in your use of the Wiley Material. Permission is also granted on the understanding that nowhere in the text is a previously published source acknowledged for all or part of this Wiley Material. Any third party content is expressly excluded from this permission. * With respect to the Wiley Materials, all rights are reserved. Except as expressly granted by the terms of the license, no part of the Wiley Materials may be copied, modified, adapted (except for minor reformatting required by the new Publication), translated, reproduced, transferred or distributed, in any form or by any means, and no derivative works may be made based on the Wiley Materials without the prior permission of the respective copyright owner. You may not alter, remove or suppress in any manner any copyright, trademark or other notices displayed by the Wiley Materials. You may not license, rent, sell, loan, lease, pledge, offer as security, transfer or assign the Wiley Materials on a stand-alone basis, or any of the rights granted to you hereunder to any other person. * The Wiley Materials and all of the intellectual property rights therein shall at all times remain the exclusive property of John Wiley & Sons Inc, the Wiley Companies, or their respective licensors, and your interest therein is only that of having possession of and the right to reproduce the Wiley Materials pursuant to Section 2 herein during the continuance of this Agreement. You agree that you own no right, title or interest in or to the Wiley Materials or any of the intellectual property rights therein. You shall have no rights hereunder other than the license as provided for above in Section 2. No right, license or interest to any trademark, trade name, service mark or other branding ("Marks") of WILEY or its licensors is granted hereunder, and you agree that you shall not assert any such right, license or interest with respect thereto. * NEITHER WILEY NOR ITS LICENSORS MAKES ANY WARRANTY OR REPRESENTATION OF ANY KIND TO YOU OR ANY THIRD PARTY, EXPRESS, IMPLIED OR STATUTORY, WITH RESPECT TO THE MATERIALS OR THE ACCURACY OF ANY INFORMATION CONTAINED IN THE MATERIALS, INCLUDING, WITHOUT LIMITATION, ANY IMPLIED WARRANTY OF MERCHANTABILITY, ACCURACY, SATISFACTORY QUALITY, FITNESS FOR A PARTICULAR PURPOSE, USABILITY, INTEGRATION OR NON-INFRINGEMENT AND ALL SUCH WARRANTIES ARE HEREBY EXCLUDED BY WILEY AND ITS LICENSORS AND WAIVED

BY YOU * WILEY shall have the right to terminate this Agreement immediately upon breach of this Agreement by you. * You shall indemnify, defend and hold harmless WILEY, its Licensors and their respective directors, officers, agents and employees, from and against any actual or threatened claims, demands, causes of action or proceedings arising from any breach of this Agreement by you. * IN NO EVENT SHALL WILEY OR ITS LICENSORS BE LIABLE TO YOU OR ANY OTHER PARTY OR ANY OTHER PERSON OR ENTITY FOR ANY SPECIAL, CONSEQUENTIAL,

INCIDENTAL, INDIRECT, EXEMPLARY OR PUNITIVE DAMAGES, HOWEVER CAUSED, ARISING OUT OF OR IN CONNECTION WITH THE DOWNLOADING, PROVISIONING, VIEWING OR USE OF THE MATERIALS REGARDLESS OF THE FORM OF ACTION, WHETHER FOR BREACH OF CONTRACT, BREACH OF WARRANTY, TORT, NEGLIGENCE, INFRINGEMENT OR OTHERWISE (INCLUDING, WITHOUT LIMITATION, DAMAGES BASED ON LOSS OF PROFITS, DATA, FILES, USE, BUSINESS OPPORTUNITY OR CLAIMS OF THIRD PARTIES), AND WHETHER OR NOT THE PARTY HAS BEEN ADVISED OF THE POSSIBILITY OF SUCH DAMAGES. THIS LIMITATION SHALL APPLY NOTWITHSTANDING ANY FAILURE OF ESSENTIAL PURPOSE OF ANY LIMITED REMEDY PROVIDED

HEREIN. * Should any provision of this Agreement be held by a court of competent jurisdiction to be illegal, invalid, or unenforceable, that provision shall be deemed amended to achieve as nearly as possible the same economic effect as the original provision, and the legality, validity and enforceability of the remaining provisions of this Agreement shall not be affected or impaired thereby. * The failure of either party to enforce any term or condition of this Agreement shall not constitute a waiver of either party's right to enforce each and every term and condition of this Agreement. No breach under this agreement shall be deemed waived or excused by either party unless such waiver or consent is in writing signed by the party granting such waiver or consent. The waiver by or consent of a party to a breach of any provision of this Agreement shall not operate or be construed as a waiver of or consent to any other or subsequent breach by such other party. * This Agreement may not be assigned (including by operation of law or otherwise) by you without WILEY's prior written consent. * Any fee required for this permission shall be non-refundable after thirty

(30) days from receipt by the CCC. * These terms and conditions together with CCC's

CCC's Billing and Payment terms and conditions (which are incorporated herein) form the entire agreement between you and WILEY concerning this licensing transaction and (in the absence of fraud) supersedes all prior agreements and representations of the parties, oral or written. This Agreement may not be amended except in writing signed by both parties. This Agreement shall be binding upon and inure to the benefit of the parties' successors, legal representatives, and authorized assigns. * In the event of any conflict between your obligations established by these terms and conditions and those established by CCC's Billing and Payment terms and conditions, these terms and conditions shall prevail. * WILEY expressly reserves all rights not specifically granted in the combination of (i) the license details provided by you and accepted in the course of this licensing transaction, (ii) these terms and conditions and (iii) CCC's

1/2s Billing and Payment terms and conditions. * This Agreement will be void if the Type of Use, Format, Circulation, or Requestor Type was misrepresented during the licensing process. * This Agreement shall be governed by and construed in accordance with the laws of the State of New York, USA, without regards to such state's conflict of law rules. Any legal action, suit or proceeding arising out of or relating to these Terms and Conditions or the breach thereof shall be instituted in a court of competent jurisdiction in New York County in the State of New York in the United States of America and each party hereby consents and submits to the personal jurisdiction of such court, waives any objection to venue in such court and consents to service of process by registered or certified mail, return receipt requested, at the last known address of such party. *WILEY OPEN ACCESS TERMS AND CONDITIONS* Wiley Publishes Open Access Articles in fully Open Access Journals and in Subscription journals offering Online Open. Although most of the fully Open Access journals publish open access articles under the terms of the Creative Commons Attribution (CC BY) License only, the subscription journals and a few of the Open Access Journals offer a choice of Creative Commons Licenses: Creative Commons Attribution (CC-BY) license Creative Commons Attribution Non-Commercial (CC- BY-NC) license and Creative Commons Attribution Non-Commercial-NoDerivs (CC- BY-NC-ND) License . The license type is clearly identified on the article. Copyright in any research article in a journal published as Open Access under a Creative Commons License is retained by the author(s). Authors grant Wiley a license to publish the

article and identify itself as the original publisher. Authors also grant any third party the right to use the article freely as long as its integrity is maintained and its original authors, citation details and publisher are identified as follows: [Title of Article/Author/Journal Title and Volume/Issue. Copyright (c) [year] [copyright owner as specified in the Journal]. Links to the final article on Wiley's website are encouraged where applicable. *The Creative Commons Attribution License* The Creative Commons Attribution License (CC-BY) allows users to copy, distribute and transmit an article, adapt the article and make commercial use of the article. The CC- BY license permits commercial and non-commercial re-use of an open access article, as long as the author is properly attributed. The Creative Commons Attribution License does not affect the moral rights of authors, including without limitation the right not to have their work subjected to derogatory treatment. It also does not affect any other rights held by authors or third parties in the article, including without limitation the rights of privacy and publicity. Use of the article must not assert or imply, whether implicitly or explicitly, any connection with, endorsement or sponsorship of such use by the author, publisher or any other party associated with the article. For any reuse or distribution, users must include the copyright notice and make

clear to others that the article is made available under a Creative Commons Attribution license, linking to the relevant Creative Commons web page. To the fullest extent permitted by applicable law, the article is made available as is and without representation or warranties of any kind whether express, implied, statutory or otherwise and including, without limitation, warranties of title, merchantability, fitness for a particular purpose, non-infringement, absence of defects, accuracy, or the presence or absence of errors.

Creative Commons Attribution Non-Commercial License The Creative Commons Attribution Non-Commercial (CC-BY-NC) License permits use, distribution and reproduction in any medium, provided the original work is properly cited and is not used for commercial purposes.(see below) ***Creative Commons Attribution-Non-Commercial-NoDerivs License*** The Creative Commons Attribution Non-Commercial-NoDerivs License (CC-BY-NC-ND) permits use, distribution and reproduction in any medium, provided the original work is properly cited, is not used for commercial purposes and no modifications or adaptations are made. (see below) ***Use by non-commercial users*** For non-commercial and non- promotional purposes, individual users may access, download, copy, display and redistribute to colleagues Wiley Open Access articles, as well as adapt, translate, text- and data-mine the content subject to the following conditions: *** The authors' moral rights are not compromised. These rights include the right of "paternity" (also known as "attribution" - the right for the author to be identified as such) and "integrity" (the right for the author not to have the work altered in such a way that the author's reputation or integrity may be impugned).** *** Where content in the article is identified**

as belonging to a third party, it is the obligation of the user to ensure that any reuse complies with the copyright policies of the owner of that content. *** If article content is copied, downloaded or otherwise reused for non-commercial research and education purposes, a link to the appropriate bibliographic citation (authors, journal, article title, volume, issue, page numbers, DOI and the link to the definitive published version on *Wiley Online Library*) should be maintained. Copyright notices and disclaimers must not be deleted. * Any translations, for which a prior translation agreement with Wiley has not been agreed, must prominently display the statement: "This is an unofficial translation of an article that appeared in a Wiley publication. The publisher has not endorsed this translation." *Use by commercial "for-profit" organisations*** Use of Wiley Open Access articles for commercial, promotional, or marketing purposes requires further explicit permission from Wiley and will be subject to a fee. Commercial purposes include: *** Copying or downloading of articles, or linking to such articles for further redistribution, sale or licensing; * Copying, downloading or posting by a site or service that incorporates advertising with such content; * The inclusion or incorporation of article content in other works or services (other than normal quotations with an appropriate citation) that is then available for sale or licensing, for a fee (for example, a compilation produced for marketing purposes, inclusion in a sales pack) * Use of article content**

(other than normal quotations with appropriate citation) by for-profit organisations for promotional purposes * Linking to article content in e-mails redistributed for promotional, marketing or educational purposes; * Use for the purposes of monetary reward by means of sale, resale, licence, loan, transfer or other form of commercial exploitation such as marketing products * Print reprints of Wiley Open Access articles can be purchased from: corporatesales@wiley.com Further details can be found on Wiley Online Library <http://olabout.wiley.com/WileyCDA/Section/id-410895.html> Other Terms and Conditions: *v1.9* *Questions? customercare@copyright.com or +1-855-239-3415 (toll free in the US) or +1-978-646-2777.* *Gratis licenses (referencing \$0 in the Total field) are free. Please retain this printable license for your reference. No payment is required.* -----

----- This is a License Agreement between Hwi Yong Lee ("You") and John Wiley and Sons ("John Wiley and Sons") provided by Copyright Clearance Center ("CCC"). The license consists of your order details, the terms and conditions provided by John Wiley and Sons, and the payment terms and conditions.

All payments must be made in full to CCC. For payment instructions, please see information listed at the bottom of this form. License Number 3497800670211 License date Oct 28, 2014 Licensed content publisher John Wiley and Sons Licensed content publication Electrophoresis Licensed content title Micro free-flow IEF enhanced by active cooling and functionalized gels Licensed copyright line Copyright © 2006 WILEY-VCH Verlag GmbH & Co. KGaA, Weinheim Licensed content author Jacob W. Albrecht, Klavs F. Jensen Licensed content date Nov 20, 2006 Start page 4960 End page 4969 Type of use Dissertation/Thesis Requestor type University/Academic Format Electronic Portion Figure/table Number of figures/tables 1 Original Wiley figure/table number(s) Fig-1 Will you be translating? No Title of your thesis / dissertation New microfluidic system to increase robustness and develop point-of-care hematocrit device Expected completion date Nov 2014 Expected size (number of pages) 200 Total 0.00 USD Terms and Conditions *TERMS AND CONDITIONS * This copyrighted material is owned by or exclusively licensed to John Wiley & Sons, Inc. or one of its group companies (each a "Wiley Company") or handled on behalf of a society with which a Wiley Company has exclusive publishing rights in relation to a particular work (collectively "WILEY"). By clicking I accept

In connection with completing this licensing transaction, you agree that the following terms and conditions apply to this transaction (along with the billing and payment terms and conditions established by the Copyright Clearance Center Inc., ("CCC's Billing and Payment terms and conditions"), at the time that you opened your Rightslink account (these are available at any time at <http://myaccount.copyright.com>). *Terms and Conditions* * The materials you have requested permission to reproduce or reuse (the "Wiley Materials") are protected by copyright. * You are hereby granted a personal, non-exclusive, non-sub licensable (on a stand-alone basis), non-transferable, worldwide, limited license to reproduce the Wiley Materials for the purpose specified in the licensing process. This license is for a one-time use only and limited to any maximum distribution number specified in the license. The first instance of republication or reuse granted by this licence must be completed within two years of the date of the grant of this licence (although copies prepared before the end date may be distributed thereafter). The Wiley Materials shall not be used in any other manner or for any other purpose, beyond what is granted in the license. Permission is granted subject to an appropriate acknowledgement

given to the author, title of the material/book/journal and the publisher. You shall also duplicate the copyright notice that appears in the Wiley publication in your use of the Wiley Material. Permission is also granted on the understanding that nowhere in the text is a previously published source acknowledged for all or part of this Wiley Material. Any third party content is expressly excluded from this permission. * With respect to the Wiley Materials, all rights are reserved. Except as expressly granted by the terms of the license, no part of the Wiley Materials may be copied, modified, adapted (except for minor reformatting required by the new Publication), translated, reproduced, transferred or distributed, in any form or by any means, and no derivative works may be made based on the Wiley Materials without the prior permission of the respective copyright owner. You may not alter, remove or suppress in any manner any copyright, trademark or other notices displayed by the Wiley Materials. You may not license, rent, sell, loan, lease, pledge, offer as security, transfer or assign the Wiley Materials on a stand-alone basis, or any of the rights granted to you hereunder to any other person. * The Wiley Materials and all of the intellectual property rights therein shall at all times remain the exclusive property of John Wiley & Sons Inc, the Wiley Companies, or their respective licensors, and your interest therein is only that of having possession of and the right to reproduce the Wiley Materials pursuant to Section 2 herein during the continuance of this Agreement. You agree that you own no right, title or interest in or to the Wiley Materials or any of the intellectual property rights therein. You shall have no rights hereunder other than the license as provided for above in Section 2. No right, license or interest to any trademark, trade name, service mark or other branding ("Marks") of WILEY or its licensors is granted hereunder, and you agree that you shall not assert any such right, license or interest with respect thereto. * NEITHER WILEY NOR ITS LICENSORS MAKES ANY WARRANTY OR REPRESENTATION OF ANY KIND TO YOU OR ANY THIRD PARTY, EXPRESS, IMPLIED OR STATUTORY, WITH RESPECT TO THE MATERIALS OR THE ACCURACY OF ANY INFORMATION CONTAINED IN THE MATERIALS, INCLUDING, WITHOUT LIMITATION, ANY IMPLIED WARRANTY OF MERCHANTABILITY, ACCURACY, SATISFACTORY QUALITY, FITNESS FOR A PARTICULAR PURPOSE, USABILITY, INTEGRATION OR NON-INFRINGEMENT AND ALL SUCH WARRANTIES ARE HEREBY EXCLUDED BY WILEY AND ITS LICENSORS AND WAIVED

BY YOU * WILEY shall have the right to terminate this Agreement immediately upon breach of this Agreement by you. * You shall indemnify, defend and hold harmless WILEY, its Licensors and their respective directors, officers, agents and employees, from and against any actual or threatened claims, demands, causes of action or proceedings arising from any breach of this Agreement by you. * IN NO EVENT SHALL WILEY OR ITS LICENSORS BE LIABLE TO YOU OR ANY OTHER PARTY OR ANY OTHER PERSON OR ENTITY FOR ANY SPECIAL, CONSEQUENTIAL, INCIDENTAL, INDIRECT, EXEMPLARY OR PUNITIVE DAMAGES, HOWEVER

CAUSED, ARISING OUT OF OR IN CONNECTION WITH THE DOWNLOADING, PROVISIONING, VIEWING OR USE OF THE MATERIALS REGARDLESS OF THE FORM OF ACTION, WHETHER FOR BREACH OF CONTRACT, BREACH OF WARRANTY, TORT, NEGLIGENCE, INFRINGEMENT OR OTHERWISE (INCLUDING, WITHOUT LIMITATION, DAMAGES BASED ON LOSS OF PROFITS, DATA, FILES, USE, BUSINESS OPPORTUNITY OR CLAIMS OF THIRD PARTIES), AND WHETHER OR NOT THE PARTY HAS BEEN ADVISED OF THE POSSIBILITY OF SUCH DAMAGES. THIS LIMITATION SHALL APPLY NOTWITHSTANDING ANY FAILURE OF ESSENTIAL PURPOSE OF ANY LIMITED REMEDY PROVIDED

HEREIN. * Should any provision of this Agreement be held by a court of competent jurisdiction to be illegal, invalid, or unenforceable, that provision shall be deemed amended to achieve as nearly as possible the same economic effect as the original provision, and the legality, validity and enforceability of the remaining provisions of this Agreement shall not be affected or impaired thereby. * The failure of either party to enforce any term or condition of this Agreement shall not constitute a waiver of either party's right to enforce each and every term and condition of this Agreement. No breach under this agreement shall be deemed waived or excused by either party unless such waiver or consent is in writing signed by the party granting such waiver or consent. The waiver by or consent of a party to a breach of any provision of this Agreement shall not operate or be construed as a waiver of or consent to any other or subsequent breach by such other party. * This Agreement may not be assigned (including by operation of law or otherwise) by you without WILEY's prior written consent. * Any fee required for this permission shall be non-refundable after thirty

(30) days from receipt by the CCC. * These terms and conditions together with CCC's

and Billing and Payment terms and conditions (which are incorporated herein) form the entire agreement between you and WILEY concerning this licensing transaction and (in the absence of fraud) supersedes all prior agreements and representations of the parties, oral or written. This Agreement may not be amended except in writing signed by both parties. This Agreement shall be binding upon and inure to the benefit of the parties' successors, legal representatives, and authorized assigns. * In the event of any conflict between your obligations established by these terms and conditions and those established by CCC's and Billing and Payment terms and conditions, these terms and conditions shall prevail. * WILEY expressly reserves all rights not specifically granted in the combination of (i) the license details provided by you and accepted in the course of this licensing transaction, (ii) these terms and conditions and (iii) CCC's

and Billing and Payment terms and conditions. * This Agreement will be void if the Type of Use, Format, Circulation, or Requestor Type was misrepresented during the

licensing process. * This Agreement shall be governed by and construed in accordance with the laws of the State of New York, USA, without regards to such state's conflict of law rules. Any legal action, suit or proceeding arising out of or relating to these Terms and Conditions or the breach thereof shall be instituted in a court of competent jurisdiction in New York County in the State of New York in the United States of America and each party hereby consents and submits to the personal jurisdiction of such court, waives any objection to venue in such court and consents to service of process by registered or certified mail, return receipt requested, at the last known address of such party. *WILEY OPEN ACCESS TERMS AND CONDITIONS* Wiley Publishes Open Access Articles in fully Open Access Journals and in Subscription journals offering Online Open. Although most of the fully Open Access journals publish open access articles under the terms of the Creative Commons Attribution (CC BY) License only, the subscription journals and a few of the Open Access Journals offer a choice of Creative Commons Licenses: Creative Commons Attribution (CC-BY) license Creative Commons Attribution Non-Commercial (CC- BY-NC) license and Creative Commons Attribution Non-Commercial-NoDerivs (CC- BY-NC-ND) License . The license type is clearly identified on the article. Copyright in any research article in a journal published as Open Access under a Creative Commons License is retained by the author(s). Authors grant Wiley a license to publish the

article and identify itself as the original publisher. Authors also grant any third party the right to use the article freely as long as its integrity is maintained and its original authors, citation details and publisher are identified as follows: [Title of Article/Author/Journal Title and Volume/Issue. Copyright (c) [year] [copyright owner as specified in the Journal]. Links to the final article on Wiley's website are encouraged where applicable. *The Creative Commons Attribution License* The Creative Commons Attribution License (CC-BY) allows users to copy, distribute and transmit an article, adapt the article and make commercial use of the article. The CC- BY license permits commercial and non-commercial re-use of an open access article, as long as the author is properly attributed. The Creative Commons Attribution License does not affect the moral rights of authors, including without limitation the right not to have their work subjected to derogatory treatment. It also does not affect any other rights held by authors or third parties in the article, including without limitation the rights of privacy and publicity. Use of the article must not assert or imply, whether implicitly or explicitly, any connection with, endorsement or sponsorship of such use by the author, publisher or any other party associated with the article. For any reuse or distribution, users must include the copyright notice and make clear to others that the article is made available under a Creative Commons Attribution license, linking to the relevant Creative Commons web page. To the fullest extent permitted by applicable law, the article is made available as is and without representation or warranties of any kind whether express, implied, statutory or otherwise and including, without limitation, warranties of title, merchantability, fitness

for a particular purpose, non-infringement, absence of defects, accuracy, or the presence or absence of errors. *Creative Commons Attribution Non-Commercial License* The Creative Commons Attribution Non-Commercial (CC-BY-NC) License permits use, distribution and reproduction in any medium, provided the original work is properly cited and is not used for commercial purposes.(see below) *Creative Commons Attribution-Non-Commercial-NoDerivs License* The Creative Commons Attribution Non-Commercial-NoDerivs License (CC-BY-NC-ND) permits use, distribution and reproduction in any medium, provided the original work is properly cited, is not used for commercial purposes and no modifications or adaptations are made. (see below) *Use by non-commercial users* For non-commercial and non- promotional purposes, individual users may access, download, copy, display and redistribute to colleagues Wiley Open Access articles, as well as adapt, translate, text- and data-mine the content subject to the following conditions: * The authors' moral rights are not compromised. These rights include the right of "paternity" (also known as "attribution" - the right for the author to be identified as such) and "integrity" (the right for the author not to have the work altered in such a way that the author's reputation or integrity may be impugned). * Where content in the article is identified

as belonging to a third party, it is the obligation of the user to ensure that any reuse complies with the copyright policies of the owner of that content. * If article content is copied, downloaded or otherwise reused for non-commercial research and education purposes, a link to the appropriate bibliographic citation (authors, journal, article title, volume, issue, page numbers, DOI and the link to the definitive published version on

Wiley Online Library) should be maintained. Copyright notices and disclaimers must not be deleted. * Any translations, for which a prior translation agreement with Wiley has not been agreed, must prominently display the statement: "This is an unofficial translation of an article that appeared in a Wiley publication. The publisher has not endorsed this translation." *Use by commercial "for-profit" organisations* Use of Wiley Open Access articles for commercial, promotional, or marketing purposes requires further explicit permission from Wiley and will be subject to a fee.

Commercial purposes include: * Copying or downloading of articles, or linking to such articles for further redistribution, sale or licensing; * Copying, downloading or posting by a site or service that incorporates advertising with such content; * The

inclusion or incorporation of article content in other works or services (other than normal quotations with an appropriate citation) that is then available for sale or licensing, for a fee (for example, a compilation produced for marketing purposes, inclusion in a sales pack) * Use of article content (other than normal quotations with appropriate citation) by for-profit organisations for promotional purposes * Linking to article content in e-mails redistributed for promotional, marketing or educational purposes; * Use for the purposes

of monetary reward by means of sale, resale, licence, loan, transfer or other form of commercial exploitation such as marketing products * Print reprints of Wiley Open Access articles can be purchased from: corporatesales@wiley.com Further details can be found on Wiley Online Library <http://olabout.wiley.com/WileyCDA/Section/id-410895.html> Other Terms and Conditions: *v1.9* *Questions? customercare@copyright.com or +1-855-239-3415 (toll free in the US) or +1-978-646-2777.* *Gratis licenses (referencing \$0 in the Total field) are free. Please retain this printable license for your reference. No payment is required.* -----

----- This is a License Agreement between Hwi Yong Lee ("You") and John Wiley and Sons ("John Wiley and Sons") provided by Copyright Clearance Center ("CCC"). The license consists of your order details, the terms and conditions provided by John Wiley and Sons, and the payment terms and conditions.

All payments must be made in full to CCC. For payment instructions, please see information listed at the bottom of this form. License Number 3495530348470 License date Oct 24, 2014 Licensed content publisher John Wiley and Sons Licensed content publication Electrophoresis Licensed content title Improving electrokinetic microdevice stability by controlling electrolysis bubbles Licensed copyright line © 2014 WILEY-VCH Verlag GmbH & Co. KGaA, Weinheim Licensed content author Hwi Yong Lee, Cedrick Barber, Adrienne R. Minerick Licensed content date Apr 15, 2014 Start page 1782 End page 1789 Type of use Dissertation/Thesis Requestor type Author of this Wiley article Format Electronic Portion Full article Will you be translating? No Title of your thesis / dissertation New microfluidic system to increase robustness and develop point-of-care hematocrit device Expected completion date Nov 2014 Expected size (number of pages) 200 Total 0.00 USD Terms and Conditions *TERMS AND CONDITIONS * This copyrighted material is owned by or exclusively licensed to John Wiley & Sons, Inc. or one of its group companies (each a "Wiley Company") or handled on behalf of a society with which a Wiley Company has exclusive publishing rights in relation to a particular work (collectively "WILEY"). By clicking I accept in connection with completing this licensing transaction, you agree that the following terms and conditions apply to this transaction (along with the billing and payment terms and conditions established by the Copyright Clearance Center Inc., ("CCC's Billing and Payment terms and conditions"), at the time that you opened your Rightslink account (these are available at any time at <http://myaccount.copyright.com>). *Terms and Conditions* * The materials you have requested permission to reproduce or reuse (the "Wiley Materials") are protected by copyright. * You are hereby granted a personal, non-exclusive, non-sub licensable (on a stand-alone basis), non-transferable, worldwide, limited license to reproduce the Wiley Materials for the purpose specified in the licensing process. This license is for a one-time use only and limited to any maximum distribution number specified in the license. The first instance of republication or reuse granted by this licence must be completed within two years of the date of the grant of this licence (although copies prepared before the end date may be distributed thereafter). The Wiley Materials shall not be used in any other manner or for any other purpose, beyond what is granted in the license. Permission is granted subject to an appropriate acknowledgement given to the author, title of the material/book/journal and the publisher. You shall also

duplicate the copyright notice that appears in the Wiley publication in your use of the Wiley Material. Permission is also granted on the understanding that nowhere in the text is a previously published source acknowledged for all or part of this Wiley Material. Any third party content is expressly excluded from this permission. * With respect to the Wiley Materials, all rights are reserved. Except as expressly granted by the terms of the license, no part of the Wiley Materials may be copied, modified, adapted (except for minor reformatting required by the new Publication), translated, reproduced, transferred or distributed, in any form or by any means, and no derivative works may be made based on the Wiley Materials without the prior permission of the respective copyright owner. You may not alter, remove or suppress in any manner any copyright, trademark or other notices displayed by the Wiley Materials. You may not license, rent, sell, loan, lease, pledge, offer as security, transfer or assign the Wiley Materials on a stand-alone basis, or any of the rights granted to you hereunder to any other person. * The Wiley Materials and all of the intellectual property rights therein shall at all times remain the exclusive property of John Wiley & Sons Inc, the Wiley Companies, or their respective licensors, and your interest therein is only that of having possession of and the right to reproduce the Wiley Materials pursuant to Section 2 herein during the continuance of this Agreement. You agree that you own no right, title or interest in or to the Wiley Materials or any of the intellectual property rights therein. You shall have no rights hereunder other than the license as provided for above in Section 2. No right, license or interest to any trademark, trade name, service mark or other branding ("Marks") of WILEY or its licensors is granted hereunder, and you agree that you shall not assert any such right, license or interest with respect thereto. * NEITHER WILEY NOR ITS LICENSORS MAKES ANY WARRANTY OR REPRESENTATION OF ANY KIND TO YOU OR ANY THIRD PARTY, EXPRESS, IMPLIED OR STATUTORY, WITH RESPECT TO THE MATERIALS OR THE ACCURACY OF ANY INFORMATION CONTAINED IN THE MATERIALS, INCLUDING, WITHOUT LIMITATION, ANY IMPLIED WARRANTY OF MERCHANTABILITY, ACCURACY, SATISFACTORY QUALITY, FITNESS FOR A PARTICULAR PURPOSE, USABILITY, INTEGRATION OR NON-INFRINGEMENT AND ALL SUCH WARRANTIES ARE HEREBY EXCLUDED BY WILEY AND ITS LICENSORS AND WAIVED

BY YOU * WILEY shall have the right to terminate this Agreement immediately upon breach of this Agreement by you. * You shall indemnify, defend and hold harmless WILEY, its Licensors and their respective directors, officers, agents and employees, from and against any actual or threatened claims, demands, causes of action or proceedings arising from any breach of this Agreement by you. * IN NO EVENT SHALL WILEY OR ITS LICENSORS BE LIABLE TO YOU OR ANY OTHER PARTY OR ANY OTHER PERSON OR ENTITY FOR ANY SPECIAL, CONSEQUENTIAL, INCIDENTAL, INDIRECT, EXEMPLARY OR PUNITIVE DAMAGES, HOWEVER CAUSED, ARISING OUT OF OR IN CONNECTION WITH THE DOWNLOADING,

PROVISIONING, VIEWING OR USE OF THE MATERIALS REGARDLESS OF THE FORM OF ACTION, WHETHER FOR BREACH OF CONTRACT, BREACH OF WARRANTY, TORT, NEGLIGENCE, INFRINGEMENT OR OTHERWISE (INCLUDING, WITHOUT LIMITATION, DAMAGES BASED ON LOSS OF PROFITS, DATA, FILES, USE, BUSINESS OPPORTUNITY OR CLAIMS OF THIRD PARTIES), AND WHETHER OR NOT THE PARTY HAS BEEN ADVISED OF THE POSSIBILITY OF SUCH DAMAGES. THIS LIMITATION SHALL APPLY NOTWITHSTANDING ANY FAILURE OF ESSENTIAL PURPOSE OF ANY LIMITED REMEDY PROVIDED

HEREIN. * Should any provision of this Agreement be held by a court of competent jurisdiction to be illegal, invalid, or unenforceable, that provision shall be deemed amended to achieve as nearly as possible the same economic effect as the original provision, and the legality, validity and enforceability of the remaining provisions of this Agreement shall not be affected or impaired thereby. * The failure of either party to enforce any term or condition of this Agreement shall not constitute a waiver of either party's right to enforce each and every term and condition of this Agreement. No breach under this agreement shall be deemed waived or excused by either party unless such waiver or consent is in writing signed by the party granting such waiver or consent. The waiver by or consent of a party to a breach of any provision of this Agreement shall not operate or be construed as a waiver of or consent to any other or subsequent breach by such other party. * This Agreement may not be assigned (including by operation of law or otherwise) by you without WILEY's prior written consent. * Any fee required for this permission shall be non-refundable after thirty

(30) days from receipt by the CCC. * These terms and conditions together with CCC's

CCC's Billing and Payment terms and conditions (which are incorporated herein) form the entire agreement between you and WILEY concerning this licensing transaction and (in the absence of fraud) supersedes all prior agreements and representations of the parties, oral or written. This Agreement may not be amended except in writing signed by both parties. This Agreement shall be binding upon and inure to the benefit of the parties' successors, legal representatives, and authorized assigns. * In the event of any conflict between your obligations established by these terms and conditions and those established by CCC's Billing and Payment terms and conditions, these terms and conditions shall prevail. * WILEY expressly reserves all rights not specifically granted in the combination of (i) the license details provided by you and accepted in the course of this licensing transaction, (ii) these terms and conditions and (iii) CCC's

CCC's Billing and Payment terms and conditions. * This Agreement will be void if the Type of Use, Format, Circulation, or Requestor Type was misrepresented during the licensing process. * This Agreement shall be governed by and construed in accordance

with the laws of the State of New York, USA, without regards to such state's conflict of law rules. Any legal action, suit or proceeding arising out of or relating to these Terms and Conditions or the breach thereof shall be instituted in a court of competent jurisdiction in New York County in the State of New York in the United States of America and each party hereby consents and submits to the personal jurisdiction of such court, waives any objection to venue in such court and consents to service of process by registered or certified mail, return receipt requested, at the last known address of such party. ***WILEY OPEN ACCESS TERMS AND CONDITIONS*** Wiley Publishes Open Access Articles in fully Open Access Journals and in Subscription journals offering Online Open. Although most of the fully Open Access journals publish open access articles under the terms of the Creative Commons Attribution (CC BY) License only, the subscription journals and a few of the Open Access Journals offer a choice of Creative Commons Licenses: Creative Commons Attribution (CC-BY) license Creative Commons Attribution Non-Commercial (CC- BY-NC) license and Creative Commons Attribution Non-Commercial-NoDerivs (CC- BY-NC-ND) License . The license type is clearly identified on the article. Copyright in any research article in a journal published as Open Access under a Creative Commons License is retained by the author(s). Authors grant Wiley a license to publish the

article and identify itself as the original publisher. Authors also grant any third party the right to use the article freely as long as its integrity is maintained and its original authors, citation details and publisher are identified as follows: [Title of Article/Author/Journal Title and Volume/Issue. Copyright (c) [year] [copyright owner as specified in the Journal]. Links to the final article on Wiley's website are encouraged where applicable. ***The Creative Commons Attribution License*** The Creative Commons Attribution License (CC-BY) allows users to copy, distribute and transmit an article, adapt the article and make commercial use of the article. The CC- BY license permits commercial and non-commercial re-use of an open access article, as long as the author is properly attributed. The Creative Commons Attribution License does not affect the moral rights of authors, including without limitation the right not to have their work subjected to derogatory treatment. It also does not affect any other rights held by authors or third parties in the article, including without limitation the rights of privacy and publicity. Use of the article must not assert or imply, whether implicitly or explicitly, any connection with, endorsement or sponsorship of such use by the author, publisher or any other party associated with the article. For any reuse or distribution, users must include the copyright notice and make

clear to others that the article is made available under a Creative Commons Attribution license, linking to the relevant Creative Commons web page. To the fullest extent permitted by applicable law, the article is made available as is and without representation or warranties of any kind whether express, implied, statutory or otherwise and including,

without limitation, warranties of title, merchantability, fitness for a particular purpose, non-infringement, absence of defects, accuracy, or the presence or absence of errors.

Creative Commons Attribution Non-Commercial License The Creative Commons Attribution Non-Commercial (CC-BY-NC) License permits use, distribution and reproduction in any medium, provided the original work is properly cited and is not used for commercial purposes.(see below) *Creative Commons Attribution-Non-Commercial-NoDerivs License* The Creative Commons Attribution Non-Commercial-NoDerivs License (CC-BY-NC-ND) permits use, distribution and reproduction in any medium, provided the original work is properly cited, is not used for commercial purposes and no modifications or adaptations are made. (see below) *Use by non-commercial users* For non-commercial and non- promotional purposes, individual users may access, download, copy, display and redistribute to colleagues Wiley Open Access articles, as well as adapt, translate, text- and data-mine the content subject to the following conditions: * The authors' moral rights are not compromised. These rights include the right of "paternity" (also known as "attribution" - the right for the author to be identified as such) and "integrity" (the right for the author not to have the work altered in such a way that the author's reputation or integrity may be impugned). * Where content in the article is identified

as belonging to a third party, it is the obligation of the user to ensure that any reuse complies with the copyright policies of the owner of that content. * If article content is copied, downloaded or otherwise reused for non-commercial research and education purposes, a link to the appropriate bibliographic citation (authors, journal, article title, volume, issue, page numbers, DOI and the link to the definitive published version on

Wiley Online Library) should be maintained. Copyright notices and disclaimers must not be deleted. * Any translations, for which a prior translation agreement with Wiley has not been agreed, must prominently display the statement: "This is an unofficial translation of an article that appeared in a Wiley publication. The publisher has not endorsed this translation." *Use by commercial "for-profit" organisations* Use of Wiley Open Access articles for commercial, promotional, or marketing purposes requires further explicit permission from Wiley and will be subject to a fee.

Commercial purposes include: * Copying or downloading of articles, or linking to such articles for further redistribution, sale or licensing; * Copying, downloading or posting by a site or service that incorporates advertising with such content; * The inclusion or incorporation of article content in other works or services (other than normal quotations with an appropriate citation) that is then available for sale or licensing, for a fee (for example, a compilation produced for marketing purposes, inclusion in a sales pack) * Use of article content (other than normal quotations with appropriate citation) by for-profit organisations for promotional purposes * Linking to article content in e-mails

redistributed for promotional, marketing or educational purposes; * Use for the purposes of monetary reward by means of sale, resale, licence, loan, transfer or other form of commercial exploitation such as marketing products * Print reprints of Wiley Open Access articles can be purchased from: corporatesales@wiley.com Further details can be found on Wiley Online Library <http://olabout.wiley.com/WileyCDA/Section/id-410895.html> Other Terms and Conditions: *v1.9* *Questions? customercare@copyright.com or +1-855-239-3415 (toll free in the US) or +1-978-646-2777.* *Gratis licenses (referencing \$0 in the Total field) are free. Please retain this printable license for your reference. No payment is required.* -----
